T.R.
ONDOKUZ MAYIS UNIVERSITY
INSTITUTE OF GRADUATE STUDIES
NANOSCIENCE AND NANOTECHNOLOGY DEPARTMENT

SYNTHESIS, CHARACTERIZATION, IN VITRO DRUG RELEASE AND CYTOTOXICTY OF NANOSPONGE AS A pH -GUIDED NANO DRUG CARRIER SYSTEM

Ph.D. Thesis

Ayhan BERGAL

Supervisor
Prof. Dr. Müberra ANDAÇ

SAMSUN
2023

T.R.
ONDOKUZ MAYIS UNIVERSITY
INSTITUTE OF GRADUATE STUDIES
DEPARTMENT OF NANOSCIENCE AND NANOTECHNOLOGY

SYNTHESIS, CHARACTERIZATION, IN VITRO DRUG RELEASE AND CYTOTOXICTY OF NANOSPONGE AS A pH -GUIDED NANO DRUG CARRIER SYSTEM

Ph.D. Thesis

Ayhan BERGAL

Supervisor

Prof. Dr. Müberra ANDAÇ

This research was funded by Ondokuz Mayıs University under Scientific Research (BAP) project (Project Number: PYO. FEN.1901.19.003).

SAMSUN
2023

ACCEPTANCE AND APPROVAL OF THE THESIS

The study entitled **"SYNTHESIS, CHARACTERIZATION, IN VITRO DRUG RELEASE AND CYTOTOXICTY OF NANOSPONGE AS A pH - GUIDED NANO DRUG CARRIER SYSTEM"** prepared by **Ayhan BERGAL**, and supervised by **Prof. Dr. Müberra ANDAÇ**, was found successful and unanimously accepted by committee members as Ph.D. thesis, following the examination on the date 27.7.2023.

	Title Name SURNAME **University** **Department/Art**	**Final Decision**
Chairman	Assoc. Prof. Dr. Bekir DİZMAN Sabancı University Faculty of Engineering and Natural Sciences, Materials Science and Nano Engineering	● Accept ☐ Reject
Member	Prof. Dr. Oğuzhan YAVUZ Çukurova University Ceyhan Faculty of Veterinary Medicine, Preclinical Sciences, Pharmacology and Toxicology	● Accept ☐ Reject
Member	Prof. Dr. Müberra ANDAÇ Ondokuz Mayıs University Faculty of Science, Chemistry	● Accept ☐ Reject
Member	Assoc. Prof. Dr. Hilal AY Yıldız Teknik University Faculty of Arts and Sciences Molecular Biology and Genetics	● Accept ☐ Reject
Member	Asst. Prof. Dr. Aydemir Güralp URAL Samsun University Özdemir Bayraktar Faculty of Aviation and Space Sciences	● Accept ☐ Reject

This thesis has been approved by the committee members that already stated above and determined by the Institute Executive Board.

.

Prof. Dr. Ahmet TABAK
Head of Institute of Graduate Studies

DECLARATION OF COMPLIANCE WITH SCIENTIFIC ETHIC

I hereby declare and undertake that I complied with scientific ethics and academic rules in all stages of my Ph.D. Thesis , that I have referred to each quotation that I use directly or indirectly in the study and that the works I have used consist of those shown in the sources, that it was written in accordance with the institute writing guide and that the situations stated in the article 3, section 9 of the Regulation for TÜBITAK Research and Publication Ethics Board were not violated.

Is An Ethics Committee Necessary?

Yes ☐ (If it necessary, please add appendices.)

No ☒

20 / 05 / 2023
Ayhan BERGAL

DECLARATION OF THE THESIS STUDY ORIGINALITY REPORT

Thesis Title : SYNTHESIS, CHARACTERIZATION, IN VITRO DRUG RELEASE AND CYTOTOXICITY OF NANOSPONGE AS A PH GUIDED NANO DRUG CARRIER SYSTEM

As a result of the originality report taken by me from the plagiarism detection program on 27 / 05 / 2023 for the thesis titled above;

Similarity ratio : 16 %

Single resource rate : 1 % has been released.

27/ 05 / 2023
Prof. Dr. Müberra ANDAÇ

ÖZET

pH GÜDÜMLÜ NANO İLAÇ TAŞIYICI BİR SİSTEM OLARAK NANOSPONGE ELDESİ, KARAKTERİZASYONU İN VİTRO İLAÇ SALINIM VE TOKSİSİTE ÖZELLİKLERİNİN ARAŞTIRILMASI

Ayhan BERGAL
Ondokuz Mayıs Üniversitesi
Lisansüstü Eğitim Enstitüsü
Nanobilim ve Nanoteknoloji Ana Bilim Dalı
Doktora, Temmuz/2023
Danışman: Prof. Dr. Müberra ANDAÇ

Tez, ALD-NS'nin sentezi ve pH'a duyarlı bir ilaç taşıyıcı olarak kullanılabilirliğini araştırmayı amaçlamıştır. Bu amaçla, aldehit (CHO) grupları ile işlevselleştirilmiş β-CD, $NaIO_4$'ün değişen molar oranları kullanılarak oksidasyon işlemi ile sentezlenmiş ve karakterizasyon sonuçları, fonksiyonel CHO gruplu OX-β-CD'lerin oluşumunu doğrulamıştır.

OX-β-CD'ler PMDA çapraz bağlayıcı ile geliştirilen yöntemle çapraz bağlanarak suda çözünür, katı ALD-NS elde edilmiş ve DOX.HCl'nin NH_2 grubunun varlığından dolayı reflux yöntemi ile hem pH'a duyarlı Schiff bazı (C=N) bağı oluşumunun sağlanması hem de ALD-NS'nin hidrofilik kısmı entegre edilmesi amaçlanmıştır. ALD-NS+DOX karakterize edilmiş ve sonuçlar bu oluşumu, kapsüllenmeyi ve morfolojik değişimi PS (372.7±8.21nm), negatif ZP (-12.8±1.54) ve yüksek EE (%85.5) ile göstermiştir.

ALD-NS+DOX'un in vitro salım davranışı, farklı pH'larda üç tampon ortamında değerlendirilmiş ve pH 5.2'de ilaç salımının pH 7.4 ortamından daha yüksek olduğu, Schiff bazı ve çapraz bağlayıcının kolay hidrolizi nedeniyle saf DOX'a kıyasla sürekli, uzun süreli ilaç salım profili meydana geldiği gözlenmiştir. ALD-NS+DOX'un doza ve zamana bağlı sitotoksisitesi ve hücresel alımı, A549 kanser hücreleri üzerinde belirlenmiştir. İlaç yüklü NC'nin hücre canlılıkları, konsantrasyon arttıkça azalmış, ancak serbest DOX ile karşılaştırıldığında daha yüksek canlılıklar ve çeşitli zaman aralığında tamamen eşdeğer konsantrasyonda hücrenin içinde veya yüzeyinde daha yoğun ilaç birikimi sergilediği bulunmuştur.

İlaç salım kinetiği en yüksek korelasyon katsayısına (R^2=0.97) dayanmasından dolayı en iyi Krosmeyyer-Peppas modeli tarafından ifade edilmiştir. Difüzyon katsayısı "n"nin pH 5.2'de PBS için 0.622 ve NaOAc için 0.71 olduğunun ortaya çıkarılması, ilaç salımının hem çözünme (Schiff bazının hidrolizi) hem de Fickian olmayan difüzyon nedeniyle gerçekleştiğini ortaya koymaktadır.

Sonuç olarak, sentezlenen yeni tür işlevselleştirilmiş nanoyapı, özellikle NH_2 yan grubu içeren ilaçlar için düşük pH ortamında aday bir ilaç taşıyıcısı olma potansiyeline sahiptir.

Anahtar Sözcükler: Nanotaşıyıcılar, Nanosponges, β-siklodekstrin, Schiff Baz, pH güdümlü ilaç salınım

ABSTRACT

SYNTHESIS, CHARACTERIZATION, IN VITRO DRUG RELEASE AND CYTOTOXICTY OF NANOSPONGE AS A pH -GUIDED NANO DRUG CARRIER SYSTEM

Ayhan BERGAL
Ondokuz Mayıs University
Institute of Graduate Studies
Department of Nanoscience and Nanotechnology
Ph.D., July/2023
Supervisor: Prof. Dr. Müberra ANDAÇ

Thesis aimed to fabricate and investigate usability of ALD-NS as a pH responsive drug delivery agent. For this aim, functionalized β-CD with aldehyde (CHO) groups were fabricated by oxidation process using varying molar ratios of $NaIO_4$ and characterization results confirmed formation of OX-β-CDs with functional CHO groups.

OX-β-CDs was crosslinked with PMDA crosslinker to obtain water soluble, solid ALD-NS with the method developed and DOX.HCl due to the presence of NH_2 group was integrated by reflux method, aiming to ensure both pH sensitive Schiff base (C=N) bond and hydrophilic part of the ALD-NS. ALD-NS+DOX was characterized, and results showed this formation, encapsulation, and morphological change with PS (372.7±8.21nm), negative ZP (-12.8±1.54), high EE (85.5%).

In vitro release behavior of ALD-NS+DOX was evaluated in three buffer conditions at different pH and observed that drug release at pH 5.2 is higher than at pH 7.4 environment occurring, sustain, prolong drug release profile compared to pure DOX due to easy hydrolysis of Schiff base and crosslinker. Time and dose dependent cytotoxicity and cellular uptake of ALD-NS+DOX were determined on A549 cancer cells. Cell viabilities of drug loaded NC decreased with increasing the concentration but have found higher viabilities and displayed the intensive drug accumulation on the surface or inside of the cell compared to free DOX in the all-equivalent concentration at various time range.

Drug release kinetics was best expressed by the Krosmeyyer-Peppas model based on the highest correlation coefficient (R^2=0.97), revealing that diffusion coefficient “n” was found 0.622 for PBS and 0.71 for NaOAc at pH 5.2 specifying drug release occurs due to both dissolution (hydrolysis of Schiff base) and non-Fickian diffusion.

As a result, the novel kind of functionalized nanostructure has the potential to be a candidate drug carrier in a low pH environment, especially for drugs containing NH_2 side group.

Keywords: Nanocarriers, Nanosponges, β-Cyclodextrin, Schiff base, pH responsive drug release

ACKNOWLEDGEMENT

I would like to express my deepest appreciation, acknowledge my indebtedness and render my warmest thanks to my Ph.D. supervisor, Prof. Dr. Muberra ANDAÇ who gave me a higher level of assistance, generous guidance, support and expert advice throughout all stages of the research. I would also like to extend my deepest and special gratitude and thanks to Prof. Francesco Trotta for all the support, advice and assistance received and provided through work who gave me the opportunity to carry out some of my Ph.D. research in the group of Polymeric Materials (MP), Department of Chemistry, University of Turin, Italy. I am deeply indebted to each person who has provided me with extensive and warm guidance.

The most importantly, I would like to manifest my deepest and sincere gratitude to my beloved family, especially my wife, my beautiful daughter and my parents, whose love, help, moral sacrifices and all kinds of support throughout my educational life with me in whatever i pursue. I owe my deepest respect, love and thanks for always encouraging, believing in me.

I wish to indicate my gratitude to doctoral committees, Faculty Members and Research Assistants of the Department of Nanoscience and Nanotechnology and the Department of Chemistry as well as the Department of Pharmacology and Toxicology, Veterinary Faculty of the University, which also carried out cytotoxicity and cell uptake studies.

This research was funded by Ondokuz Mayıs University with the project number PYO.FEN.1901.19.003 within the scope of the Scientific Research (BAP) project. Also, I would like to state my sincere thanks to YOK for the 100/2000 Ph.D. scholarship and TUBITAK for the 2214-A - International Research Fellowship Program for Ph.D. students (1059B142100007) and the 2211-C National Ph.D. Scholarship Program in the Priority Fields of Science and Technology (1649B032000188) for providing scholarship opportunities.

Ayhan BERGAL

CONTENTS

SYMBOLS AND ABBREVIATIONS

^{13}CNMR	: Carbon Nuclear Magnetic Resonance Spectroscopy
^{1}HNMR	: Proton Nuclear Magnetic Resonance Spectroscopy
A549	: Adenocarcinomic human alveolar basal epithelial cells
ALD-NS	: Aldehyde functionalized Nanosponge
ALD-NS+DOX	: Doxorubicin loaded Nanosponge complex
AMOX	: Amoxicillin trihydrate
CBNPs	: Carbohydrate-Based Natural Polymers
CDs	: Cyclodextrins
CHO or OD	: Aldehyde amounts or Oxidation Degree
DFC	: Diphenyl Carbonate
DL	: Drug Loading Capacity
DLS	: Dynamic Light Scattering
DMSO	: Dimethyl Sulfoxide
DOX or DOX.HCl	: Doxorubicin Hydrochloride
EE	: Entrapment Efficiency
EPR	: Enhanced Permeability and Retention
FDA	: Food and Drug Administration
FTIR	: Fourier Transform Infrared Spectroscopy
GDTDS	: Guided Drug Targeting and Delivery Systems
HAHCl	: Hydroxylamine Hydrochloride
IC_{50}	: The concentration that inhibited cell growth by 50 %
MIC	: Minimum Inhibition Concentration
$NaIO_4$	: Sodium Periodate
NaOAc	: Sodium Acetate Buffered Saline
NCDS	: Nano-Carrier based Delivery Systems
NCs	: Nanocarriers
NPs	: Nanoparticles
NSs	: Cyclodextrin Based Nanosponges
OX-β-CDs	: Oxidized Beta-Cyclodextrins
PBS	: Phosphate-Buffered Saline
PDI	: Polydispersity Index
PMDA	: Pyromellitic Dianhydride

PS	: Particle Size
SEM	: Scanning Electron Microscope
SIF	: Simulated Intestinal Fluid
TEA	: Triethylamine
TGA	: Thermogravimetric Analysis
TUBITAK	:Scientific and Technological Research Council of Türkiye
UV-Vis	: Ultraviolet Visible Spectroscopy
WST-8	:2-(2-methoxy-4-nitrophenyl)-3-(4-nitrophenyl)-5-(2,4-disulfophenyl)-2H tetrazolium, mono-sodium salt
XRD	: X-ray diffractometry
YOK	: Council of Higher Education
ZP(ζ)	: Zeta Potential
β-CD	: Beta-Cyclodextrin

FIGURES LEGENDS

TABLES LEGENDS

1. INTRODUCTION

Most drugs recently used in the treatments are not specifically targeted and may have weak biopharmaceutical properties limiting their use in clinical applications, including:

- Low water/ lipid solubility (delivering hydrophobic drugs is a major obstacle). About 70% of drugs are weakly soluble in water, which inhibits their clinical implementation) (Bhalani et al., 2022)
- Deterioration in gastrointestinal fluids
- Short in vitro stability (shelf life)
- Weak bioavailability
- Strong dose dependent side effects
- Lack of selectivity
- Low permeability
- Short blood circulation time which causes various toxic side effects
- High molecular weight and/or
- Quick excretion as well as other adverse side effects (Mitchell et al., 2021; Afzal et al., 2022).

Free drugs prone to be distributed evenly after application to the body, therefore, a tendency to apply high doses is required to achieve sufficient concentration of effect at the desired region. In order to accomplish the disadvantages of classical therapeutic applications, guided drug targeting and delivery systems (GDTDS), particularly nano-carrier-based delivery systems (NCDS), have been broadly investigated, developed and researched (Afzal et al., 2022; Sultana et al., 2022).

The primary purpose of NCDSs developed is to deliver and controlled release of therapeutic drugs to the targeted regions. It is significant that the nanocarriers (NCs) used for this purpose should have some important properties such as:

- **The reduced dosage** (Reduce the drug's toxicity issues and side effects) (Poon et al., 2020).

- **High drug loading capacity**
- **The surface modification of NCs** (Protecting drugs from undue degradation and extending their circulation in the blood and providing peculiar targeting) (Ahmad et al., 2022).
- **The larger surface-to-volume ratio** (NCs, which allow a broader contact region of the drug with the body under the same drug concentration situation, help to transport, bind and adsorb compounds such as drugs, proteins and probes.) (Ahmad et al., 2022; Joudeh and Linke, 2022).
- **Modifiable Flexibility** (Making them suitable for loading or encapsulating anti-cancer drugs to enhance their stability, solubility and in vivo behavior) (Joudeh and Linke, 2022; Yagublu et al., 2022).
- **Adjustable physio- chemical properties** (Depending on their application, NCs can be designed to be more functional by gaining certain physicochemical properties such as surface charge, size, geometry, hydrophilic or hydrophobic properties.) (Yagublu et al., 2022; Chandrakala et al., 2022).

NCs used for targeted delivery should be soluble in water, responsive under internal or external stimulation, biocompatible, safe as well as bioavailable. In addition, the toxicity regarding nanomaterials for drug delivery could be very low so that they utilized to target the particular diseased tissue in a safe concentration (Sharma et al., 2021; Patnaik et al., 2021).

The most important feature of NCs is to protect drugs from hydrolytic and enzymatic degradation in the gastrointestinal tract as well as Reticuloendothelial system (RES) to assist in bypassing the “first-pass” metabolism in the liver and spleen regardless of their morphology or composition. RES and systemic circulations are two of the major phases in NC delivery system. Thus, blood circulation time and clearance depend on interaction NCs with RES. Circulation of NCs coated with hydrophilic polymers such as polyethylene glycol generally remains for longer time (Kaushik et al., 2022). Hence, they are suitable for enhancing the blood circulation time and efficacy of drugs with short half-lives depending on their size and surface characteristics. Overall, accumulation of nanocarriers in specific targeted areas (such as tumors) depends on their circulation time, chemical characteristics and size. Thus,

they can be used to monitor drug as release formulation as well as for delivering DNA (Fam et al., 2020; Ulldemolins et al., 2021).

1.1. Nanocarriers Drug Delivery System

In order to design an effective NC system, the combinatorial effects of surface chemistry, shape, size, patient-specific information, and other parameters require comprehension (Bozzer et al., 2022). So, the ideal carrier as mentioned might be efficient, safe and have optimal bioavailability. In addition, non-immunogenicity, nontoxicity, stability as well as targeting ability to a specific site are especially significant. By following this approach, many nanoparticulate systems (Figure 1.1) such as nanosponges, metallic/bimetallic NPs (silver, gold), solid lipid nanoparticles, polymeric micelles, liposomes, dendrimers, microspheres, inorganic structures, nanotubes, nanocrystals, hydrogels, magnetic nanoparticles and microcapsules have been developed, designed and manufactured (Patnaik et al., 2021; Kaushik et al., 2022; Bozzer et al., 2022).

However, due to the drawback of NCs, developing an optimal drug delivery system to achieve the desired result is a difficult task. Some nanomaterials are inconvenient to apply as a drug delivery agent due to their degradation or toxicity effects in the body parts. Therefore, it requires ample time and detailed research to develop (Bergal and Andac, 2021). For instance, the disadvantage of solid lipid NPs is that they possess a crystalline structure that causes drug release due to unexpected polymeric degradation (Dhiman et al., 2021). Dendrimers, on the other hand, may display toxic properties due to the presence of peripheral amine carboxylate, phosphonate, sulfonate groups. In addition, the fact that they manifest non-specific drug delivery and sudden and uncontrolled drug release due to their open network (Chis et al., 2020). Liposomes also have disadvantages to possesses low content of drug loading, high cost, poor stability and undesired drug release. The toxicity and non-degradable property of some nanomaterials also limit their applications as drug carriers (Su and Kang, 2020; De et al., 2022).

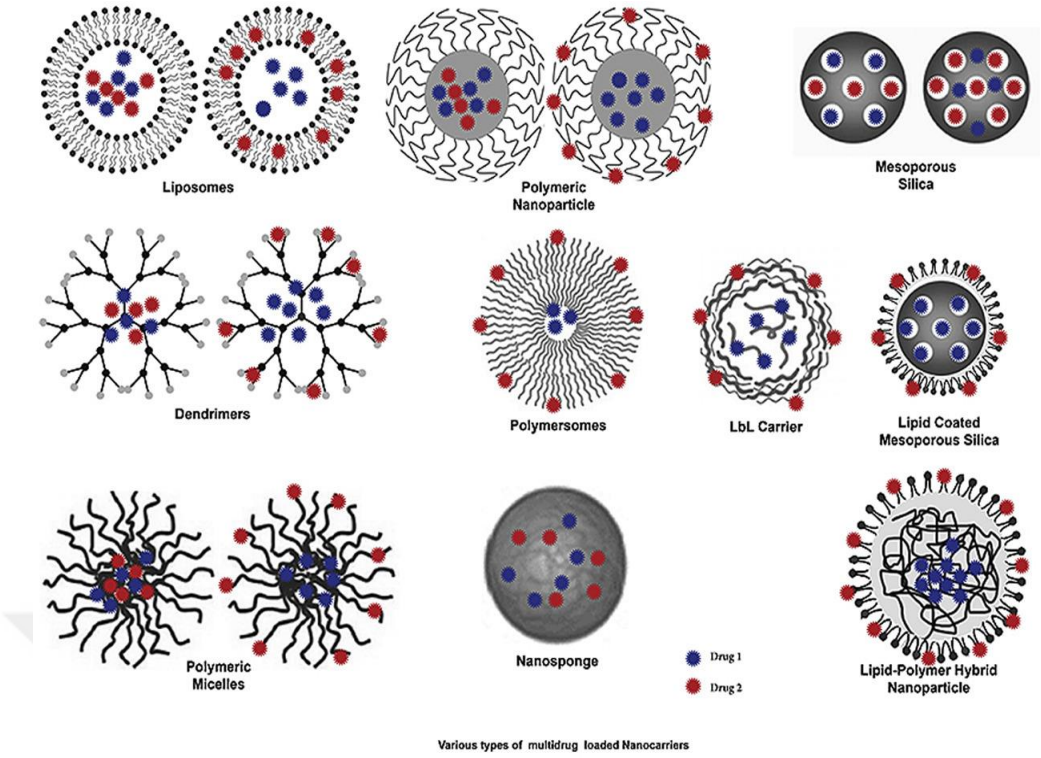

Figure 1.1. Various types of drugs loaded Nanocarriers (Reproduced with permission from Elsevier) (Pushpalatha et al., 2017)

1.1.1. Methods to Transport Drug-Loaded NCs

The primary function of the above mentioned nanocarriers is to deliver the therapeutic drugs to the targeted site. Due to their characteristic structure and properties, delivering of drug loaded NCs to the diseased site (e.g., tumor cells) can be achieved using three main mechanisms (Ding and Li, 2017; Su and Kang, 2020; Bozzer et al., 2022) which is shown in Figure 1.2.

- Passive targeting,
- Active targeting, and
- Physical targeting.

The targeting of NCs to the tumor site is due to the leaky vascular and the structural feature of the tumor tissue, called the enhanced permeability and retention (EPR) effect, as well as the weak excretory system (Subhan et al., 2021). Passive targeting as shown in Figure 1.2(a) leads to an increased EPR effect, which allows tumor cells to absorb preferably NC-sized bodies (Rahim et al., 2021). Although most tumor types have variations in pore size, they are reported to have much larger pores (approximately 380-780 nm) than healthy organs (Rahim et al., 2021). Therefore, the

size of the carrier is important for the tumoral vasculature permeability of EPR as well as for deposition at the tumoral site due to its effect on the vessel walls (Hoshyar et al., 2016).

The active targeting approach as illustrated in Figure 1.2(b) is the method of applying surface modifications of nanocarriers using specific ligands such as antibodies, sugars, folic acid, peptides, and the binding of liganded nanostructures to a specific cell receptor presented on tumor cells (Hoshyar et al., 2016; Din et al., 2017; Teixeira et al., 2023). Physical targeting as displayed in Figure 1.2(c) is a method for directing NCs to the target site and controlling the release process using external sources such as photothermal, light or magnetic field (Ding and Li, 2017; Fam et al., 2020; Bozzer et al., 2022).

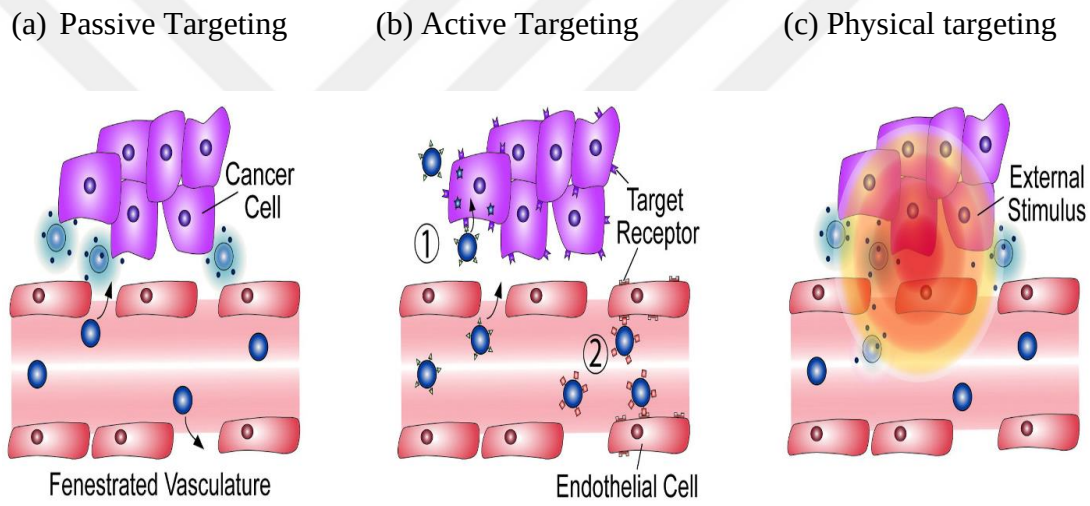

Figure 1.2. Schematic illustration of drug targeting strategies (Reproduced with permission from Elsevier) (Wicki et al., 2015)

1.1.2. Drug Release Mechanism

Nanostructures differ from conventional materials in that they exhibit rapid physicochemical properties in response to environmental stimuli. Once an ideal drug nanocarrier has been designed and the targeting method determined based on tumor structure and environmental influences, the release of a cancer drug at the selected target site can be triggered from the nanocarrier by an internal or external stimulatory response mechanism. Systems that respond to **internal stimuli** drug release such as:

- pH mediated (Wibowo et al., 2020)
- Enzyme responsive (Li et al., 2020)

- Ligant- Receptor stimulus (Liu et al., 2021)
- Temperature mediated (Khodaei et al., 2022)
- Redox Responsive (Abed et al., 2023)

are based on environmental differences between diseased and normal tissue.

On the other hand, the accumulation of drug loaded nanostructures in diseased tissues can be achieved through **external effects** such as;

- Light (UV, Infrared) (Zhao et al., 2019)
- Ultrasound (Moradi Kashkooli et al., 2023)
- Magnetic Field (Jiang et al., 2022)
- Electric Field (Kolosnjaj-Tabi et al., 2019)
- Voltage Excitations (Griffiths and MacLeod, 2003) or
- Other Chemicals (Broaders et al., 2011; Korin et al., 2012) and designed NCs may release the drug in the cell.

Among them, pH-sensitive systems are widely applied in tumor tissues, cell organelles or some organs to selectively release cancer drugs to avoid side effects and to achieve better efficacy. Nanomaterials sensitive to pH environment, especially to low acidic environment, have been accepted as the most promising systems for intracellular drug release and delivery applications, which are not affected by mildly acidic environmental regions (pH 4-5) such as endosomal / lysosomal.

NCs that are sensitive to physicochemical changes in response to pH changes such as charge conversion, hydrolysis, or swelling can often be used for pH-guided therapeutic drug release applications in locally lower pH regions such as tumor tissue (pH 5.7-7.8) in addition to infectious and inflammatory sites (pH 6.5) (He et al., 2013; Yan and Ding, 2020).

NCs such as dendrimers, liposomes, polymeric micelles, non-polymeric or solid lipid nanostructures and next-generation nano-delivery systems such as cyclodextrin, noisome, and nanospoges could target by passive diffusion and pH/temperature/light/magnetic field assisted drug release occur in cancer cells. In addition, NCs bound to ligands such as amino acid, protein, dopamine, hyaluronic acid and folic acid target cancer cells with ligand-receptor interaction and release drugs

with internal or external effects. Figure 1.3 demonstrates the various drug release mechanisms from multidrug loaded NCs.

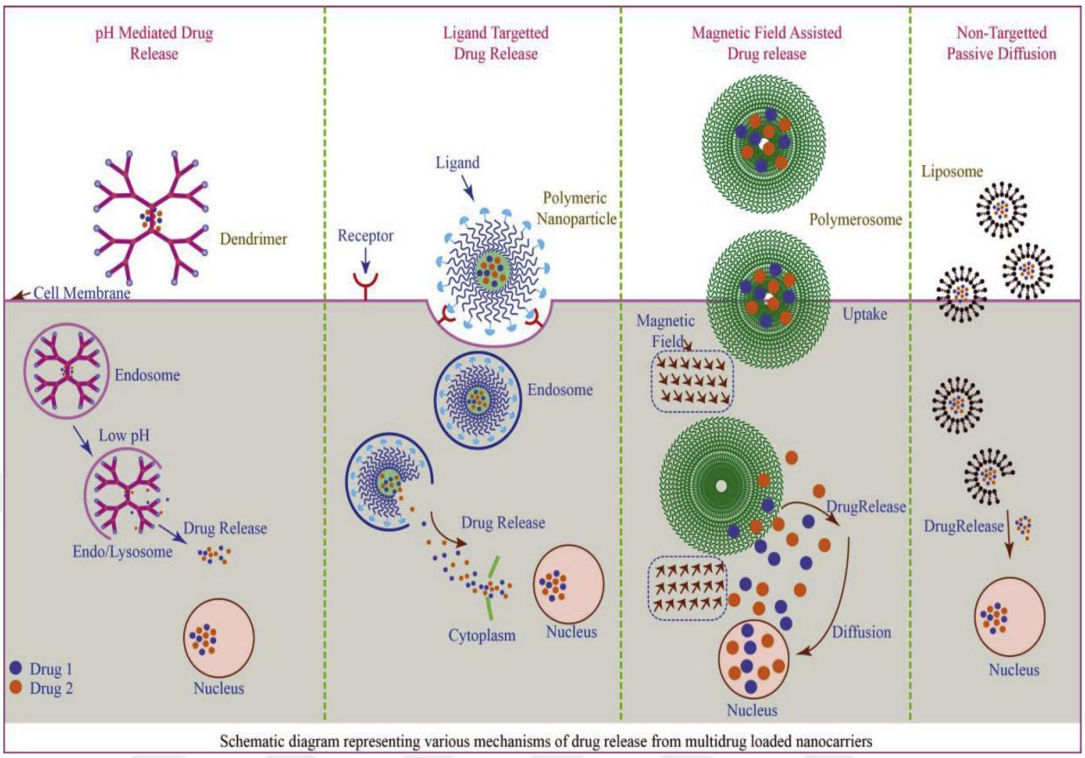

Figure 1.3. Various mechanism of drug release from multidrug loaded Nanocarriers (Reproduced with permission from Elsevier) (Pushpalatha et al., 2017)

1.2. Carbohydrate-Based Natural Polymers (CBNPs)

CBNPs such as monosaccharides, polysaccharides as well as oligosaccharides (cellulose, starch, chitosan, dextran, hyaluronic acid, sodium alginate, unilin, xanthan, or cyclodextrin) (Gim et al., 2019) are important naturally abundant macromolecular substances consisting of long chains of saccharide units linked by glycosidic bonds. The generations of materials from carbohydrate-based polymers for biomedical, pharmaceutical applications, and particularly for drug delivery systems have taken notable interest in recent years (Gim et al., 2019; Westin et al., 2020; Di et al., 2022; Kumar et al., 2022; Zhang et al., 2022). Due to their appealing features such as biocompatibility, availability, biodegradability, chemical reactivity, nontoxicity and tunable properties, those polymers have found several applications to the formation of NCs, nanogel, hydrogel in drug delivery (Zhang et al., 2022) and tissue engineering (Westin et al., 2020; Alibolandi et al., 2022). In addition, carbohydrate-based polymers could be functionalized to advance encapsulation, responsiveness, stability, and solubility due to physical and biological advantages which are fundamental

requirements for biomedical field (Khalid et al., 2021; Di et al., 2022). Therefore, carbohydrate-based polymers possess several qualities that make them advantageous, and they have been used increasingly in drug targeting, sustained drug release in drug delivery applications.

Chemical modifications using different appropriate methods such as oxidation, sulfonation, amidation, graft polymerization, esterification ensure a set of derivatives due to carboxyl hydroxyl, and amine groups on the main backbone of biomacromolecules (Kumar et al., 2022; Zhang et al., 2022). Therefore, structural changes alter the chemical, physical, and biological properties of saccharides to obtain their various derivatives and enable them to study their structure-activity relationships (Khalid et al., 2021; Kumar et al., 2022).

Among the above-mentioned saccharides, Cyclodextrins (CDs) appear as a new pharmaceutical approach with promising strategies for drug delivery systems, particularly through the assembly of CD-based delivery (Santos et al., 2021; Păduraru et al., 2022). CDs, which were discovered by Antoine Villiers in 1891, are truncated cone-shaped oligosaccharides composed of α-1,4-glucopyranose units with a hydrophobic inner cavity and a hydrophilic outer surface (Poulson et al., 2021). Among the three naturally occurring CDs (α-, β- and γ-CD), β-CD is broadly utilized in drug delivery due to their distinctive ability to form inclusion with both hydrophobic and hydrophilic drug molecules (Santos et al., 2021; Poulson et al., 2021). This appealing property is promising for a broad application such as gene delivery, drug delivery and biomedical applications (Zhang et al., 2020; Poulson et al., 2021). Since γ-CD has a relatively expensive production cost, α-CD has a small cavity and can only trap low molecular weight molecules, β-CD has become the most widely used CD in pharmaceutical research with low production cost and its convenient cavity (Zhang et al., 2020; Poulson et al., 2021).

They are usually used as carriers in pharmaceutical formulations such as nanosponges, hydrogels, nanoparticles, microspheres, liposomes, nanogels to encapsulate drugs to protect them or particularly to improve biopharmaceutical properties of drugs. Natural CDs exhibit low water solubility due to strong intermolecular hydrogen bonding, limiting their use for pharmaceutical purposes compared to their chemically modified counterparts. To resolve low solubility problems, researchers have developed multiple delivery systems based on CDs, which

have proved useful results (Liu et al., 2019).

1.3. Cyclodextrin-Based Nanosponge (CD-NS)

CD-NSs are one of the nanocarriers that researchers have recently studied and designed as a drug carrier agent in order to eliminate the disadvantages of conventional drugs and increase their effectiveness for the reasons explained in detail above. Therefore, before detailing this concept, it is useful to briefly describe one of the main components, Cyclodextrins.

1.3.1. Cyclodextrins (CDs)

1.3.1.1. Properties and Chemical Structure of CDs

CDs which consist of enzymatic decomposition of starch by *Bacillus amylobacter* bacteria (Jansook et al., 2018) and composed of the binding of D-glycosupranoses with α-1,4-glycosidic bonds (Fig. 1.4a-b) are one of the most basic oligosaccharides in nature. CDs are partly water soluble, biocompatible and have lipophilic cavity and hydrophilic outer surface. Since the 1970s, it has been used in the fields of biotechnology, food medicine, cosmetics, textiles and as catalyst as well as a drug delivery system in pharmaceutical industry, pharmacology, and nanotechnology (Osmani et al., 2018).

As shown in Figure 1.4b, they are named as α-CD, β-CD and γ-CD according to the number of glycosupranose units in their structure. For example, the structure consisting of 6, 7 and 8 glycosupranose units linked by glycosidic bonds is defined as α-CD, β-CD and γ-CD respectively. Despite the fact that higher units of CDs in their structures are found in nature, it is not preferred in terms of research due to the difficulty of obtaining and forming inclusion complex with very few substances.

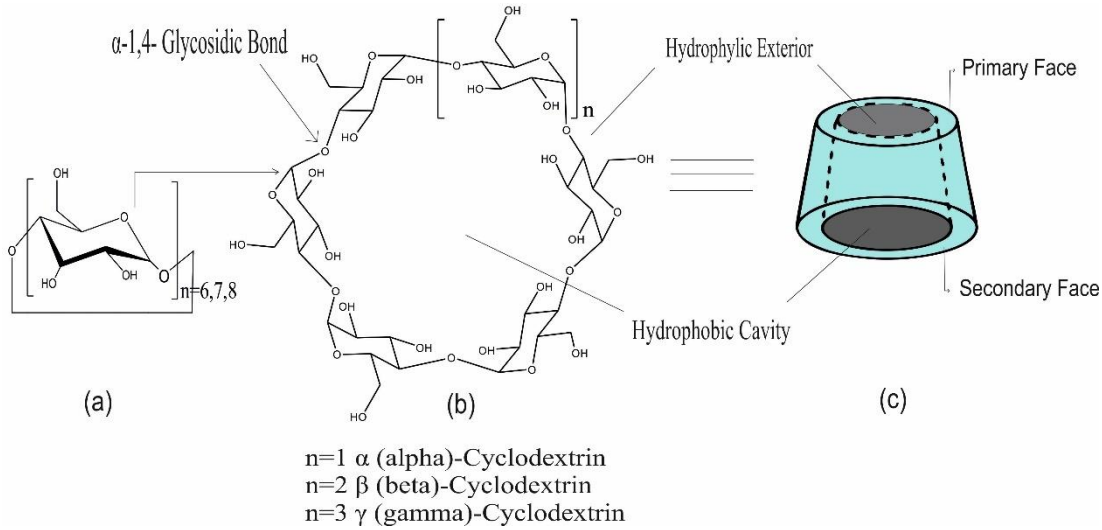

Figure 1.4. Schematic representations of CDs (a) the general chair conformation (b) two-dimensional chemical structure of α-, β- and γ-CD and (c) tridimensional structure

The CDs molecules are shaped into a truncated cone or funnel with two open ends due to the sequence of glycopyranose units with primary hydroxyl groups (OH) at one end and secondary hydroxyl groups (OH) at the other end (Figure 1.4b, c). In this funnel-shaped structure for β-CD, the primary 7 OH group is located at one end and the secondary 14 OH group is located at the other end.

Table 1.1. Physical properties of α-, β-and γ-cyclodextrin

Property	**Alpha α-Cyclodextrin**	**Beta β-cyclodextrin**	**Gamma γ-Cyclodextrin**
Glucose subunits Synonyms	Hexa Cyclo-hexaamylose	Hepta Cyclo-heptaamylose	Octa Cyclo-octaamylose
Number of Glucose units	6	7	8
Cavity diameter (Å)	4.5-5.3	6-6.5	7.5-8.3
External diameter (Å)	14.6	15.4	17.5
Water solubility at 25^0C (mg/ml)	14.5	1.85	23.2
Molecular weight (DA)	972	1135	1297

The physical properties of cyclodextrins are shown in Table1.1. Among these, β-CD has been preferred as the most studied structure due to its solubility in water, ability to complex with many organic and inorganic substances due to its suitable cavity, high drug loading capacity, easy availability, and affordability (Crini et al., 2018). It has been recognized by the FDA that β-CDs are safe for humans (Jansook et

al., 2018; Paiva-Santos et al., 2022). Normally, CDs are not toxic when administered orally because they are not absorbed by the gastrointestinal tract (Loftsson et al., 2005a).

Natural CDs do not form inclusion complexes with certain drugs that display hydrophilic property or possesses high molecular weight. In addition, some CDs limit in their use since they exhibit toxic properties when injected intravenously (Davis and Brewster, 2004; Loftsson et al., 2005b). Therefore, some chemical modification studies have been performed in order to use them as a drug carrier system to eliminate the disadvantages of CDs, and to improve their physical and chemical properties. One of these modifications is the formation of NSs by reacting natural CDs with the crosslinkers described below. In 1998, DeQuan Li and Min Ma were the first researchers (Trotta et al., 2012) to obtain and use cyclodextrin-based nanosponges by bonding β-CD with a cross-linker (such as diisocyanate) for the treatment and purify of wastewater (Li and Ma, 2000).

1.3.2. Nanosponges (NSs)

NSs are hyper-crosslinked cyclodextrins having nanoscale spongy pores and a three-dimensional network with non-toxic, stable in high temperature (Trotta et al., 2012; Swaminathan et al., 2016) materials which can be obtained by crosslinking α-, β- and γ-CDs with a certain quantity of crosslinking agents such as carbonyl-diimidazole, diphenyl carbonate, hexamethylene diisocyanate and pyromellitic anhydride (Figure 1.5). NSs are generally obtained from β-CD, because among natural α- and γ-CDs, β - CD has the highest complexity and stability due to the appropriate cavity size with cross-linkable polymers.

Compared with native CDs, NSs form higher interaction sites and drug encapsulation complexes with many molecules including drugs. Therefore, they can retain and preserve the hydrophobic and hydrophilic drugs in their cavity. NSs have being researched and developed as a promising nanocarrier system to prevent drug degradation, improve drug solubility, increase permeability and control drug release (Swaminathan et al., 2016). For this purpose, they have been investigated as nanocarriers on various insoluble or soluble drugs such as ibuprofen, captopril, telmisartan, meloxicam, camptothecin, tamoxifen, paclitaxel, quercetin, erlotinib, enalapril, acetylsalicylic acid, lansoprazole and nifedipine (Mognetti et al., 2012; Rao

et al., 2013; Swaminathan et al., 2016; Sherje et al., 2017).

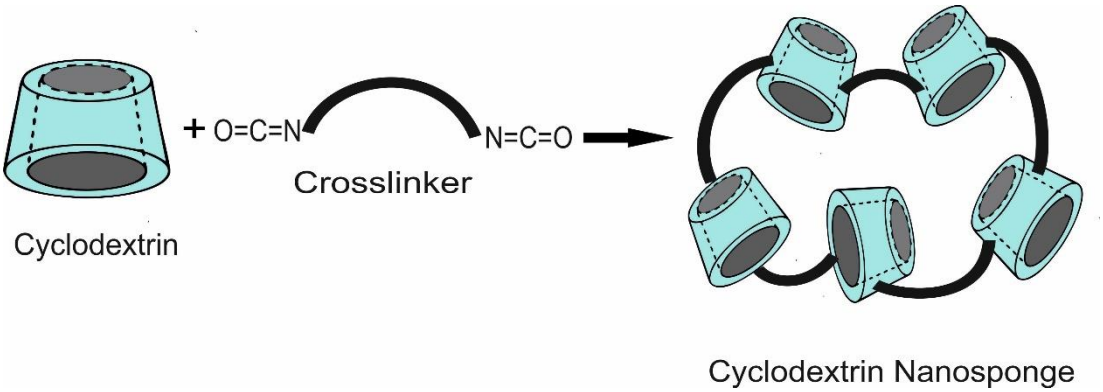

Figure 1.5. Formation of NSs by crosslinking cyclodextrins with one of the crosslinker material.

Although different types of crosslinkers are applied, NSs are synthesized by cross-linking polymer materials with four main categories such as carbonyl crosslinkers, diisocyanate linkers, anhydride crosslinkers and epichlorohydrin. A brief summary of the main crosslinkers used is summarized below in Figure 1.6.

The development of CD-based NSs by the reaction of natural CDs with crosslinkers and the application of NSs as a nano drug delivery system were demonstrated for the first time by Trotta (Trotta et al., 2012; Swaminathan et al., 2016) and his team. Studies by Trotta et al. revealed that new types of CD-based NSs have the potential to be utilized as drug carriers.

It has been shown in a study of injecting CD-NS into Swiss albino mice that NSs did not show any toxic properties. In that research, its acute systemic toxicity between 500 and 5000 mg/kg was demonstrated by the absence of any side effects or signs of toxicity (van de Manakker et al., 2009). In addition, it has been revealed that NSs do not display a significant adverse effect of cytotoxicity, both in oral administration studies on mice (Shende et al., 2015) and in in vitro studies using cell cultures such as HELA, MCF7, COS by applying the MTT test (Trotta et al., 2012).

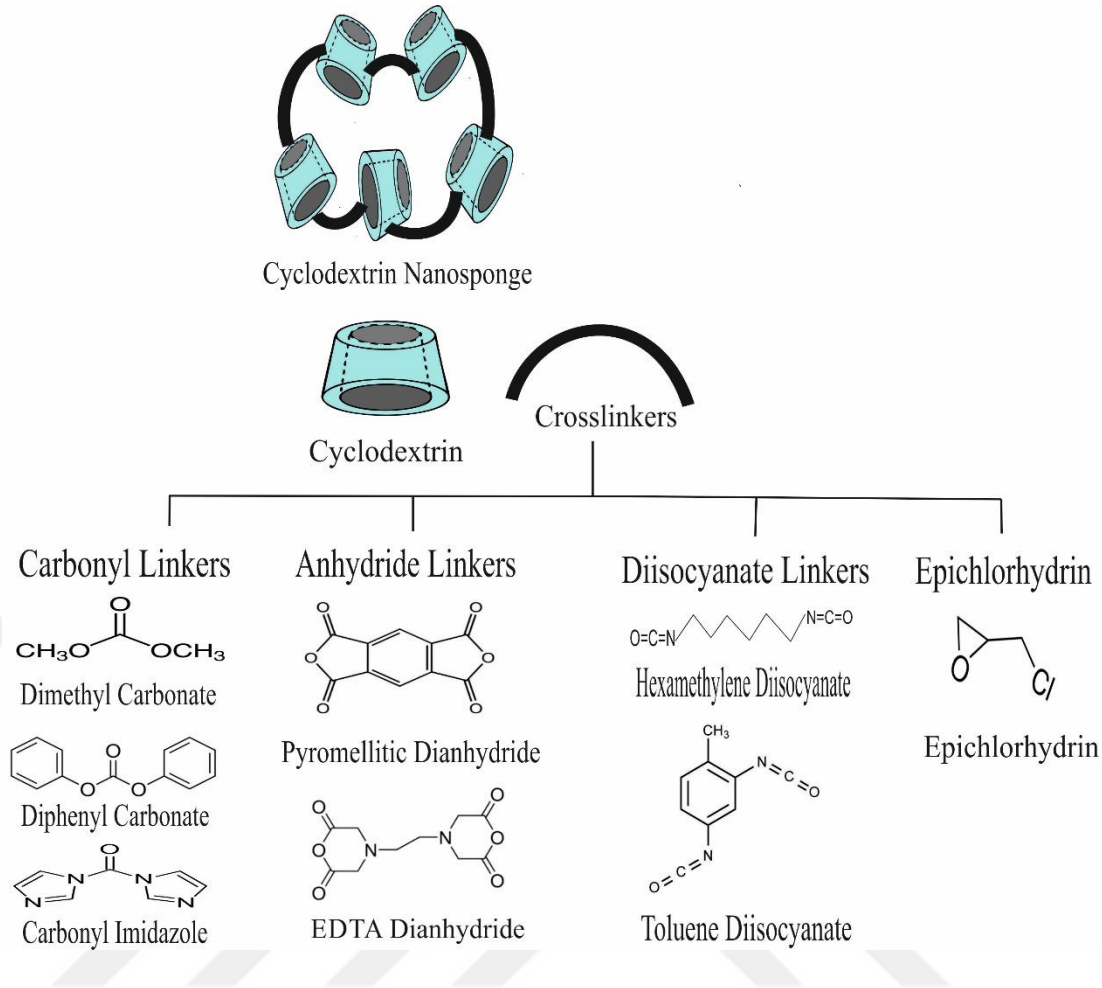

Figure 1.6. Cross-linking agetns consisting of four main categories used in the synthesis of NSs

CD-NSs form inclusion complexes with drugs of different properties which provide superior drug encapsulation and higher interaction sites compared to native CDs. Due to their biocompatibility, ability to form encapsulation complexes with various molecules and versatility, they could also be utilized as adjuncts in the preparation of tablets, capsules, solid dispersions, or topical dosage forms as nanotechnological multifunctional carriers (Dhakar et al., 2019). Therefore, NSs are being investigated in the pharmaceutical field as a promising drug delivery system to increase drug solubility, prevent drug degradation, increase permeability and bioavailability of lipophilic drugs and control drug release (Swaminathan et al., 2016). Swaminathan et al. (2007) aimed to increase the solubility of BCS II Class Itraconazole which is a low-bioavailable anti-cancer drug with limited solubility in water by integrating with NS using solid dispersion technique (Swaminathan et al., 2007). NS were obtained with crosslinked carbonate bonds of β –CD. As a result of this study, they showed that dissolution profile of the drug increased by more than 27-fold in the presence of two NS formulations compared to the plain drug. This ratio increased to

55-fold when copolyvidonum (PVP) was added as an auxiliary component in the NS formulation. As a result, the crosslinked NS formulation enhanced the bioavailability of itraconazole.

Another study investigating how the solubility of the drug Telmisartan (TEL) was affected by the encapsulation of NS obtained by using the solvent method (Rao et al., 2013). It has been demonstrated that the solubility of TEL increased from 9.9 µg/ml to 45.92 µg/ml due to complexation with NS (Rao et al., 2013). In the in vivo study of the same research, they emphasized that the Cmax value of NS-TEL increased from 141 ng/ml to 258 ng/ml compared to pure TEL, increasing the bioavailability.

Pushpalatha et al. (2018) investigated the anticancer activity and photoreactive effects of NS prepared by using two different crosslinkers with low water-soluble drug Curcumin (CUR) (Pushpalatha et al., 2018). For this purpose, various molar ratios of β-CD with DFC and PMDA were prepared by solvent method. Solubility, drug release, stability and cytotoxicity of NS were compared with pure drug as well as with respect to each other. Accordingly, the solubility of the pure drug increased by 63.98% with PMDA cross-linked drug-loaded NS (PMDA-CUR-NS) and 18.6% with DFC cross-linked drug-loaded NS (DFC-CUR-NS) proving that the solubility effect of NS prepared with PMDA linker was approximately 3.4 times higher than that of DFC linker. In addition, in vitro drug release from PMDA-CUR-NS increased 16-fold and 5-fold compared to pure CUR and DFC-CUR-NS, respectively. Moreover, the in vitro cytotoxicity study also showed decreased in IC_{50} value of PMDA-CUR-NS 2.2 times, and 1.5 times compared to pure drug and DFC-CUR-NS, respectively. As a result, they emphasized that PMDA-NS is a more potential nanocarrier compared to DFC-NS (Pushpalatha et al., 2018).

NSs can be used as a drug delivery agent to preserve the encapsulated drugs from light, physical and chemical degradation. For this aim, Anandam and Selvamuthukumar (2014) studied the protective effect of NSs on photodegradation of quercetin by conducting separate irradiation tests for pure and quercetin loaded NSs at the same concentration proving that pure quercetin degradation was faster than that of quercetin encapsulated NSs (Anandam and Selvamuthukumar, 2014a). In the same study, pure drug concentration displayed more than 50% reduction in simulated intestinal fluid (SIF) over 6 hours, but no fundamental reduction was observed with NS encapsulated formulations. Therefore, NSs could be utilized effectively to protect

drugs from the stomach. In addition, they pointed out that quercetins' DPPH radical scavenging activity increased 569-fold by NS complex with significantly increasing its antioxidant activity (Anandam and Selvamuthukumar, 2014a). Swaminathan et al. (2010) investigated the protection potential of NS (Swaminathan et al., 2010a). They demonstrated that the shelf life of camptothecin, an anticancer drug, by encapsulation into NSs extended and protected from deterioration (Swaminathan et al., 2010a; Swaminathan et al., 2016).

In another study (Minelli et al., 2012) also demonstrated how NS protects a drug called camptothecin (CPT), which inhibits the DNA topoisomerase enzyme and is used especially in the treatment of prostate cancer from deterioration and increases its in vitro anti-tumor activity. Minelli et al. (2012) emphasized that the inclusion of CPT in β-CD based NS facilitates the cellular uptake of the drug by showing intracellular drug content increase over time up to 6 hours from the treatment. This result confirmed the prevention of physiological deterioration that may occur in the intracellular environment by introduction of CPT into the NC system and facilitates the accumulation of the drug into the cells (Minelli et al., 2012).

NSs are also used as a cosmetic agent for the skin in the form of hydrogel as a topical drug release application. Such a study was conducted by Sharma and Pathak (2011) as an alternative carrier for targeting econazole nitrate (EN) to the skin using polymeric NSs with topical hydrogel formulations (Sharma and Pathak, 2011). The pharmaceutical properties and irritation studies of EN loaded NS hydrogels were tested on the mouse skin by selecting the best hydrogel that performs swelling, low stiffness, high viscosity, and controlled release for 12 hours. As a result, it was emphasized by the researchers that EN-loaded NSs may provide sustain drug release profile as well as benefits such as decrease in total dose and application frequency due to the reduction of dose-related systemic side effects (Sharma and Pathak, 2011).

On the usability of hydrogel NS in topical applications, Gangadharappa et al. (2017) investigated skin irritation and pharmacokinetic properties on mice by integrating lipophilic and low water-soluble celecoxib with the prepared hydrogel NS (Gangadharappa et al., 2017). They emphasized that the optimized formulation of NS-4 is non-irritating to mouse skin, so this dosage form can meet the requirements for human use and the obtained NS hydrogels can be used in topical drug applications (Gangadharappa et al., 2017).

In addition to the use of NSs as a drug delivery agent, NSs are applied in protein delivery (Swaminathan et al., 2010b), maintenance of catalytic efficiency, transmission and storage of gases such as oxygen and carbon dioxide (Cavalli et al., 2010), increase enzymes stability (Boscolo et al., 2010), as well as a carrier system for biomedical applications such as, peptides, antibodies and their derivatives. Moreover, it is used in cosmetics (Sapino et al., 2013) or in water purification purposes (Euvrard et al., 2016). In particular, the storage and transmission of gases is an important issue in diagnostic or therapeutic biomedical applications. The delivery of oxygen gas in the appropriate vehicle and dose in clinical treatments is sometimes complicated, and therefore the lack of oxygen supply can cause diseases ranging from inflammation to cancer. Cavalli et al. researched NSs structure for topical applications with regard to storage and slow release of oxygen gas over time (Cavalli et al., 2010). NSs can selectively absorb a measurable substance in an organism known biomarkers for the diagnosis purposes.

Such research conducted by Longo et al. (2011) also demonstrated that NSs can gather rare cancer markers from blood (Longo et al., 2011). NSs can be a very effective substance in environmental application for removing persistent organic pollutants from water such as chlorotoluenes, polychlorobiphenyls or chlorobenzenes and eliminating in water contaminated heavy metals such as lead, chromium, zinc, cadmium, etc. (Longo et al., 2011).

Unlike many other NCs, the reason for selecting this material is that it does not show toxic properties, it can carry both hydrophobic and hydrophilic drugs simultaneously due to its physical and chemical properties and can be modified to the desired size. In addition to all these, many advantages such as being easily obtained and synthesized, not being affected by the aqueous environment and not being dispersed, having a high loading capacity, and effect on the slow and sustain release of the drug can be counted. The EU commission report pointed out the use of NSs as a promising, innovative system for drug delivery (Trotta et al., 2012).

1.3.2.1. Method of Preparation of NSs

The most commonly known and applied NSs synthesis method can be briefly described as dissolving any selected type of CD in a suitable solvent followed by the addition of a desired type of crosslinker under continuous mixing or sonication by

adding a catalyst if necessary (Pawar et al., 2011; Ali M. Osmani et al., 2015; Sherje et al., 2017). In some cases, melt polymerization process if the crosslinking agent is in liquid form and dissolves CDs, increasing the temperature to initiate the crosslinking process may also be applicable (Ali M. Osmani et al., 2015).

Different synthesis methods such as melting (Jain et al., 2020), solvent method (Bano et al., 2019), ultrasound assisted synthesis (Trotta et al., 2007) microwave assisted synthesis (Anandam and Selvamuthukumar, 2014b) can be used to obtain NSs with various sizes and properties. For example, NSs with spherical morphology with high solubility can be obtained for molecules that are poorly soluble in water with the solvent method, while NSs with a submicron dimensional spherical structure can be synthesized by ultrasound assisted synthesis (Trotta et al., 2007).

1.4. Modification of Carbohydrates (Polysaccharides or Oligosaccharides)

Although different types of CD-based NPs are prepared and used in drug delivery applications, the exact definition of the structure-function mechanism has not been established yet (Liu et al., 2019). Better understanding of the mechanism and relationships between drugs and chemically modified β-CD oligosaccharides, a new generation drug delivery vehicle was created for the drug delivery purposes by modifying β-CD so that new type NS nanocarrier can be obtained and used as a more effective drug delivery vehicle for the drugs which contain NH_2 groups as demonstrated in this study.

Modification procedures are employed to develop and improve the properties of carbohydrates (polysaccharides or oligosaccharides). Chemical modification methods such as excessive sulfation (Gunasekaran et al., 2021), phosphorylation (Liu et al., 2019) and oxidation applied to alter the properties of saccharides and common synthesis methods used by researchers. Some of hydroxyl groups in the saccharides are oxidized to form carboxyl or aldehyde depending on oxidants used so that performances and characteristics of oxidized carbohydrates are significantly improved.

Hydroxyl groups provide active sites for chemical modification and these properties give CDs remarkable prospective for functionalization. Hence, they are used in particular applications such as antimicrobial agents (Yamamura et al., 2014),

smart carriers and targeted drug delivery systems (Tian et al., 2020). Substitution of that hydroxyl group can improve their solubility. This way, several non-crystallizable or amorphous β-CD derivatives have been developed via well-known chemical modifications. Modifications by using different suitable methods involve based on the breaking of intramolecular hydrogen bond of β-CD hydroxyl groups and the resulting substitution of the desired functional moieties (Yamamura, 2017). Several chemically modified derivates (e.g., 2- hydroxypropyl-β-CD or methylated -β-CD or others) have been obtained for pharmaceutical applications to demonstrate advanced capacities, such as complexation efficiency, diminishment of toxic drug side effects and release accuracy, then unmodified CDs (Liu et al., 2019; Matencio et al., 2020).

1.4.1. Periodate Oxidation of Polysaccharides or Oligosaccharides

Periodate oxidative cleavage was discovered by Malaprade who observed that polyols are rapidly oxidized by periodate ion and since then, the method has found many implementations in synthesis and as an analytical means in carbohydrate chemistry (Perlin, 2006). Chemical modification of saccharides by periodate oxidation which is a straightforward and most commonly used method have a variety of attractive practices in tissue engineering (Chen et al., 2017), drug delivery (Ijaz et al., 2017), flocculating agents (Sirviö et al., 2011), electron transfer mediator (Zheng et al., 2008) and food packaging application (Dou et al., 2015).

Periodate oxidation of polysaccharides or oligosaccharides produces "dialdehyde groups in polymers" to give aldehyde functionality to obtain newly modified materials by cleaving the C-C bond of adjacent diols in the structure of polymer molecules such as cellulose (Strätz et al., 2019), sodium alginate (SA) (Chen et al., 2020), starch (Ziegler-Borowska et al., 2018), dextran (Nonsuwan et al., 2019), carboxymethyl chitosan (CMC) (Zhang et al., 2020), Inulin (Afinjuomo et al., 2020), Hyaluronic acid (HA) (Pandit et al., 2019), xanthan gum (Guo et al., 2014), xylan (Amer et al., 2016) or CDs (Lou et al., 2020a).

Several research studies such as oxidized β cyclodextrin (Ye et al., 2017), aldehyde dextran (Chan et al., 2015), dialdehyde cellulose (Zhang et al., 2017), oxidized amylose (Zi et al., 2018) and oxidized κ-carrageenan (Zhu et al., 2017) conducted and outlined earlier that those oxidized saccharides had prominent antibacterial activity on several food related bacteria. Dineen was the first to

demonstrate that oxidized cellulose had antibacterial activity against variety of bacteria due to pH effect of carboxyl groups (Spangler et al., 2003).

Intramolecular hydrogen bonds of crude β-CD prevent and reduce its solubility in water, and the cavity size can encapsulate molecules of a certain size and molecular weight, which prevents the use of pure β-CD for different purposes. Chemical modifications of β-CD are made in order to eliminate the above-mentioned disadvantages and increase its properties. Modifications of the hydroxyl groups of β-CD are based on the formation of novel functional groups in the chain of the polymer, conversion to a flexible structure, increasing its solubility in water, and this feature allows it to be easily modified chemically and used in desired areas and purposes.

Oxidation of β-CD is a catalysis-free aqueous reaction and could be obtained using varied oxidants such as sodium periodate ($NaIO_4$) (Lou et al., 2020), hydrogen peroxide (H_2O_2) (Ye et al., 2017), 2, 2, 6, 6- tetramethylpiperidine-1-oxyl (TEMPO) (Isogai et al., 2011; Coseri, 2017) and nitrogen oxides (Duan and Kasper, 2011). In $NaIO_4$ oxidation, stabilizer and catalyst are not required for the reaction, and oxidation can be carried out at room temperature as well as the product which has high aldehyde content could be obtained. There are several disadvantages to using other oxidation processes. For example, oxidations processes using TEMPO or hydrogen peroxide are difficult to control and as a result of the breaks in and/or between the glucose units, the carboxyl group is formed as a by-product with excessive oxidation of the aldehyde group.

Periodate oxidation of β-CD is a highly specific reaction to introduce aldehyde groups at the C-2, C-3- *vicinal di-hydroxyl (glycol)* position of D-glucose molecule without significant side products. Thus, two aldehyde groups are formed in the structure by opening the hydroxyl at the C2-C3 bond of each repeating unit in the macromolecule. Addition of aldehyde groups improves the performance of oxidized saccharides such as showing higher solubility, more importantly, performing good antibacterial activity as an antibacterial agent (Ye et al., 2017; Ouyang et al., 2022).

1.5. Purpose of the Thesis

Doxorubicin Hydrochloride (DOX.HCl or DOX) is one of the most efficacious hydrophilic anticancer drugs used in several different types of cancer such as ovarian, soft tissue sarcoma, lung, stomach, leukemia, and especially in the treatment of breast

cancer.

A high drug concentration is needed for a drug substance to have a minimum effect on cancer cells. However, high drug doses can cause cytotoxicity in normal cells. For example, DOX.HCl has serious adverse effects such as kidney and cardiac toxicity, which limit its use and effectiveness (Argenziano et al., 2020). DOX may also show adverse effects such as poisoning of topoisomerase II cleavage complexes (antiproliferative effect), and serious cytotoxic side effects that limit the dose effectiveness including palmar plantar erythrodysynthesis, myelosuppression, and cardiotoxicity (Argenziano et al., 2020). Furthermore, cancer cells often become resistant to DOX therapy, and some conditions of the tumor microenvironment, such as lymphatic vessels, acidity, hypoxia and defective vasculature limit DOX anticancer efficacy (Argenziano et al., 2020).

One of the effective attempts to resolve these issues is the development and improvement of tumor targeted NCs system for delivery of DOX anticancer drug for reducing its doses and side effects as well as promote the accumulation of the drug at the tumor regions. So that drug delivery systems could enhance the delivery of anticancer drug and to alter its biodistribution to support its concentration.

Although several carrier systems have been developed for DOX, only PEGylated Liposomal Doxorubicin (Doxil®) was ratified by the FDA in 1995 for the treatment of Kaposi's sarcoma (Barenholz, 2012). However, while Doxil® reduces cardiotoxicity in breast cancer treatment or “decrease uptake by the mononuclear phagocyte system in the spleen and liver” (Aldughaim et al., 2020) and increases the circulation time, Doxil® displays some disadvantages such as high production cost, low volume of distribution, early release of the drug. In addition, most of it being trapped without leakage and most importantly, it may cause the hand-foot syndrome that “results in accumulation of liposomes in capillaries below the skin due to increased circulation times” (Aldughaim et al., 2020).

To our knowledge, there have been no reports of a drug delivery platform based on oxidized β-CD, specifically functionalized by $NaIO_4$ to fabricate pH-sensitive nano drug delivery systems.

The objective of this study is to fabricate and investigate in detail the usability of aldehyde functionalized Nanosponge (ALD-NS) as a pH sensitive drug delivery

agent and to investigate its effects on DOX.HCl. In order for the synthesized nanostructure to be a pH sensitive carrier, a pH sensitive binding was ensured in the interaction between the model drug and the nano drug carrier system.

For this aim, first, functionalized β-CD with aldehyde (CHO) groups were fabricated to enhance its physical, chemical properties as well as to determine its biological activities (such as antibacterial) at this state and crosslinked with PMDA crosslinker to have functionalized, water-soluble, solid, 3-dimensional more complexed pH sensitive ALD-NS with the method developed.

DOX was chosen as the model drug due to the presence of NH_2 group in its molecular structure and easy availability to create pH sensitive Schiff base bound among drug and nanostructure (Ibrahim et al., 2022). Integration of the model drug into the nanostructure is aimed to ensure both the Schiff base (C=N) bond and hydrophilic part of the ALD-NS nanostructure. In vitro drug release study was performed by creating acidic buffer conditions due to the easy hydrolysis of Schiff base in acidic medium and crosslinker (PMDA). Such NCs fabricated by chemical process are described in the experimental section and possible drug loading mechanism explained schematically in Figure 2.5 below. The current thesis informs a novel kind of functionalized NS (ALD-NS) that is capable of effective drug loading and delivery.

1.6. Question and Hypothesis of the Research

It is necessary to develop natural and new drug carrier systems in order to reduce the toxic properties of DOX alone, which is widely used in cancer treatment, and to release it in a controlled manner. In addition, there is still a need for increasing the drug loading capacity of nanocarriers, ensuring pH-controlled release of the drug in cancerous tissue, and in vitro and in vivo studies.

The most important feature of the prepared thesis that distinguishes is the synthesis of a new type of functionalized NS using modified β-CD with PMDA crosslinker, integration of the DOX drug by binding to the three-dimensional part of nanocarrier, as well as loading it to the functionalized NS by the Schiff base reaction, thereby increasing the drug loading capacity. Along with that, to investigate in vitro drug release mechanism, in vitro cellular DOX uptake and release in A549 cell culture based on low pH effect as well as cytotoxicity studies of DOX loaded Nanosponge

complex (ALD-NS+DOX). Such studies on this approach have not been encountered so far in literature revealing the originality of this thesis.

Based on this approach, a hypothesis can be formed by asking the following question:

If β-CD is functionalized by periodate ($NaIO_4$) oxidation method (if aldehyde (CHO) group is added), will there be a change in the characteristic feature of β-CD? For example, does its solubility in water increase in this state? According to the literature, it is stated that some carbohydrates with aldehyde group exhibit antibacterial properties, could functionalized β-CD with added aldehyde group display antibacterial properties at this state as well? Can functionalized β-CD react with the crosslinkers and transform it into a new more complex and functional structure? If this new nanostructure can be used as a drug delivery agent, what kind of integration can be established with DOX? Could Schiff base (C=N) bonding (the bond that will occur between the CHO group of the nanostructure and the NH_2 group of the drug) be formed with a drug containing NH_2 group with the ALD-NS nanostructure that obtained by binding to the functionalized β-CD with a crosslinker. Besides, can the drug loading capacity be increased if the drug binds to the hydrophilic or lipophilic structure of the ALD-NS nanostructure and can perform multiple loading? In addition to this question, since the drug-loaded nanostructure will exhibit pH-sensitive degradation (both Schiff base bond and cross-links degradation are predicted), what will be the "in vitro drug release rate and mechanism" of the structure in physiological buffer pH environments (slow release, fast or constant sustained release depending on time or whether more drug release will occur in acidic environment or in alkaline environment). How will the in vitro cellular uptake or entry of the obtained drug-loaded nanostructure in the cancer cell line change and what will be its in vitro cytotoxicity. Finally, which mathematical models will explain the drug release mechanism and kinetics and which model will best fit the drug release mechanism.

In terms of the scientific novelty and originality of the subject, the hypotheses to be developed in answering the questions asked above can be given as follows:

a) **The β- form of cyclodextrins (β-CD), which is a natural monosaccharide mentioned in detail above was used as the main core material of**

fabricating the pH sensitive nanocarrier.

Among natural CDs, β-CD, formed by the binding of 7 glucopyranose units, can be used as an excellent drug delivery agent because of its ability to both encapsulate the drug in its hydrophobic cavity and integrate it into its hydrophilic outer surface due to its appropriate cavity size, high complexing ability and stability. In addition, cavity dimensions and low production cost are some of the main advantages of β-CD (Jansook et al., 2018; Zhang et al., 2020; Poulson et al., 2021). In addition, it is used as a primary material in the synthesis of multi-molecular structures such as NSs and Nanocapsules.

Chemical modification of β-CD was made in order to eliminate the above-mentioned disadvantages and increase its physical and chemical properties. Modifications of the hydroxyl groups of β-CD are based on the formation of new functional groups in the structure of the polymer, conversion to a flexible structure, increasing its solubility in water. This feature allows it to be easily modified chemically and performed as a convenient drug delivery system.

In this context, functionalized β-CD was obtained with chemical modification by using different molar amounts of $NaIO_4$ by applying the periodate oxidation method, which is a fast, practical and safe application in order to answer the question of how the degree of oxidation would affect the morphological and structural integrity of β-CD and the most importantly which chemical modification is required for β-CD to have a certain characteristic. In this thesis, periodate method was preferred due to the fact that the oxidation does not require a catalyst, the reaction takes place at room temperature, and most importantly, high aldehyde content is obtained. Periodate oxidation of β-CD produces “dialdehyde groups in polymers” to give aldehyde functionality to obtain newly modified materials by cleaving the C-C bond of adjacent diols in the structure of polymer molecules. Therefore, a detailed synthesis and characterization research was carried out in order to investigate characteristic property of oxidized β-CDs and in addition, whether the influences of aldehyde groups on the antibacterial activity of OX-β-CDs.

The OX-β-CDs were prepared through sodium periodate at certain molar ratios and the properties and structure of OX-β-CDs were examined by XRD, FTIR, proton ^{1}HNMR and SEM technique. The FTIR and ^{1}H-NMR studies were analyzed to

determine whether the aldehyde group was added to the synthesized structures, and the SEM and XRD images were analyzed to determine whether the increasing degree of oxidation showed a morphological or structural change in OX-β-CDs. Moreover, the aldehyde content of OX-β-CDs was determined depending on the increasing $NaIO_4$ molar ratio using theoretical and experimental data.

In addition to determining its antibacterial properties, it sheds light on the development of this structure for different purposes as a more efficient, more functional water-soluble structure.

b) **Modified (aldehyde group added) β-CD (OX-β-CDs) will be transformed into a three-dimensional more functional nanostructure (ALD-NS) with using pyromellitic dianhydride (PMDA) crosslinker by the synthesis method developed.**

Native CDs cannot form inclusion complexes with high molecular weight drugs or certain hydrophilic molecules. On the other hand, β-CD shows low water solubility (1.85% w/v at 25°C) and demonstrated renal toxicity when injected intravenously (N.d. from Europa.eu website, 2023). Apart from this, and most importantly, the drug loading capacity is low in its pure form, and as a result, it shows insufficient drug release profile. Therefore, chemical modifications of CDs have been carried out in order to overcome their disadvantages and enhance their physicochemical and technological properties to apply them as a nanotechnological drug delivery system.

In the ALD-NS synthesis method, only deionized water was used as a solvent. Because adding (modifying) an aldehyde group on β-CD will ensure complete dissolution of the structure in water. The use of water as a solvent will allow the use of the freeze dryer method to obtain a purer water-soluble substance. The synthesis method, which is not demonstrated in the literature, is also important because of the difference in the nature of the subject and its methodologically original contributions.

In the literature, only different sponge types (sponges' structures) which do not contain any functional groups were obtained with the above-mentioned NS synthesis methods by using DMSO, DMF, DCM as solvents and by using different crosslinkers. In addition, it has only been widely studied in the pharmaceutical field as a method of forming inclusion complex capability of NSs with various molecules to increase aqueous solubility and hence the bioavailability of lipophilic drugs (Swaminathan et

al., 2010a; Selvamuthukumar et al., 2012; Swaminathan et al., 2016; Moreira et al., 2016; Cinà et al., 2017).

For instance, Shende et al. (2015) investigated the effect of meloxicam on solubility, stability and prolong release with complexes containing β-CD and NS (Shende et al., 2015). For this purpose, meloxicam drug was incapsulated on NS obtained by using PMDA crosslinker. They showed that the solubility of meloxicam in aqueous medium increased from 9.45 ug/ml to 19.07 ug/ml by integration with β-CD alone and increased to 36.61 ug / ml by integration with NS. Thus, NS carrier increased the solubility of the drug compared to β-CD alone. In addition, they showed that the drug was released from NS in a controlled manner for 24 hours (release of pure drug during the first 2 hours was 45.23%, release in the formulation was 73.09% for 24 hours) and controlled release reduced the toxic side effect of the drug. They emphasized that drug loaded NS increased anti-inflammatory and analgesic activity compared to pure meloxicam (Shende et al., 2015).

Therefore, it can be considered as a new approach with the feature of investigating the effects of functionalized NS with different properties on certain drugs.

c) **Integration of DOX.HCl cancer drug on ALD-NS nanocarrier with the reflux method based on both the Schiff base bond formation and the hydrophilic part of the ALD-NS.**

Formation of acid-sensitive bonds with Schiff base reaction has been the most preferred and promising approach due to their biodegradability by hydrolysis and their decreased stability as the environmental pH decreases (Su et al., 2016; Jalalvandi et al., 2017; Zhao et al., 2017). The reason for forming a Schiff base bond (C=N) is both creating a pH-sensitive hydrolysis profile and increasing the integration of the DOX drug into the nanostructure with this bond and the hydrolysis of Schiff base bond under acidic conditions. Therefore, the release of conjugated DOX via Schiff base linkages will be pH dependent**.**

Schiff bases are structures with the general formula $R_1R_2C=N-R_3$, which are obtained from the nucleophilic addition reaction of aldehydes or ketones with amines. Here R_3 can be an alkyl or aryl group, which makes the Schiff base a stable imine. Schiff base chemistry also plays a fundamental role in biological systems as a result

of high yield and harmless by-product (water only), which can also be characterized by biological activity, and is used in biomedical applications (Meyer et al., 2007; Xin and Yuan, 2012). β-CD is easily modified by periodate's oxidation and turns into an aldehyde-β-CD structure with many aldehydes' groups (-CHO) in its molecular chain, and this transformation is made ready for Schiff base formation during the polymer-drug integration preparation.

In this thesis, DOX.HCl was selected as model drug (because it contains both NH_2 group and is a cancer drug). In addition to demonstrating the scientific novelty of the subject in terms of its synthesis method and nanostructure containing functional groups, the cancer drug DOX.HCl was integrated into ALD-NS by reflux synthesis method both by creating a Schiff base bond and conjugating to the hydrophilic part of ALD-NS (so that increasing the drug loading capacity). So, this thesis is again having the feature of being a first in terms of the subject of drug integration. Therefore, this thesis exhibits scientific quality and innovation, especially in terms of eliminating the existing deficiency in this direction.

d) Examination of the release behavior of the DOX cancer drug from the synthesized ALD-NS+DOX complex by the dialysis membrane (cut-off=12-14 kDa) method under neutral (0.1 M PBS at pH 7.4) and acidic conditions ((0.1 M PBS at pH 5.2 and 0.1 M NaOAc buffer solution at pH 5.2)) that mimic the physiological and endo-lysosomal environment.

The expected and designed mechanism is that the release behaviors of DOX loaded nanostructure could be higher (in % amount) in an acidic environment (at pH 5.2) and could display controlled sustain drug release profile. Some studies in literature also confirm that the drug release is high in the low pH environment. For example, Su et al. (2018) developed dextran-based nanogel containing covalently combined DOX with Schiff base linkage using inverse microemulsion technique (Su et al., 2018). In vitro drug release studies showed DOX under acidic conditions (pH 2.0, 5.0) has been shown to be released much faster than at pH 7.4. Approximately 66.28% and 9% of the drug released were observed within 72 h at pH 2.0 and 7.4 respectively. DOX-loaded dextran nanogel was taken up into the cell (MCF-7) by endocytosis and dispersed into the endocytic compartments inside the tumor cells (Su et al., 2018).

Xiong et al. (2015) synthesized β-CD-modified polyaldehyde dextran (PAD-

CD) between amino β-CD and polyaldehyde dextran through the Schiff base formation to obtain injectable DOX-loaded hydrogel (Xiong et al., 2015) and they investigated in vitro release behavior of DOX from DOX-loaded hydrogels at pH 5.8, 6.8 and 7.4. They concluded that DOX was released much faster under acidic conditions (pH 6.8 and 5.8) than that of physiological (pH 7.4) condition (Xiong et al., 2015).

Jia et al. (2017) reported pH-sensitive drug release of the anticancer drug DOX in copolymer micelles with CD cores (Jia et al., 2017). In this study, DOX was covalently bonded with the benzaldehyde groups of the polymer via a pH sensitive Schiff-base bond. Covalently bound DOX resulted in greater drug loading compared to unimolecular micelle β-CD-poly (lactic acid)-b-poly [(oligo ethylene glycol) methyl ether methacrylates]. In vitro release studies have shown a more controlled release of DOX compared to encapsulated DOX, emphasizing increased tumor-targeting release of the drug due to the Schiff-base bond. The results showed that the Schiff base-containing nanogel can function as a pH-sensitive drug delivery system (Jia et al., 2017).

e) Investigation of cytotoxicity and cellular uptakes of synthesized ALD-NS+DOX complex in cancer cell culture

When drug carriers sensitive to pH-triggered stimuli attain tumor tissues, enzymes in tumor cells or the weak acidic environment on the surface of cancer cells cause drug carriers to collapse and drugs to be released. Thus, drug-targeted release can be obtained with this method. In this thesis, the cytotoxicity and cellular uptake of the ALD-NS+DOX complex in the A549 cell line were investigated. It was aimed that the cytotoxicity of the drug loaded structure would be lower and its cell uptake would be higher than that of free DOX. In addition, the nano drug carrier alone is expected to show very low or no cytotoxicity.

Such a study was conducted to investigate cellular interaction and protein binding ability of NS (Singh et al., 2018). For this aim, NS was synthesized using β-CD with DMC crosslinker and its surface was biofunctionalized with cholesterol hydrogen succinate (CHS). Singh et al. (2018) reported in their study using doxorubicin as a model drug that cellular binding activity and cellular uptake increased by the surface interaction between CHS and the model drug. They emphasized preferable internalization in cells due to the interaction among cell membrane and

CHS. In the study, the in vitro cytotoxicity of modified β-CD-NS was examined, and the obtained data demonstrated that the surface modified structure did not display substantial toxicity in HeLa cells and samples were biologically friendly (Singh et al., 2018).

1.7. The objectives of the thesis are presented below in articles;

- Synthesis of OX-β-CDs with various aldehyde content by adjusting the molar ratio between pure β-CD and sodium periodate ($NaIO_4$), gaining functional properties, performing all structural and morphological characterizations of the structure (determining the optimum molar ratio, determining the aldehyde group formation with different analysis techniques, determination of aldehyde content). In addition, it has been seen in the literature that OX-β-CDs have antibacterial properties due to their aldehyde functional group. Depending on the synthesis method and various molar ratios, it has been investigated whether the structure to be synthesized exhibit antibacterial properties in this stage.

- Synthesis of more functional pH sensitive drug carrier (ALD-NS nanocarrier) by using OX-β-CDs and PMDA crosslinker in various molar ratios (1:2 1:4 1:6 OX-β-CDs:PMDA) and performing all characterization techniques (Determining the optimum molar ratio between OX-β-CDs:PMDA according to drug loading capacity, determination of ALD-NS nanocarrier formation and the presence of aldehyde group on the nanostructure). The freeze-drying synthesis method has been applied for the first time in this thesis. Obtaining ALD-NS using this technique has not been found in the literature.

- Establishing the integration of ALD-NS with the DOX.HCl cancer drug by applying the Reflux method and increasing the drug loading capacity of the anti-cancer drug into the ALD-NS nanocarrier by both binding drug with Schiff base bond and the hydrophilic outer surface of the ALD-NS nanocarrier. Then, integration was verified by applying all characterization techniques. The reason for the application of this method is the creation of Schiff base bonding between the aldehyde group on ALD-NS with the NH_2 group of the DOX.HCl drug, which is sensitive to the acidic environment. Drug integration in this method is not available in the literature, and it is one of the most important goals that was conducted for the first time in this thesis.

- Adjusting the weight ratio between DOX.HCl and ALD-NS to be 1:10

(DOX: ALD-NS). Integration of drug into nanocarrier by a mechanism based on Schiff base reaction to increase drug loading capacity or amount of drug content with bidirectional mechanism (the drug both binds to the functional group of ALD-NS and integrates into the three-dimensional space of ALD-NS).

- Investigation of in vitro drug release from ALD-NS+DOX complex in body temperature environment (37 ^{0}C) in 3 different buffer solutions (under neutral and acidic conditions) mimicking physiological and endo-lysosomal environment by comparing with free DOX.HCl using dialysis membrane (cut-off=12-14 kDa). Due to the acidic nature of the cancer cell culture, the drug release in acidic buffers was performed (the drug will form a pH-sensitive degradation profile as a result of both the hydrolysis of the Schiff base bond under acidic conditions and the pH-sensitive crosslinker being used). Thus, the release of the drug is provided to increase the amount and effectiveness of the anti-cancer drug.

- Measuring the absorbance value of DOX release at different time intervals (from 0.5 h to 168 h) using UV-vis spectroscopy and calculating the DOX release amount by creating a standard DOX calibration curve. The expected target is that the DOX release from the nanostructure would be higher than that of free DOX in the acidic environment compared to the neutral or basic environment. Moreover, expected drug release behavior would be slow and sustain drug release depending on time. In this system, DOX molecules are chemically bonded to the polymer shell of ALD-NS+DOX. Therefore, drug release mainly depends on two mechanisms; firstly, the bond is in the form of Schiff base, so cleavage of the imine (C=N) bond occurs to release DOX. Secondly, diffusion of DOX drug from the matrix of ALD-NS+DOX complex into the surrounding dialysis medium takes place. Due to the acidic property of the cancer cell culture, the drug is released in the cell due to the pH gradient (The drug performs a pH sensitive degradation profile under acidic conditions due to the hydrolysis of the Schiff base bond and the pH sensitivity of the crosslinker used in the formed structure).

- Determination of in vitro cytotoxicity of the ALD-NS+DOX complex on A549 lung cancer cell culture at 24, 48 and 72 h of incubation with WST-8 [2- (2-methoxy-4-nitrophenyl) -3- (4-nitrophenyl) -5- (2,4-disulfophenyl) -2H-tetrazolium, mono-sodium salt] test and its cellular uptake behavior. The cytotoxicity study of DOX and ALD-NS+DOX complex in the proliferation of WST-8 test was performed to

determine the in vitro cytotoxicity of the developed ALD-NS to its free drug counterpart at all concentrations studied. IC_{50} value of the system will be gained for the first time within the scope of this thesis using WST-8 test on A549 cell line. In the cell entry behavior, it is aimed to demonstrate more concentration and higher drug accumulation profile in the cell cytoplasm compared to the free drug.

- It is necessary to use mathematical models to determine the in vitro drug release mechanism and kinetics of a particular system. In this thesis, using numerical data obtained from in vitro drug release studies for each pH in different buffer solutions at body temperature, the release mechanism and kinetics of DOX.HCl from ALD-NS compared with pure DOX.HCl was determined by using the most suitable mathematical models such as zero order, first order, Higuchi and Korsmeyer-Peppas models.

1.8. Stages of the Thesis

The thesis consists of 6 stages and is described both as items below and schematically in Figure 1.7.

1.8.1. Definition as Items

1. Synthesis of OX-β-CDs and modification of optimum values

1.1. Preparation of OX-β-CDs from β-CD by using $NaIO_4$.

1.2. Characterization and Results of OX-β-CDs obtained

a. Determination of Aldehyde (CHO) content

b. Aldehyde peak observation of OX-β-CDs by FTIR, ^{1}H-NMR Spectroscopy, SEM, XRD images of OX-β-CDs.

1.3. **Antibacterial activity studies of OX-β-CDs**

a. MIC Method

b. Disc Diffusion Method

2. Synthesis of ALD-NS and Determination of Optimum Values and Characterizations

a. Detection of optimum values by activating OX-β-CDs with PMDA in 1: 2, 1: 4, 1: 6 molar ratios with drug loading study

2.1. Characterization of ALD-NS obtained

a. FTIR, XRD and ^{1}H-NMR of ALD-NS

3. Integration DOX.HCl anti-cancer drug on ALD-NS nanocarrier

3.1 Synthesis of ALD-NS+DOX.HCl Complex

3.2 Characterization of DOX loaded ALD-NS

a. UV-vis measurement, FTIR**,** SEM Images, TGA, ^{13}C-NMR Spectroscopy, XRD analysis, PS and ZP (ζ) measurement, EE and DL percentage calculation

4. In vitro DOX Release Studies from ALD-NS+DOX Complex

5. Cytotoxicity Testing and Cellular Uptake

5.1 In Vitro Cytotoxicity Test (WST-8 test)

5.2 Determination of time-dependent cellular uptake of DOX + ALD-NS complex by Fluorescence microscopy

6. Mathematical Modeling (drug release kinetics)

1.8.2. Schematic Representation

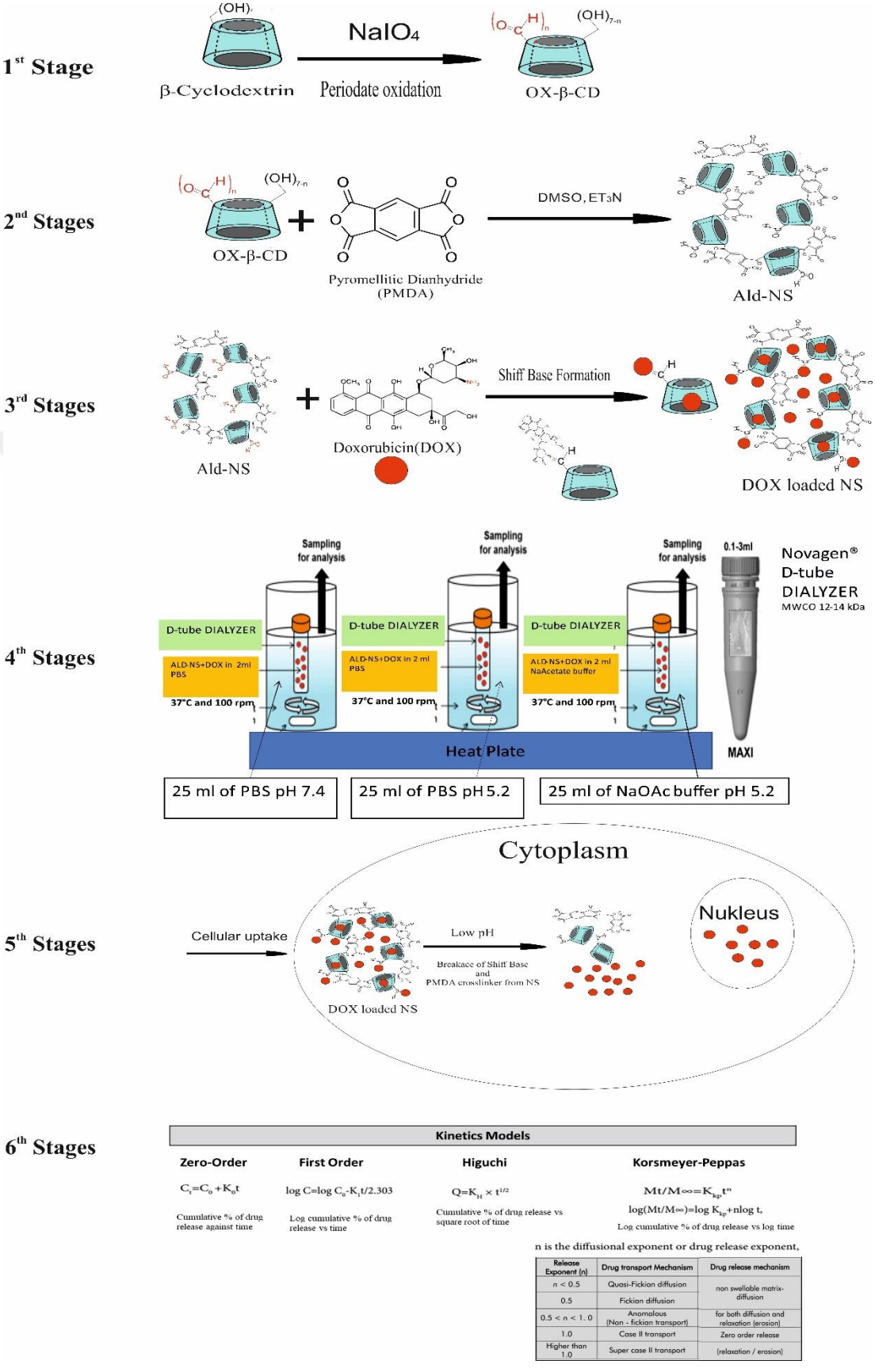

Figure 1.7. Schematic representation of thesis stages

2. MATERIALS AND METHOD

2.1. Materials and Reagents

β-Cyclodextrin (purity > 98%) and pyromellitic dianhydride (PMDA ≥ 99%) was obtained from Acros Organics. Sodium periodate (purity ≥ 99.8%), ethylene glycol (≥ 99%), TEA (≥ 99%), hydroxylamine hydrochloride (HAHCl), and DOX.HCl (200mg) were purchased from Sigma–Aldrich. Spectra/por® cellulose ester (CE) dialysis membrane (MWCO of 100-500 Da) and D-Tube™ Dialyzer Maxi dialysis tube (Spectra/Por® MWCO 12-14 kDa) was acquired from Repligen Corporation, USA. A Macherey-Nagel paper filter (MN 640w 125mm) was used in the vacuum filtration process. Avantor VWR® hydrophobic PTFE (13 mm 0.22 µm) was used in the syringe filtration process. WST-8 cell counting kit were obtained from Sigma-Aldrich, Germany. A549 lung cancer cells were obtained from the Turkish Type Culture Collection. A549 were cultured in Ham's F-12K supplemented with 10% FBS (ATCC, USA) and 1% Penicillin-Streptomycin (Biowest, France). Cells were grown in a humidified incubator (EC-160, Nuve, Turkey) with 5 % CO_2 at 37°C, and were passaged at 80% confluence. All procedures were performed in a sterile laminar flow hood (MN 120, Nuve, Turkey).

All other chemicals used were of analytical grade, so they were utilized as they were received without any further processing.

2.2. Characterizations of All Samples

2.2.1. UV-vis Spectrophotometer

UV-vis measurement was performed using a Thermo Scientific Evolution™ 201/220 in the range of 250–700 nm with Quartz cuvette.

2.2.2. FT-IR Spectroscopy

The dried powder of samples was used for FTIR analysis using a PerkinElmer Spectrum two instrument. All spectra were acquired in the 4000–400cm^{-1} range with a resolution of 4cm^{-1} for 20 scans.

2.2.3. SEM Images

The surface morphology of all samples was investigated by SEM with JEOL JSM-7001f. Small quantity of samples in liquid form were placed on a carbon-coated copper plate and dried under vacuum to prepare a thin sample layer.

2.2.4. XRD Analysis

The XRD of all samples were operated by a Rigaku Smart Lab diffractometer in the reflection mode at 40 kV and 30 mA using a fixed CuKα radiation (λ = 1.54 Å) at a scan speed of 2°/min with a 2θ range from 5 to 50 ^{0} at ambient temperature.

2.2.5. ^{1}H-NMR Spectroscopy Analysis

The proton NMR spectra for the β-CD and OX-β-CDs was obtained in DMSO-d_6 using the Bruker Avance III 400 MHz NMR Spectrometer. Then, all the spectra acquired were analyzed using the MNova NMR software.

2.2.6. TGA Analysis

The thermal behavior of samples was carried out on a TA Instruments Hi-res Q500 Thermo Analyzer by heating 5 mg of the sample in an aluminum open crucible under a nitrogen (flow, 10 mL min^{-1}) with a 20 °C/min heating rate over 30–700°C range.

2.2.7. ZP and PS Measurements

ZP(ζ) and PS were measured by dynamic light scattering (DLS) with water dispersion method using Malvern Zetasizer Nano ZS 90 at a detection angle of 174°. 10 mg samples were dispersed in 5 mL ultra-DI water and planetary ball mill (RETSCH Models PM 200) was used ultrafine colloidal grinding for mixing and homogenizing materials on a nanometer scale for 30 min at 500 rpm. Samples were filtered by 0.24 µm syringe filter before measurement.

2.2.8. Statistical Analysis

Characterizations, in vitro cytotoxicty and celluar uptake studies in this thesis were repeated in triplicate (n = 3). Characterizations data were shown as mean value ± standard deviation (SD). In vitro cytotoxicty and celluar uptake data was shown as Mean±S.E.M. The normality of the data was evaluated with the Shapiro-Wilk Test. Inhibitor Concentrations (IC) of the compounds were calculated by the Probit-Regression analysis. Dose-response data of the compounds were compared with the One-Way Analysis of Variance (ANOVA) followed by the Tukey's and Duncan tests. Statistical data was obtained with SPSS programme. Differences were considered statistically significant when P values were less than 0.05.

2.3. First Stage

2.3.1. Synthesis of OX-β-CDs and Determination of Optimum Values

2.3.1.1. Periodate Oxidization of β-CD

OX-β-CDs were synthesized by the oxidation of β-CD with $NaI0_4$ by the method described elsewhere with some modification (Lou et al., 2020) as follows in Figure 2.1.

Specified amount of dried β-CD and various amounts of $NaIO_4$ (based on molar ratios of $NaIO_4$/β-CD 2, 3, 4, 5.3 and 7) were mixed with 50 ml of deionized water in glass Erlenmeyer flask. The Erlenmeyer flask was covered with aluminum foil and magnetically stirred in the dark for 3 h at room temperature. Then, a certain amount of ethylene glycol ($NaIO_4$/ ethylene glycol 1 molar ratio) was added to the mixture to stop the reaction without aluminum foil, and it was stirred for 1 more hour at room temperature. After this step, a certain amount of $CaCl_2$ is added, mixed, and the $Ca(IO_3)_2$ formed is removed by vacuum filtration. Excess $Ca(IO_3)_2$ and ions remaining in the filtrate are removed using the dialysis membrane (MWCO = 1-5 kDa) and solid white OX-β-CD powder is obtained by freeze-drying. The freeze dried of OX-β-CDs synthesized at the $NaIO_4$/β-CD molar ratio of 2/1, 3/1, 4/1, 5.3/1 and 7/1 were named as OX-β-CD2 (74.9%), OX-β-CD3 (83.73%,) OX-β-CD4 (86.64%), OX-β-CD5 (89.27%) and OX-β-CD7 (94.17%) respectively.

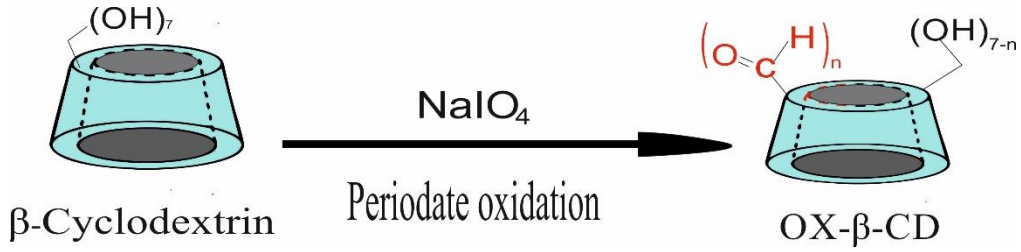

Figure 2.1. Schematic representation of oxidation of β-CD with sodium periodate ($NaIO_4$)

2.3.2. Characterization of OX-β-CDs

2.3.2.1. Aldehyde Content Determination

The amount of aldehyde (or oxidation degree) in the OX-β-CDs (OX-β-CD2, OX-β-CD3, OX-β-CD4, OX-β-CD5 and OX-β-CD7) were calculated by hydroxylamine hydrochloride (HAHCl) acid-base titration method (Yin et al., 2020). The aldehyde group reacts with HAHCl to form oxime and hydrochloric acid (HCl)

(Figure 2.2). The HCl in the mixed solution was titrated with 0.1 M sodium hydroxide (NaOH) to calculate the experimental aldehyde content with equations given below.

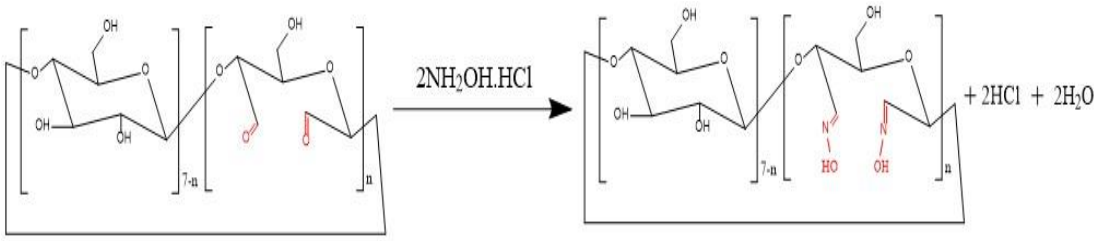

Figure 2.2. Reaction equation between aldehyde in OX-β-CDs and hydroxylamine hydrochloride to form oxime and hydrochloric acid.

In brief, accurately weighed OX-β-CDs were dissolved in HAHCl solution (25 mL, 0.25 M), into which 2 drops of methyl orange indicator was added. After addition, the color of the solution changed to a reddish appearance. The red mixture is reacted for 2 hours at room temperature and then titrated with 0.1 M NaOH solution. At this stage, the color of the sample solution is matched with the blank one until the red-to-yellow end point is reached. Blank titration was also performed by using the raw β-CD powder and the consumed volume of NaOH (Va, mL) was recorded as well.

The yield of the dried OX-β-CDs were determined using the Eq. (2.1). Aldehyde amounts (CHO) (or oxidation degree (OD)) was calculated experimentally by Eq. (2.2) and Eq. (2.3) and theoretically by Eq. (2.4) and Eq. (2.5) given below as percentage (CHO %) and amount ([CHO] mmol /g).

$$\text{Yield}\ (\%) = \frac{\text{OX}-\beta-\text{CD(g)}}{\beta-\text{CD(g)}} \times 100 \quad \textbf{(2.1)}$$

$$\text{CHO}(\%) = \frac{[V_b - V_a] \times 0.1M \times 29}{m \times 1000} \times 100 \quad \textbf{(2.2)}$$

$$[\text{CHO}](\text{mmol/gr}) = \frac{[V_a - V_b] \times C}{m} \quad \textbf{(2.3)}$$

$$[\text{TDO}_{\text{CHO}}](\text{mmol/gr}) = \frac{\text{mmol of NaIO}_4 \times 2}{\text{initial amount of } \beta-\text{CD used}} \quad \textbf{(2.4)}$$

$$\text{TOD}_{\text{CHO}}(\%) = \frac{\text{amount of NaIO}_4 \text{ for each molar ratios (mol)}}{\left(\frac{\text{Initial amount of } \beta-\text{CD}}{\text{M.W.of initial glucose unit of } \beta-\text{CD}}\right)} \times 100 \quad \textbf{(2.5)}$$

Where 29 is the molecular weight of aldehyde (g/mol); m is the weight of OX-β-CD used (g); C (mol/L) is the concentration of NaOH; 0.1M is the concentration of NaOH (mol/L); Va is the volume of NaOH spent in control titration (mL); Vb is the volume of NaOH spent in titration (mL).

2.3.2.2. FTIR, SEM, ^{1}H-NMR, XRD, PS Studies

FTIR, SEM, ^{1}H-NMR, XRD, PS studies were performed, and all the results are explained in detail in the results and discussion part (section 3.1.1.).

2.3.3. Antimicrobial Activity of OX-β-CDs

Antibacterial activity of OX-β-CDs was investigated against Gram-negative (*Escherichia coli*, *Pseudomonas aeruginosa)* and Gram-positive (*Staphylococcus aureus*, *Bacillus cereus*) bacteria strains by using the minimal inhibitory concentration (MIC) and the Disk diffusion method (Yakan et al., 2020; Matar and Andac, 2021). Mueller Hinton II Broth (MHB) Agar was used to cultivate bacteria. MIC values were calculated by microdilution method to evaluate the antibacterial activity of OX-β-CDs.

2.3.3.1. MIC Method

100 µL MHB broth was added to each well (1 to 12) in a sterile 96-well plate. 100 µL OX-β-CDs (16.3 mg/mL) and β-CD as well as antibiotics (amoxicillin (2.048 mg/mL) were added to the first well, mixed and serially diluted to 12 well. 1 mL of the 0.5 McFarland -adjusted bacterial solution (~10^{8} colony-forming units (CFU)/mL) was mixed with 9 mL of MHB, and five microliters of this solution was added to all wells. The plate was kept in a refrigerator at +4 °C for 2 hours and then incubated at 37 °C for 24 hours. Amoxicillin (AMOX) was used as standard antibiotics. Broth containing bacteria with β-CD alone was used as the control.

2.3.3.2. Disk Diffusion Method

Bacteria strains were added to 5 mL of sterile saline (0.85% NaCl) solution and the McFarland value was adjusted to 0.5 (~10^{8} CFU/mL). 25 mL of MHA (Mueller Hinton Agar) was added to sterile petri dishes and the bacterial solution (adjusted to McFarland 0.5 value) was spread on MHA agar. 50 µL of the OX-β-CDs samples prepared at different concentrations were absorbed into the discs (6 mm diameter) and the discs were placed on MHS agar. Each bacteria strain was incubated for 24 hours at 37 °C. After 24 h of incubation, an inhibition zone diameter in millimeters (mm) was measured. Amoxicillin antibiotic was used as the standard and dilution of antibiotic 2048 µg/mL was prepared (Yakan et al., 2020; Rafaque et al., 2020).

2.4. Second Stages

2.4.1. Synthesis of ALD-NS and Determination of Optimum Values

ALD-NS was obtained in the reaction of OX-β-CD4 and PMDA crosslinker using 1:2, 1:4 and 1:6 molar ratios of OX-β-CD4: PMDA with using only water as a solvent (Figure 2.3). 0.1 gr OX-β-CD4 was initially dissolved in deionized water containing very low quantity of TEA. PMDA (molar ratio of 1:2,1:4,1:6 (OX-β-CD4: PMDA)) was dissolved in acetone then added drop by drop in above solution under vigorous stirring at room temperature for 3h. The acetone is removed by evaporation and dialyzed against deionized water for 1 day and aqueous solution is freeze dried to give a solid white substance.

2.4.2. Characterization of ALD-NS

FTIR, XRD, ^{1}H-NMR, SEM, TGA, PS, ZP measurement and calculation of DL and EE of ALD-NS prepared in different molar ratios was conducted. The results are explained in the results and discussion part (section 3.2.1.).

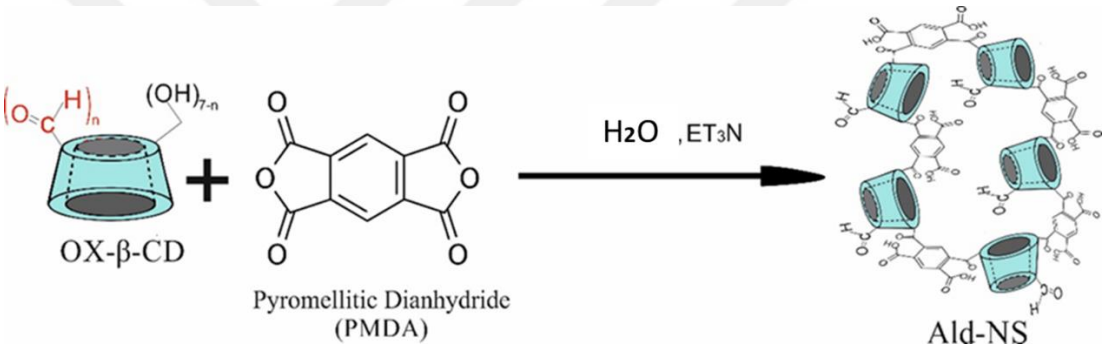

Figure 2.3. Schematic representation of obtaining ALD-NS as a result of oxidized β-CD with PMDA crosslinker

2.5. Third Stages

2.5.1. Integration of Doxorubicin Hydrochloride (DOX.HCl) Anti-Cancer Drug on ALD-NS

2.5.1.1. Synthesis of ALD-NS+DOX.HCl Complex

In order to form the most important part of the thesis research, the reflux mechanism shown in Figure 2.4 below was established and the DOX anti-cancer drug was integrated into the synthesized ALD-NS nanocarrier in two mechanisms as shown in Figure 2.5. One of them is the connection of C=N (Schiff base) between the NH_2 group in the structure of DOX and the aldehyde (CHO) group of synthesized ALD-NS, shown in Figure 2.5. The second will be in the form of binding of the DOX drug to the hydrophilic outer surface of the ALD-NS due to its hydrophilic nature.

A certain amount of DOX.HCl and ALD-NS (1:10 w/w) were added to 10 ml methanol. Establishing an experimental setup as in Figure 2.4a, solution was refluxed at 65 ^{0}C -70 ^{0}C for 4-5 h in the dark. Solution was precipitated by adding diethyl ether. Resulted red solid dissolved by methanol and water in respectively and dried in the oven. At the end of the synthesis, a red solid was obtained (Figure 2.4b Yield %= 80%-87%) (Fonkui et al., 2019).

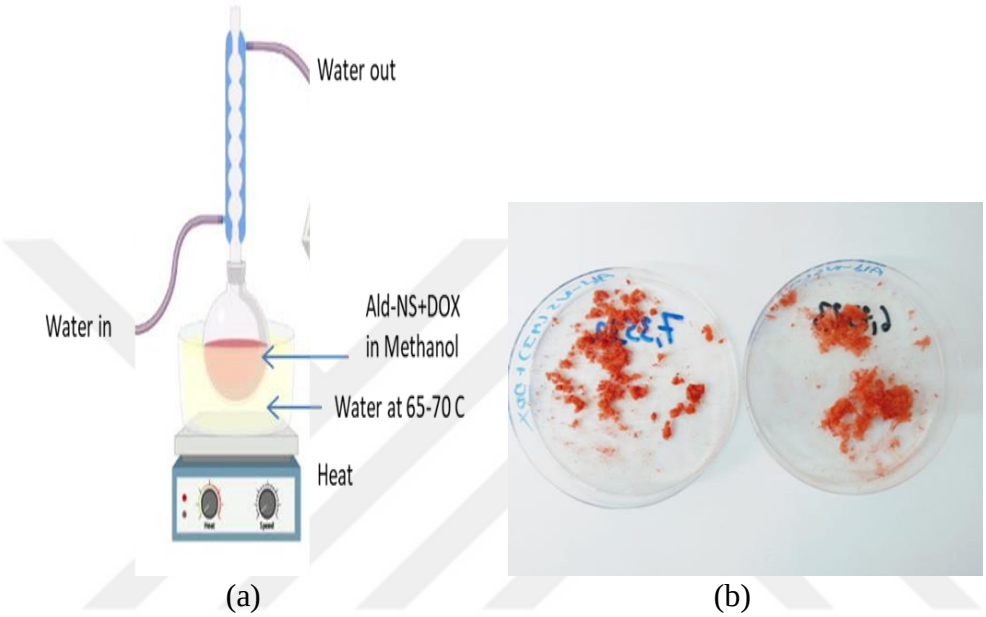

Figure 2.4. (a) Experimental schematic representation of the reflux method and (b) DOX loaded nanocarrier (ALD-NS+DOX)

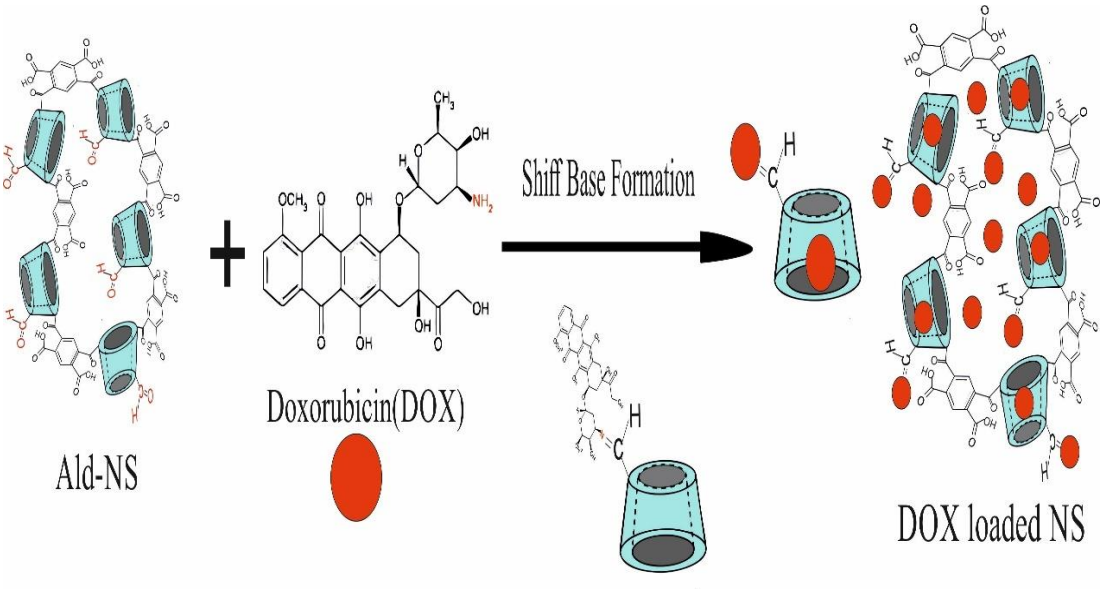

Figure 2.5. Possible bidirectional DOX drug loading mechanism into ALD-NS Nanocarrier (Schiff base bond formation and binding to the hydrophilic moiety)

2.5.2. Characterization of DOX loaded ALD-NS+DOX Complex

UV, FTIR, SEM, TGA, XRD, ^{13}C-NMR PS, ZP(ζ) measurement analysis were carried out. The results are explained in detail in the results and discussion part (section 3.3.2.).

2.5.3. EE and DL Calculation

EE and DL were determined by quantitative estimation of drug loaded into ALD-NS (ALD-NS+DOX). The precise amount of ALD-NS+DOX (10 mg) was dissolved in methanol, sonicated 15s for breaking the complex and centrifuged for 15 min. Centrifuged supernatant was diluted with water and then analyzed by UV-vis at 480 nm (0.1–1 mg/ml, R^2= 0.9916). EE and DL of ALD-NS+DOX complex was determined using following equations (Eq 2.6 and 2.7).

$$\text{EE (\%)} = \frac{\text{Total Drug Added (mg)-Drug Unentrapped (mg)}}{\text{Total Drug (mg)}} \times 100 \quad \textbf{(2.6)}$$

$$\text{DL (\%)} = \frac{\text{Total Drug Added (mg)-Drug Unentrapped (mg)}}{\text{Total Nanocarrier (mg)}} \times 100 \quad \textbf{(2.7)}$$

2.6. Forth Stages

2.6.1. In Vitro DOX Release Studies from ALD-NS+DOX Complex

It is known that the Schiff base linkages are degradable via hydrolysis in low acidic medium. On the other hand, their stability decreases as the surrounding pH decreases. Therefore, the release of DOX from the ALD-NS+DOX complex will occur as pH dependent degradation of the Schiff base linkages as well as the crosslinked structure. Therefore, the drug release behaviors of ALD-NS+DOX complex were investigated through a dialysis method (cut-off=12-14 kDa) under neutral (0.1 M PBS at pH 7.4) and acidic conditions (0.1 M PBS at pH 5.2 and 0.1 M NaOAc buffer solution at pH 5.2), imitating the physiological (pH 7.4) and tumor environment (pH 4.5–6.5).

The prepared drug loaded nanocarriers (ALD-NS+DOX) containing 0.94 mg of DOX were suspended in 2 mL of 0.1 M PBS at pH 7.4 and 2 ml of acidic conditions (0.1 M PBS at pH 5.2 and 0.1 M NaOAc buffer solution at pH 5.2) by slight vortexing and placed in a dialysis tube (Novagen® D-tube dialyzer MWCO 12-14 kDa) to determine in vitro release of DOX (Figure 2.6). The tube immersed in a glass container containing 25 mL of release medium (PBS at pH 7.4 and pH 5.2 and 0.1 M NaOAc

buffer solution at pH 5.2). The container was placed in a horizontal shaking incubator at 37°C and 100 rpm. The dialysis bags were dialyzed against three different buffers. About 1 mL of the release medium was withdrawn at different time intervals (0.083, 0.16, 0.3, 0.5, 1, 2, 3, 4, 8, 24, 48, 72, 96, 120, 144 and 168 h) and the amount of DOX was determined from the standard calibration curve of DOX at 482.6 nm for PBS at pH 7.4, 482 nm for PBS at pH 5.2 and 481 nm for NaOAc buffer solution at pH 5.2 (Figure 2.7). The withdrawn release medium was replaced with fresh buffers. Under similar conditions, release of free DOX (0.94 mg) from fresh buffers (PBS at pH 7.4 and pH 5.2 and 0.1 M NaOAc buffer solution at pH 5.2) was also carried out and compared with release of DOX from the ALD-NS+DOX. Cumulative release of DOX at different time intervals was calculated from the Eq. (2.8) (Li et al., 2017).

$$\text{Cumulative release of DOX (\%)} = \frac{V_e \sum_1^{n-1} C_i + V_0 C_n}{m_0} \times 100 \qquad \textbf{(2.8)}$$

Where V_e is the volume taken from the released medium for measurement for each time (1 mL); V_0 is the total volume of release buffers (25 mL); C_n is the concentration of DOX in the release buffers, and m_0 is the total mass of DOX loaded in ALD-NS; C_i is the concentration of DOX taken from the released medium for each measurement.

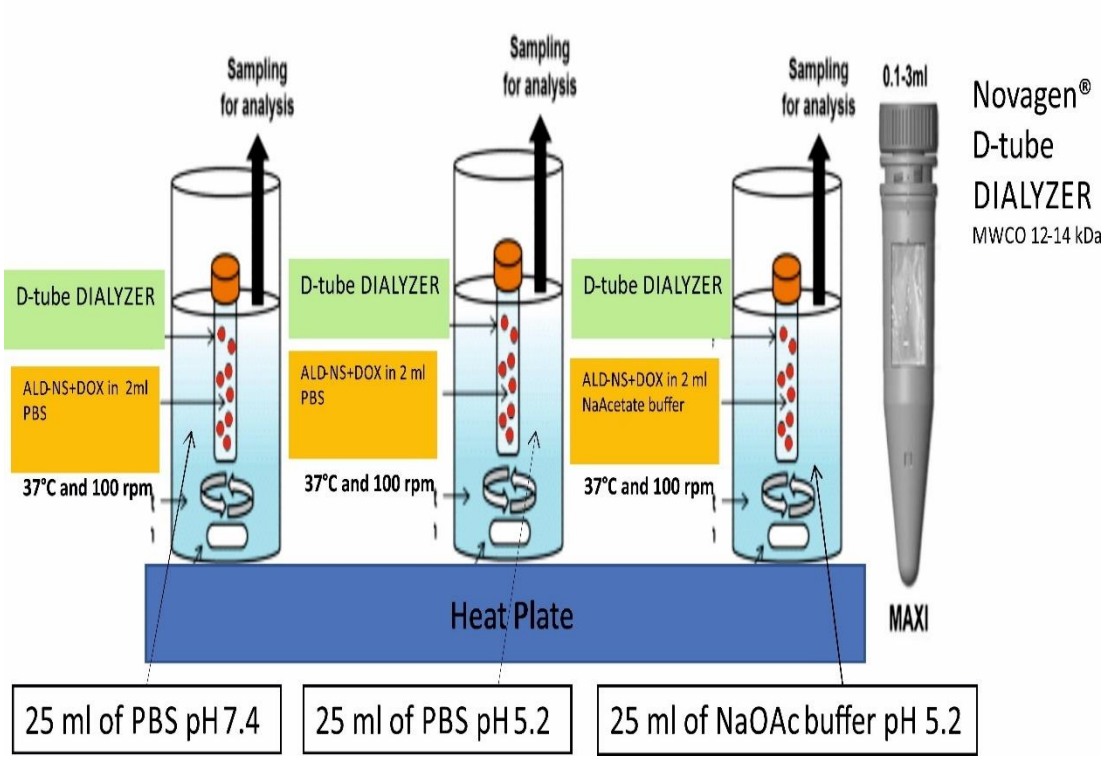

Figure 2.6. Experimental schematic representation of the drug release through a dialysis method.

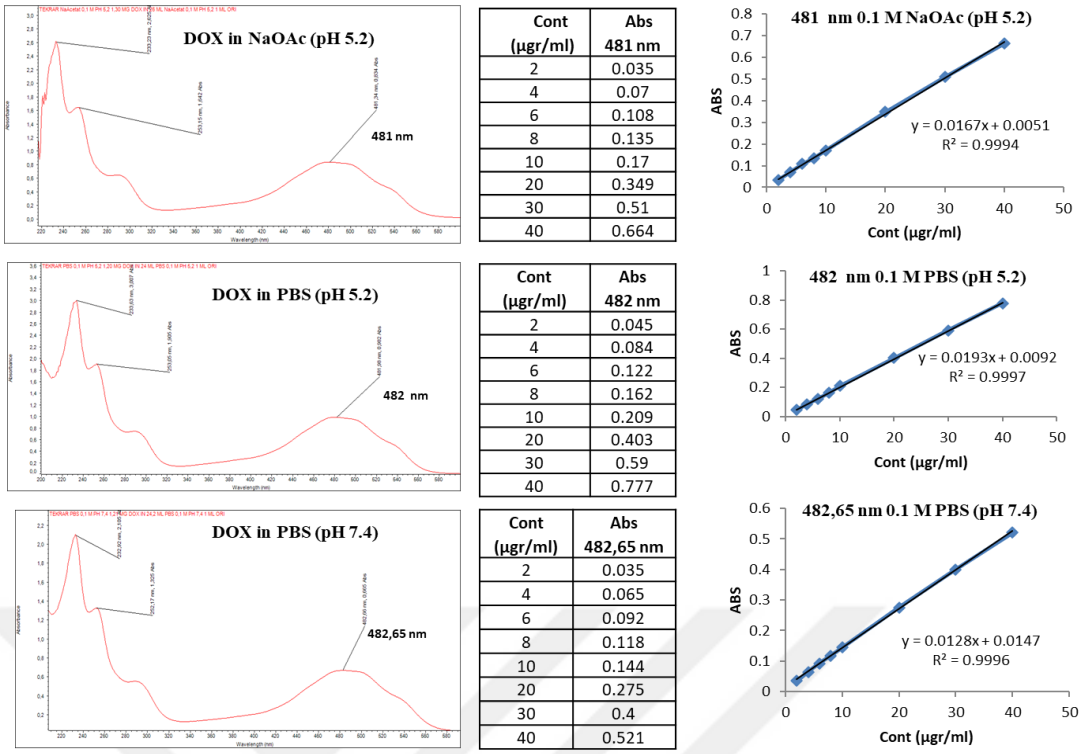

Cont (µgr/ml)	Abs 481 nm
2	0.035
4	0.07
6	0.108
8	0.135
10	0.17
20	0.349
30	0.51
40	0.664

Cont (µgr/ml)	Abs 482 nm
2	0.045
4	0.084
6	0.122
8	0.162
10	0.209
20	0.403
30	0.59
40	0.777

Cont (µgr/ml)	Abs 482,65 nm
2	0.035
4	0.065
6	0.092
8	0.118
10	0.144
20	0.275
30	0.4
40	0.521

Figure 2.7. Standard calibration curve of DOX.HCl in 0.1M PBS (pH 7.4), 0.1M PBS (PH 5.2) and 0.1M NaOAc buffer (pH 5.2)

2.7. Fifth Stages

2.7.1. Cytotoxicity Testing and Cellular Uptake

2.7.1.1. In Vitro Cytotoxicity Test (WST-8 Test)

The in vitro cytotoxicity test, which is the most basic test for determining the toxic effect and level of a substance, is a test performed on living cells in vitro and provides basic information about the toxic behavior of the related compound and subsequent in vivo studies. For this purpose, the efficiency of the synthesized ALD-NS + DOX complex was evaluated in A549 lung cancer cell culture.

Cytotoxicity was determined by WST-8 tetrazolium test. According to this test principle, the WST-8 compound is reduced by electrons carried by NADH molecules in living cells to the formazan compound in orange color, and since there is no metabolic activity in dead cells, no orange color is formed. Thus, the live / dead cell ratio according to the intensity of color formation can be determined by absorbance measurement. Cancer cells microenvironment is more acidic than normal cells due to their high metabolic rate. The ALD-NS+DOX complex is designed to bind/enter the cancer cell and release DOX inside the cell at acidic pH values of cancer cells. Thus,

it is expected to specifically destroy the cancerous cell and show a higher cytotoxic effect at lower doses compared to free DOX.

The cytotoxicity test was performed for 24 h and 48 h exposure periods. Stock solutions of samples (control, free DOX and two formulations of ALD-NS nanocarrier and ALD-NS+DOX complex) were prepared in sterile-filtered DMSO (ATCC, USA). Stocks were diluted with FBS-free medium to final concentrations of 20, 10, 5, 2.5, 1.25, 0.625, 0.3125 µM (test mediums).

Cells were trypsinized (0.25% Trypsin & 0.05% EDTA, Biological Industries, Israel), and were seeded into 96-well sterile plates at a density of $2.5x10^4$ and cultured for 24 h. After 24 h of incubation, mediums were removed, and the test mediums containing free DOX, ALD-NS nanoparticle and ALD-NS+DOX complex at various drug concentrations (0.1, 0.25, 0.5, 0.75, 1 ve 5 µM) were added. Then the cells were exposed to samples for either 24 h or 48 h. Test mediums were drawn, and wells were washed with PBS at the end of the exposure period. After adding fresh medium, cells were incubated for 30 minutes.

At the end of the exposure period, 10 µl of WST-8 solution was added to each well, and the cells were incubated for 2 h. The absorbance was measured at 450 nm wavelength (RT-6000, Rayto, China). Blank wells containing only medium were used to subtract the background. Untreated cells were used to obtain 100% viability. All tests (24 h and 48 h) were repeated three times. Inhibitor concentrations of the samples were calculated by probit-regression analysis. Calculated viability rates will be subjected to statistical processes and the IC_{50} value will be determined.

2.7.1.2. Determination of Time-Dependent Cellular Uptake of ALD-NS+DOX Complex by Fluorescence Microscopy

The degree of intracellular drug release and cellular internalization of NCs are two key indicators of a NCs system that are valuable for measuring the cell entry potential, drug delivery, and concentration within cells.

DOX cancer drug, which gains its natural fluorescence feature (Mohan and Rapoport, 2010; Yildiz et al., 2018) thanks to its central anthracycline chromophore group, can be visualized in tissues or cells under fluorescent imaging systems in the visible range (Tahir et al., 2019). Therefore, to evaluate the targeting behavior of free DOX and ALD-NS+DOX formulations, in vitro cellular uptake study was performed and further monitored at 12 h incubation after adding 1.25 µm of each sample on A549

cell culture with a Zeiss™ Axio Vert.A1 FL LED-based fluorescence microscopy. Intracellular distribution and the cellular uptake of cells were then observed with fluorescence microscope by excitation at 490 nm.

Doxorubicin in the cells was excited by sending light at a wavelength of 470 nm on the cells (i.e., excitation wavelength = 470 nm). At this time, the excited doxorubicin emitted light at a wavelength of 590 nm and this scattering was recorded with a camera (i.e., emission wavelength = 590 nm) (Mohan and Rapoport, 2010).

2.8. Sixth Stages

2.8.1. Mathematical Modeling (Drug Release Kinetics)

The most relevant kinetic models applied to understand drug release mechanisms for the transport of material subject to change in ambient conditions base on driving forces such as swelling, erosion, diffusion and dissolution or degradation from polymeric delivery systems (Fu and Kao, 2010; Elmas et al., 2020). To investigate drug release kinetics and the release rate from obtained NCs, the in vitro drug release data was fitted and analyzed with the several well written mathematical models such as zero order (Eq. 2.9), first order (Eq. 2.10), Higuchi model (Eq. 2.11) and Korsmeyer-Peppas model (Eq. 2.12). The models and fitting parameters are shown in Table 2.1 and Table 2.2.

The zero-order model describes the process of sustained drug release from the drug-loaded nanocarrier, regardless of concentration. A dissolution of the drug occurs, which does not dissociate from the various dosage forms, causing slow drug release and can be expressed as:

$$M_t = k_0 t \quad \textbf{(2.9)}$$

Therefore, a graph of cumulative drug release versus time is plotted to examine drug release kinetic data from the in vitro dissolution study (Table 2.1).

The first order kinetic is a process which releases the drug from the system where the drug release rate is subject to concentration. i.e., the greater the concentration, the faster the reaction. After rearranging and integrating the equation it can be expressed as:

$$\mathrm{Log}M_t = \log M_o + {}^{k_1 t}\,/_{2.203} \quad \textbf{(2.10)}$$

Thus, it defines the drug release from matrices as a graphical representation of the

log cumulative % versus time (Table 2.1).

The Higuchi model was considered that the drug release is takes place due to both dissolution and diffusion so that drug release from solid matrices described as:

$$M_t = k_h\sqrt{t} \quad \textbf{(2.11)}$$

Obtained data from drug release study could be plotted as cumulative percentage drug release versus square root of time (Table 2.1).

Korsmeyer and Peppas demonstrated a relationship describing what type of dissolution (both fickian law and non-fickian law) drug release from the polymeric delivery system and they developed a factual equation as follows:

$$\log(M_t/M_\infty) = \log k_{kp} + n\log t \quad \textbf{(2.12)}$$

The result of drug release occurs based on the release component "n" (Table 2.2). For instance, Fickian diffusion takes place when n = 0.5 or 0.5<n<1 and the release obeys zero order kinetics when n=1. The Korsmeyer-peppas model accepts mostly 60% of the drug release data, which helps to find the drug release mechanism. Graphical representation of drug release for this model could be described as log cumulative % drug release versus log time (Table 2.1).

Where M_0 is the initial drug amount in the formulation; Mt is the amount of drug release at time t; k_0, k_1, k_h, and k_{kp} are release rate constants for zero-order, first-order, Higuchi model and Korsmeyer–Peppas models, respectively; M_∞ is the amount of drug release at time ∞ and "n" is the diffusion coefficient for Korsmeyer–Peppas models.

Table 2.1. Kinetic parameters for drug release models

Kinetic Models	**Zero-Order**	**First-Order**	**Higuchi Model**	**Korsmeyer and Peppas Model**
Equations	$M_t = k_0 t$	$\log M_t = \log M_o + {k_1 t}/{2.203}$	$M_t = k_h \sqrt{t}$	$\log (M_t/M_\infty) = \log k_{kp} + n \log t$
Plots	Cumulative % drug release vs. time	Log cumulative % of drug release vs time	Cumulative % drug release vs square root of time.	Log cumulative % drug release vs. log time.

Table 2.2. Different release mechanisms of Korsmeyer and Peppas Model depends on "n".

Release Exponent ("n")	Drug Transport Mechanism	Drug Release Mechanism
$n < 0.5$	Quasi-Fickian Diffusion	Non-Swellable Matrix Diffusion
0.5	Fickian Diffusion	
$0.5 < n < 1.0$	Anomalous (non Fickian Transport)	For both Diffusion and Relaxations
1.0	Case II Transport	Zero Order Release
higher than 1.0	Super Case II Transport	Relaxation or Erosions

3. RESULTS AND DISCUSSION

3.1. Synthesis of OX-β-CDs and Degree of Oxidation

β-CD was oxidized using varying molar ratios of $NaI0_4$, which eventually resulted in the formation of CHO (aldehyde) functional group on β-CD units (Figure 3.1) with different degrees of oxidation. As shown in Figure 3.1(a), this oxidation reaction results in the cleavage of the C2–C3 bond of the pyranose ring and two aldehyde groups formed at these carbon atoms. As a byproduct, IO_3^- and water are also formed. In addition to that, one of the aldehyde functional groups at C2 or C3 could react with the neighboring hydroxyl (OH) group within and around the oxidized β-CD which eventually causes the formation of either intramolecular or intermolecular hemiacetal groups (Figure 3.1b, c). The formation of hemiacetals depicted in Figure 3.1(b, c) is reversible reactions and exists in equilibrium that can revert to free aldehyde form.

The formation of $NaIO_3$ as by product has a negative effect on the structure's color. My experimental study has shown that after a certain period of time (3-4 months) OX- β-CD starts to turn slightly yellow which showed that the by product (IO_3-) formed was still present in the structure. Therefore, before the dialysis membrane stage, the exact amount of $CaCl_2$ which is calculated based on the

stoichiometric ratio as shown in Eq. (3.1 and 3.2) was used to precipitate the IO_3- ion as $Ca(IO_3)_2$ and was removed by suction filtration. The iodometric titration method (see Appendix 1) applied to calculate IO_3- ion and shows that the amount of iodate was removed by approximately 95% (see Appendix 1) from the solution. This allowed us to obtain the oxidized structure in a purer form. During the periodate oxidation, two or more secondary hydroxyl groups are affected rather than that of primary hydroxyl groups in CD structure. The amount of added periodate has an impact on the degree of oxidation. Therefore, different molar ratios of $NaI0_4$/ β-CD were investigated in the search for desired properties in order to preserve original cyclic structure of β-CD.

$$\beta\text{-CD} + NaIO_4 \longrightarrow \text{OX-}\beta\text{-CD} + NaIO_3 + H_2O \quad \textbf{(3.1)}$$

$$2NaIO_3 + CaCl_2 \longrightarrow Ca(IO_3)_2 + 2NaCl \quad \textbf{(3.2)}$$

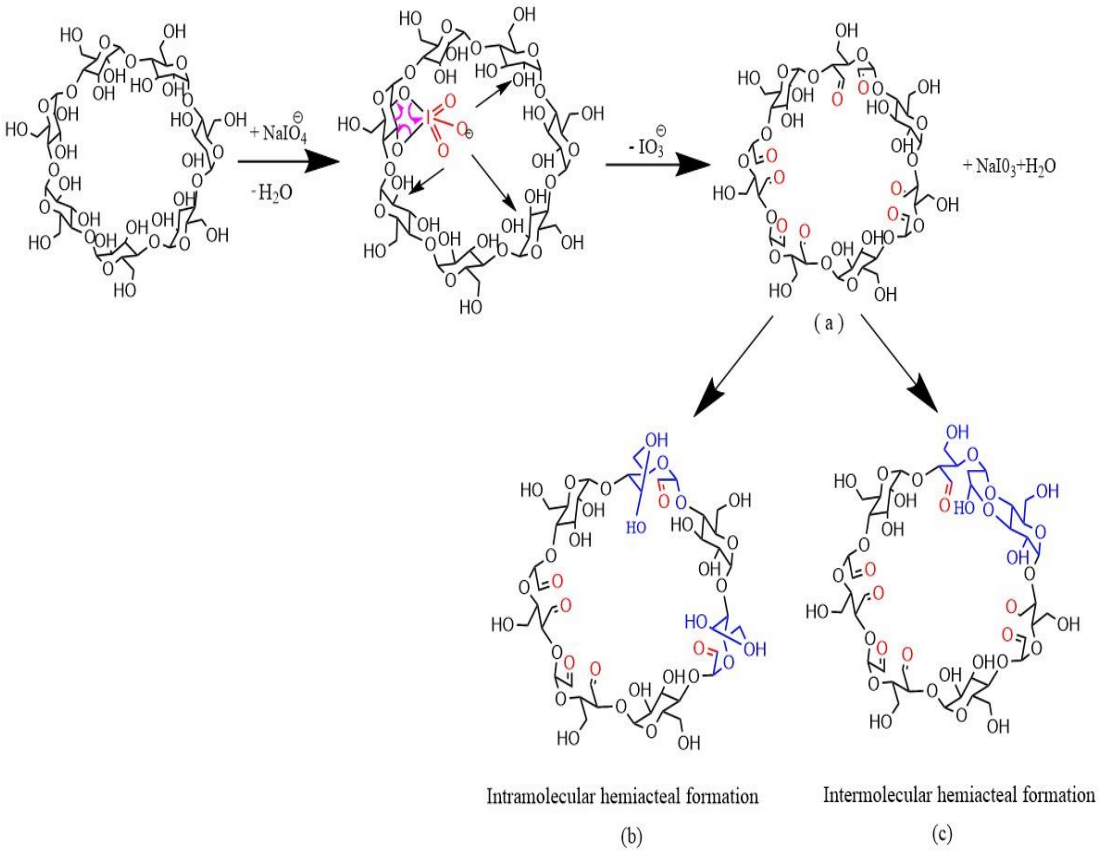

Figure 3.1. Potential structures of OX- β-CDs: (a) free aldehyde, (b) intramolecular hemiacetal and (c) intermolecular hemiacetal formations.

The theoretical and experimental aldehyde contents (or oxidation degree) of OX-β-CDs were calculated using titration method (Table 3.1) and presented in Table 3.2. It shows that the aldehyde functional groups are successfully introduced into β-CD molecules. The result of this experiment indicates that aldehyde content was increased

when increasing the concentration of $NaIO_4$ up to 7 molar ratios. During the oxidation, there was an increase in the aldehyde content from 9.51% to 29.11% (Table 3.2) in the experimentally which is quite high compare to other studies (Ijaz et al., 2015, Ren et al., 2018) and as expected, degree of oxidation in theoretically increase from 28,5% to 100% when the molar ratios of $NaIO_4$ increased to 7. The same results were also observed when the aldehyde content of OX-β-CDs was calculated as mmol/gr. I found an increase in the amount of aldehyde from 3.28 mmol/g to 10.03 mmol/g and from 3.52 mmol/g to 12.33 mmol/g in both experimental and theoretical calculations respectively, with increasing molar ratios of $NaIO_4$ up to 7. As seen in Table 3.2, the experimental aldehyde amounts are lower than the theoretical aldehyde value. The difference between the experimental and theoretical results is due to the fact that not all the aldehyde functional groups participated in the reaction during oxidation and some of oxidized glucose was converted into intramolecular or intermolecular hemiacetal (Afinjuomo et al., 2019; Afinjuomo et al., 2020). This fact was further supported by NMR result. Hemiacetal formation as shown in Figure 3.1(b, c) is coherent with results in the literature for some oxidized polysaccharides such as inulin (Afinjuomo et al., 2019), dextran (Pan et al., 2014), cellulose (Nypelö et al., 2021) and chitosan (Kristiansen et al., 2010).

3.1.1. Characterization of OX-β-CDs

In order to investigate the changes and modification of β-CD structure as a result of the periodate oxidation, both the dried powder of β-CD and modified OX-β-CDs (2,4,5 and 7) were analyzed using FTIR spectroscopy. As results shown in Figure 3.2, β-CD present characteristic O-H stretching vibration peak at 3302 cm^{-1}, C-H stretching vibration at 2925 cm^{-1}, H-O-H bending at 1643 cm^{-1}, symmetric stretching vibration of glycosidic C-O-C at 1152 cm^{-1} and C-O stretching vibration bond at 1077 cm^{-1}. As we can see in Figure 3.2, a new vibration band at 1730 cm^{-1} is noticed in the spectra of OX-β-CD4, OX-β-CD5and OX-β-CD7, which was attributed to the existence of C=O stretching of the aldehyde (CHO) groups on OX-β-CDs. However, peak around 1730 cm^{-1} was not observable in the FTIR spectra of the OX-β-CD2 sample in our work. This is because the aldehyde group may exist in the hemiacetal form or possibly because FTIR is not strong enough to identify the masked aldehyde functional group (Ren et al., 2018). Similar studies were reported that the characteristic band for C=O bond at 1730 cm^{-1} was observed in FT-IR spectrum of different oxidized

polysaccharides (Lou et al., 2020).

β-CD has a cyclic ring structure and the glycopyranose units are linked by 1-4 glycosidic C-O-C bonds. The C-O-C peak of FTIR spectrum of β-CD at 1152 cm^{-1} and the C-O peak at 1077cm^{-1} confirm this connection (Figure 3.2). When Figure 3.2 is examined carefully, the C-O-C (1-4 glycosidic) bonds break down as the oxidation degree increases and the cyclic structure of β-CD deteriorates. Especially, the disappearance of the C-O-C vibration band of both OX-β-CD5 and OX-β-CD7 at 1152 cm^{-1} and the decrease in the intensity of the C-O vibration of OX-β-CD5 and OX-β-CD7 at 1077 cm^{-1} confirms this fact.

In OX-β-CD2 and OX-β-CD4 however, the presence of C-O-C glycosidic bond and C-O stretching vibration peaks at 1152 cm^{-1} and 1077 cm^{-1} respectively, confirms that there is no fragmentation in the original structure of β-CD except oxidation so that the integrity of the structure is preserved. In addition, as can be seen in Figure 3.2, the broad-spectrum OH vibration peak of β-CD at 3302 cm^{-1} changed as the $NaIO_4$ molar ratio increased (at 5 and 7), which can be considered as clear evidence that there is degradation in the β-CD unit. This result shows that as the $NaIO_4$/β-CD molar ratio increases (5/1 to 7/1), the original glucopyranose unit and cavity of β-CD are fragmented.

Table 3.1. Titration results of β-CD (Control), OX-β-CD2, OX-β-CD4, OX-β-CD5 and OX-β-CD7 obtained by colorimetric titration of HAHCl

OX-β-CD2 + HAHCl Titration		**OX-β-CD4 + HAHCl Titration**		**OX-β-CD5 + HAHCl Titration**		**OX-β-CD7 + HAHCl Titration**		**Control Titration β-CD + HAHCl**	
pH	$V_{b(NaOH)}$ (ml)	pH	$V_{b(NaOH)}$ (ml)	pH	$V_{b(NaOH)}$ (ml)	pH	$V_{b(NaOH)}$ (ml)	pH	$V_{a(NaOH)}$ (ml)
2.14	0 (red)	1.88	0 (red)	1.72	0 (red)	1.61	0 (red)	3.46	0
2.60	1,1	2.34	1.8	2.21	1.2	2.34	3.3	4.21	0.3 (yellow)
3.00	1.5	3.29	2.9	3.20	3.5	3.34	4.3		
3,68	2.0 (yellow)	4.11	3.7 (yellow)	4.16	4.5 (yellow)	4.14	5.5 (yellow)		

Table 3.2. Aldehyde content and degree of oxidation of OX-β-CD2, OX-β-CD4, OX-β-CD5 and OX-β-CD7 calculated by Experimental (colorimetric titration) and Theoretical

Sample	Yield (%)	Experimental Aldehyde Content		Theoretical Oxidation Degree	
		*CHO (%)	**[CHO] (mmol/g)	***TOD_{CHO} (%)	****$[TOD]_{CHO}$ (mmol/g)
OX-β-CD2	74.90	9.51	3.28	28.50	3.52
OX-β-CD4	86.64	19.60	6.56	57.09	7.05
OX-β-CD5	89.27	23.51	8.10	75.00	9.34
OX-β-CD7	94.11	29.11	10.03	100.00	12.33

*CHO is experimental aldehyde content (%) of OX-β-CDs calculated by titration according to the equation 2.2
** [CHO] (mmol/gr) is the experimental aldehyde content of OX-β-CDs calculated by titration according to the equation 2.3
***TOD is theoretical oxidation degree (aldehyde content) of OX-β-CDs Calculated according to the equation 2.4
**** [TOD] mmol/gr is theoretical oxidation degree (aldehyde content) of OX-β-CDs calculated according to the equation 2.5

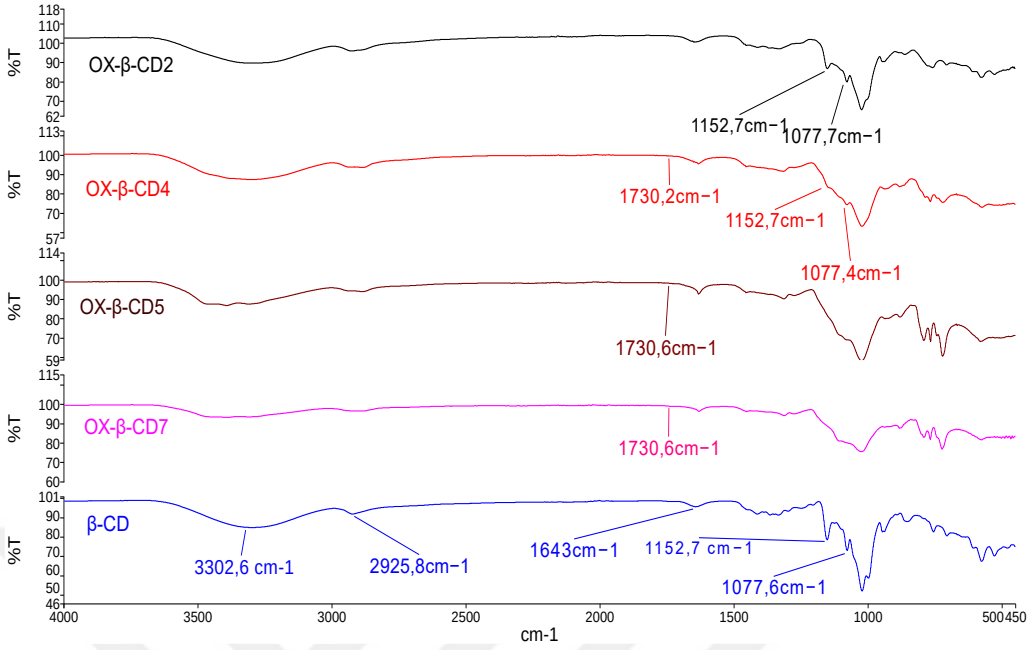

Figure 3.2. FTIR spectrum of β-CD and OX-β-CDs (OX- β-CD2, OX- β-CD4, OX- β-CD5 and OX-β-CD7).

The surface morphology of β-CD and OX- β-CD2, OX- β-CD4, OX- β-CD5 and OX- β-CD7 was investigated by SEM and images of β-CD and OX- β-CDs presented in Figure 3.3. When the β-CD structural morphology is examined, it is seen in Figure 3.3 (a) that the surface is quite rough, and it exhibits rectangular and square structures of different sizes. It can be seen clearly that the SEM of OX- β-CDs in Figure 3.3 (b-e) is different from that of β-CD. OX-β-CDs transform from rough granular type structure to smooth scaly, crusty structures. It has been reported that there is a same change in the structural morphology of polysaccharides, both in size and shape, as a result of the partial loss of hydrogen bonds and the formation of aldehyde groups in the oxidation reaction (Zhu et al., 2017).

Since the periodate oxidation reaction is based on the oxidation of the hydroxyl group and the formation of the aldehyde as a result of the breaking of the C-C bond by the periodate ion, the aldehyde groups in the molecular chains of OX-β-CDs make the molecules disordered and form less hydrogen bonds. Increasing molar amount of $NaIO_4$ caused in increasing oxidation degree of β-CD and leading production of aldehyde functional groups (Zhu et al., 2017; Zi et al., 2018). Therefore, SEM images of OX-β-CD2 and OX-β-CD4 in Figure 3.3 (b, c) confirm the slight degradation with smooth scaly structures. Although the periodate oxidation oxidizes the molecular

structure, it transforms the structure in a very small amount, but it is seen that it does not damage the organic structure much compared to OX-β-CD5 and OX-β-CD7 which contain rough striped and crustal structures on the surface (Figure 3.3 d, e). This result confirms that the molecular structure of OX-β-CD5 and OX-β-CD7 is disrupted when the degree of oxidation is increased.

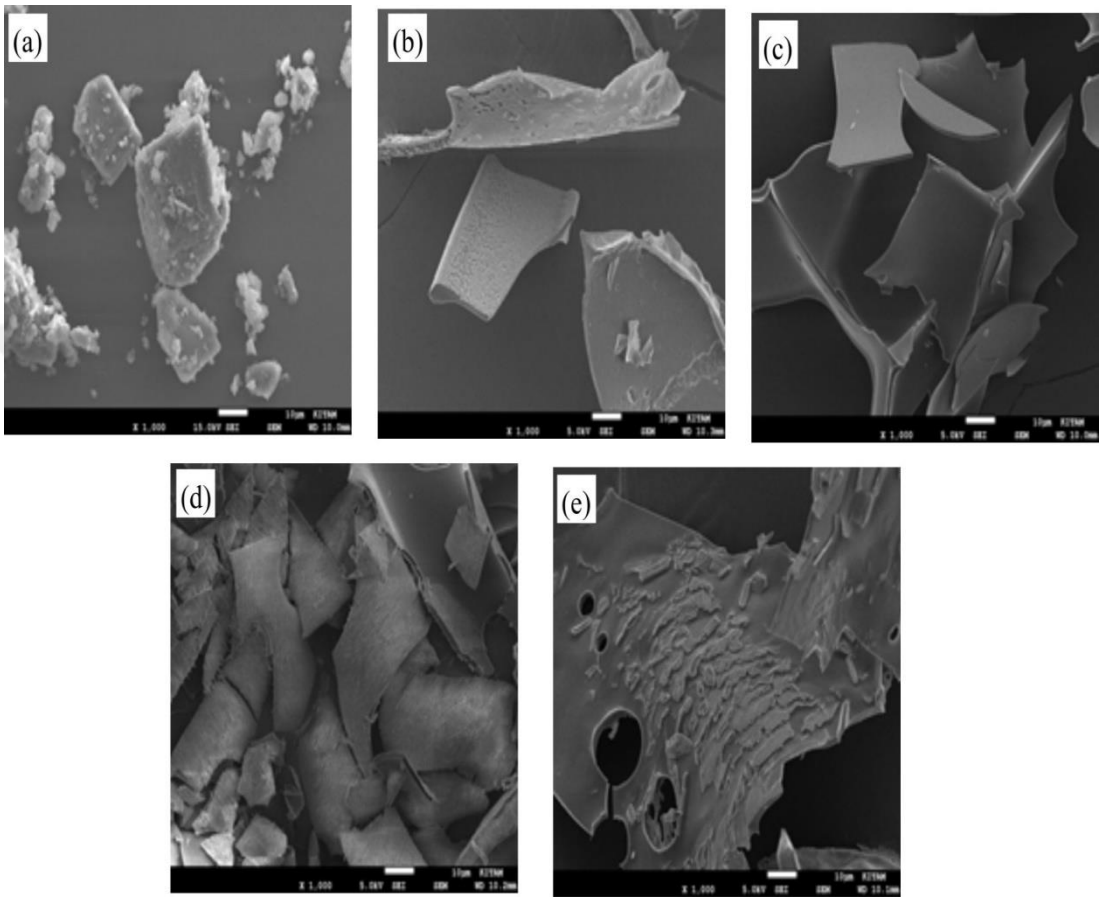

Figure 3.3. SEM image of (a) β-CD (b) OX-β-CD2 (c) OX-β-CD4 (d) OX-β-CD5 and (e) OX-β-CD7 (scale bar: 10μm and resolution: X1000)

XRD were used to determine the crystal structure of β-CD, OX-β-CD2, OX-β-CD4, OX-β-CD5 and OX-β-CD7. XRD patterns in Figure 3.4 reveal so many details of the differences among β-CD and OX-β-CDs.

Several sharp peaks at 2θ= 9.71°, 10.6°, 12.4°, 15.3°, 16.04°, 17.6°, 18.8°, 19.5°, 20.6°, 22.6° and 27.02° are evidently observed in the XRD of β-CD (Figure 3.4), which is demonstrating the crystalline nature (Ye et al., 2017; Ren et al., 2018; Lou et al., 2020). Basically, the crystallization of β-CD can be explained by the ability of multiple hydroxyl groups in their molecular structure to form hydrogen bonds (Ye et al., 2017; Afinjuomo et al., 2019). In OX-β-CDs, some of these hydroxyl groups are

oxidized to aldehyde groups which make the molecules irregular and interaction of the hydrogen bond between molecules is reduced. Especially, as the oxidation degree increases (increase in molar ratio of $NaIO_4$ to β-CD), the crystallinity of OX-β-CDs gradually decrease and also several of these corresponding peaks become weaker (Figure 3.4) or even disappear completely in the patterns of OX- β-CDs which illustrates that OX-β-CD2 and OX-β-CD4 become almost amorphous structure (Figure 3.4). The reason why the crystal structure of OX-β-CD5 and OX-β-CD7 is not amorphous but partially composed of the crystalline peaks is based on deterioration of the molecular structure depending on the higher degree of oxidation and the presence of hemiacetal groups in its structure which form hydrogen bonds with molecules. Although OX-β-CD2 and OX-β-CD4 partially contain hemiacetal group (see NMR spectrum), the less effect of hemiacetal formation on the structure compared to OX-β-CD5 and OX-β-CD7 as well as preservation of its molecular structure (cyclic structure) due to low periodate oxidation explain the reasons why OX-β-CD2 and OX-β-CD4 are amorphous. It has been observed in Figure 3.4 that some XRD peaks of β-CD are also present in the structures formed as a result of oxidation. For example, the XRD peaks at 12.4°, 18.8°, 22.6° and 27.02° are seen in OX-β-CD2, OX-β-CD5 and OX-β-CD7, which is the proof that the oxidized structures have the crystal property of β-CD.

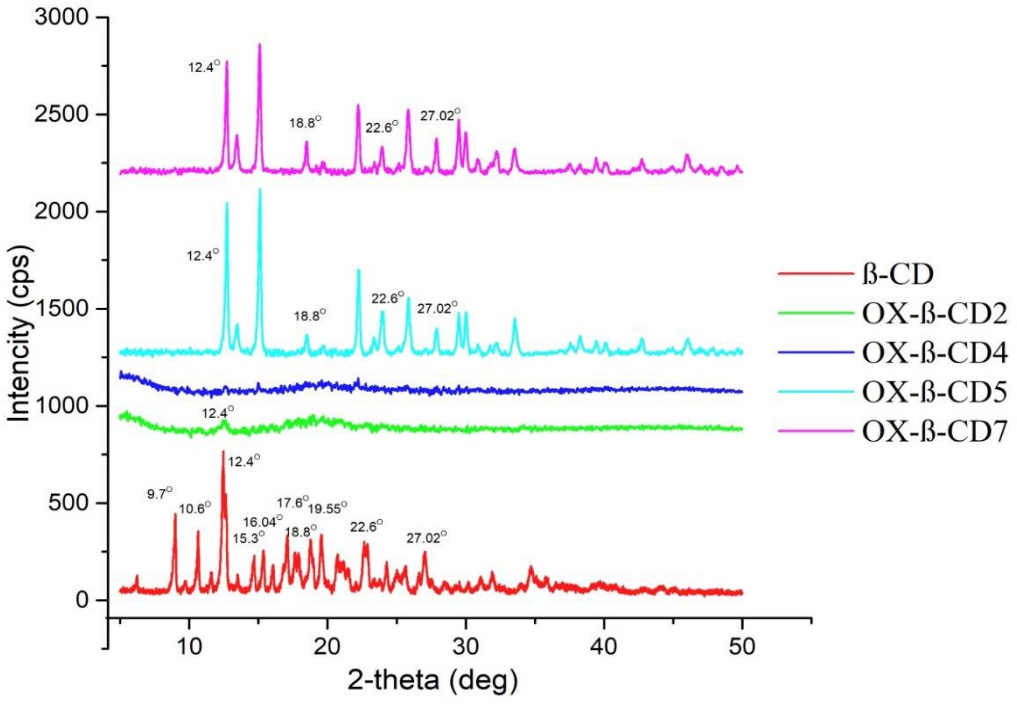

Figure 3.4. XRD image of β-CD, OX- β-CD2, OX- β-CD4, OX- β-CD5 and OX- β-CD7

The ^{1}H-NMR spectra of β-CD and OX-β-CDs were displayed in Figure 3.5. The signals ascribed to the H atom in each glucose at 4.84 ppm (C_1-H), 3.34 ppm (C_2-H), 3.62 ppm (C_3-H), 3.31 ppm (C_4-H), 3.56 ppm (C_5-H), 3.64 ppm (C_6-Ha,b), 5.69 ppm (OH-3), 5.74 ppm (OH-2) and 4.48 ppm (OH-6) are observed in the ^{1}H-NMR spectra of β-CD (Figure 3.5).

As seen in Figure 3.5, the peak intensity of H atoms bonded to O2, O3 and O6 of β-CD decreased remarkably after oxidation, indicating that the OH groups at C_2, C_3 and a bit of C_6 positions of β-CD units are partially oxidized. Aldehyde H proton was expected between 9.0 and 10 ppm (Nonsuwan et al., 2019; Lou et al., 2020) in NMR spectrograph of OX-β-CDs. Therefore, the aldehyde (CHO) protons peaks appeared in the spectrum of OX- β-CD2 (9.20 ppm, 9.31ppm and 9.62 ppm), OX- β-CD4 (9.29 ppm, 9.32 ppm and 9.33 ppm), OX- β-CD5 (9.28 ppm, 9.33ppm and 9.64 ppm) and OX- β-CD7 (9.28 ppm, 9.58 ppm and 9,62 ppm) but were absent in that of β-CD (Figure 3.5).

Moreover, as seen in Figure 3.5, appearance of several distinctive peaks in the ^{1}H-NMR spectra of the OX-β-CDs also be observed in the region of 6.20–7.10 ppm, indicating the inter and intramolecular hemiacetals formation of CHO with neighboring OH groups. Therefore, the formation of hemiacetal groups was proven in the spectrum of OX-β-CD2 (6,30 6,52 7,10 ppm), OX-β-CD4 (6,52 6,82 7,04), OX-β-CD5 (6,51 7,02) and OX-β-CD7 (6,21 6,52 6,82 7,03) in Figure 3.5 but were absent in that of raw β-CD. The same phenomenon has been observed in previous works (Ye et al., 2017; Lou et al., 2020; Ouyang et al., 2022). These observations confirmed the oxidation of OX-β-CD2, OX-β-CD4, OX-β-CD5 and OX-β-CD7 that produced aldehyde groups on the β-CD chain.

As can be seen in Figure 3.5, when the degree of oxidation of β-CD increases, the decrease in the intensity of OH2 and OH3 hydrogen atoms attached to the C_2 and C_3 carbons in the unit of each oxidized product can be considered as evidence of the formation of aldehyde groups in the oxidation process, as well as the formation of intramolecular hemiacetal groups. Most importantly, when the NMR spectrum of OX-β-CD2 and OX-β-CD4 prepared with a lower molar ratio of $NaIO_4$ (2 and 4) is examined, the presence of H atoms attached to each carbon atom and hydroxyl in the spectrum (C_1-H, C_2-H, C_3-H, C_4-H, C_5-H, C_6-H and OH-6) shows that there is no fragmentation based on ring opening in the cyclic structure. On the other hand, as seen

in Figure 3.5, depending on the increasing amount of sodium periodate in OX-β-CD5 and OX-β-CD7, some of the hydrogen peaks (C_1-H, C_2-H, C_3-H, C_4-H and C_5-H) bonded to carbon atoms and hydroxyls disappear in the NMR spectrum of oxidized structure (cyclic structure), indicates that there is degradation in the organic structure of OX-β-CD5 and OX-β-CD7. This result shows that the molecular structure of OX-β-CD5 and OX-β-CD7 deteriorated.

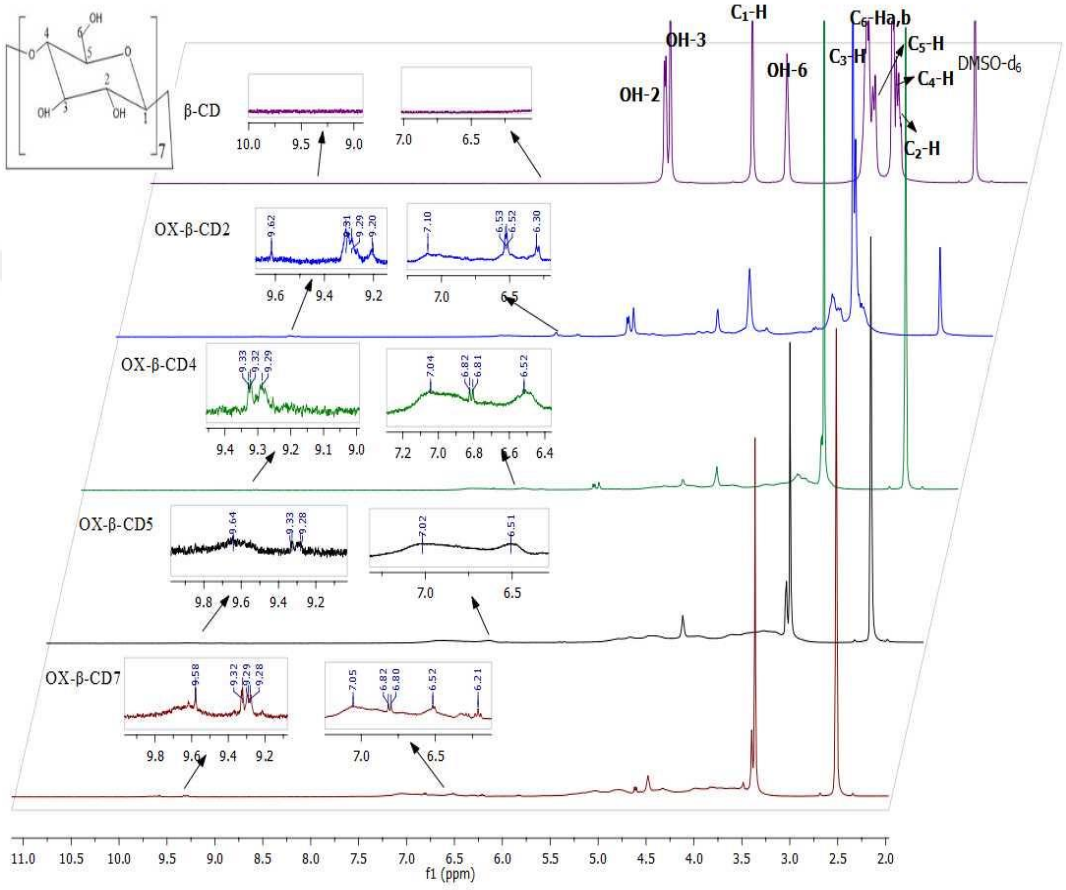

Figure 3.5. ^{1}H-NMR spectra of β-CD and OX-β-CDs (OX- β-CD2, OX- β-CD4, OX- β-CD5 and OX-β-CD7)

3.1.2. Antimicrobial Activity of OX-β-CDs

3.1.2.1. MIC Method

MICs are defined as the minimum antimicrobial concentrations at which microbial growth is inhibited after incubation. The MIC values of β-CD and OX-β-CDs against *E. coli, P. aeruginosa and S. aureus and B. cereus* were measured along with amoxicillin as standard antibiotics and the results are shown in Table 3.3. It is worth noting that all OX-β-CDs presents antibacterial activity against both Gram-positive and Gram-negative bacteria, but raw β-CD has no antibacterial activity

(Figure 3.6 a-d).

OX-β-CDs (16.3 mg/mL), β-CD (16.3 mg/mL) and antibiotic (amoxicillin (2.048 mg/mL) were added to the first well and serially diluted to 12 well. Serial microdilution method is applied to determine the lowest concentration where no bacterial growth was observed to determine MIC value. The photographs in Figure 3.6 (a-d) showed that the growth of bacterial colonies increases as the concentration of the oxidized product decreases. These growths are visible in all MHB broth well containing different concentrations of OX-β-CDs for each bacteria strain except the first well. For example, in OX-β-CD4, it is seen that broth was turbid due to bacterial growth in the 3rd well (at 4.096 mg/mL) for *E. coli* bacteria.

MIC values of OX-β-CDs decreased thus, the antibacterial properties of OX-β-CDs increased with increasing oxidation degree or aldehyde content (Ye et al., 2017; Zhu et al., 2017). For example, it was seen in Table 3.3 that the highest MIC value was observed in OX-β-CD2 in all bacteria species (8192 μg/mL). However, the MIC values of OX-β-CD4, OX-β-CD5 and OX-β-CD7 were found to be the same in both *P. aeruginosa* and *B. cereus* bacterial strains (8192 μg/mL), but lower in both *E. coli and E. faecalis* bacterial strains (4096 μg/mL) compared to OX-β-CD2. Thus, it was seen in Table 3.3 that due to increased aldehyde content of OX-β-CD4, OX-β-CD5 and OX-β-CD7 showed more antibacterial properties compared to OX-β-CD2 in *E. coli and E. faecalis* bacterial culture but nearly the same with those of OX-β-CD2 in *P. aeruginosa* and *B. cereus* bacteria. In addition, it has been observed that the antibacterial properties based on MIC values of OX-P-CD4, OX-P-CD5 and OX-P-CD7 may remain approximately the same in all bacterial strains. This result can be explained in this way. The amount of aldehyde increases due to the increasing degree of oxidation (increasing the Periodate molar ratio) but as previously explained, the aldehyde content may decrease as a result of the inter or intramolecular hemiacetal formations of the oxidized structure and the deterioration in the molecular integrity of the structure unit. Therefore, MIC values look the same in oxidized structures prepared after periodate molar ratio 4.

A former study reported that the MIC values of oxidized β-CD prepared by H_2O_2 oxidation against *S. aureus, E. coli* were found as 4 mg/mL, 8 mg/mL respectively (Ye et al., 2017). The MIC values of dextran aldehyde prepared by $NaIO_4$ against *S. aureus and E. coli* were 4 and 32 mg/mL, respectively (Aziz et al., 2012).

MIC values of oxidized κ-carrageenan prepared by H_2O_2 and copper sulfate against *P. aeruginosa*, *S. aureus and E. coli* were 2 mg/mL 4 mg/mL and 5 mg/mL, respectively (Zhu et al., 2017).

It is known that aldehyde groups are very reactive compounds and can impart antimicrobial activity to oxidized polysaccharides (Zhu et al., 2017). The ability of aldehyde groups to form a strong complex with amine compounds in the bacterial cell membrane structure creates an inhibitory effect on the transport and enzyme systems and causes the deterioration and death of bacterial cells by damaging the bacterial cell wall.

3.1.2.2. Disc Diffusion Method

The antibacterial activity of all OX-β-CDs against *E. coli, P. aeruginosa* and *S. aureus and B. cereus* were determined by measuring their various inhibition zones according to disc diffusion test and the results are given in Table 3.4. The zone of inhibition is a circular area where there is no bacterial growth around an antimicrobial agent. The more sensitive the bacteria are to the antimicrobial agent, the wider the inhibition zone will be on the agar disc. By measuring the diameter of the inhibition zone in mm, evaluations are made according to the standard zone disc and the resistance of the bacteria to the antimicrobial agents used is determined.

As shown in Table 3.4, when the inhibition values of OX-β-CDs in all molar ratios are examined, it has been proven that oxidized β-CDs have high inhibition values compared to control. As can be seen in Table 3.4, inhibition zone was formed in all bacterial cultures in OX-β-CD5 and OX-β-CD7, whereas in OX-β-CD2 and OX-β-CD4, inhibition zone was formed in only three bacterial cultures. This result can be explained by the increased amount of aldehyde in OX-β-CD5 and OX-β-CD7 as a result of the increased $NaIO_4$ molar amount.

It is shown in Table 3.4 that OX-β-CD2, OX-β-CD4 OX-β-CD5 have the highest zone of inhibition (11.0± 00 mm) on *E. coli* compared to *P. aeruginosa and S. aureus and B. cereus*. It was also observed that the inhibition zone value of OX-β-CD7 in *Bacillus cereus* bacteria was even higher than that of Amoxicillin antibiotic and thus exhibits antibacterial properties.

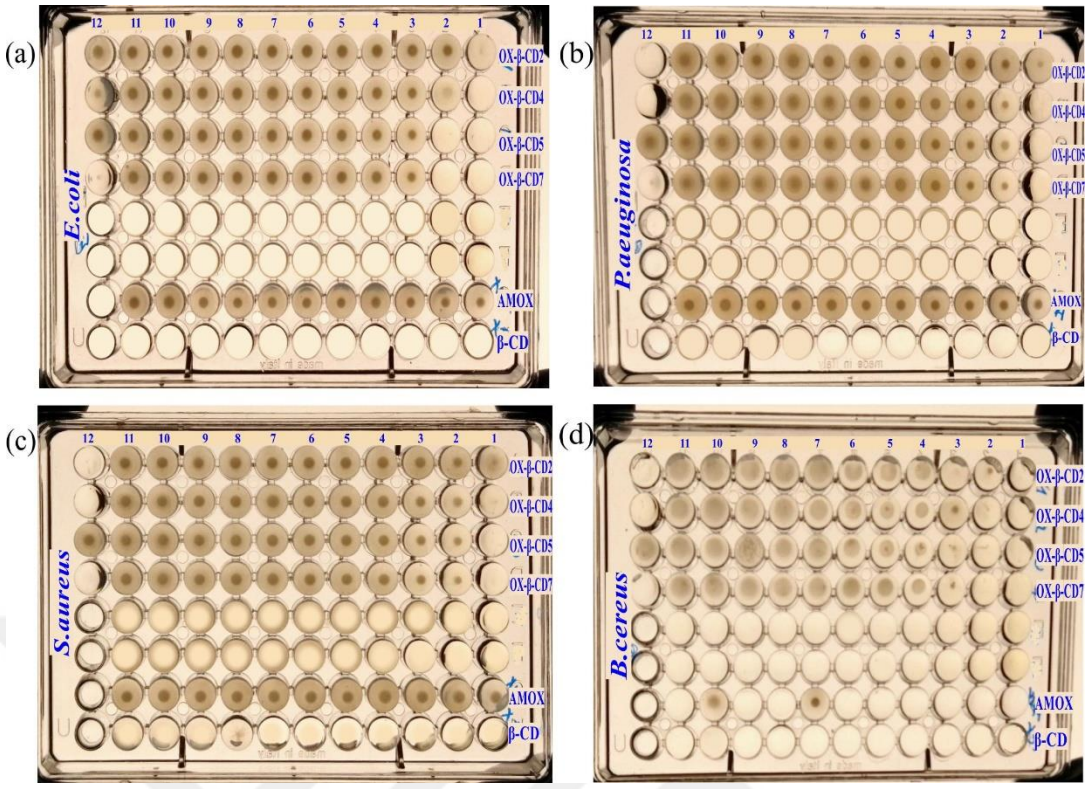

Figure 3.6. Photographs of antibacterial activity of β-CD, OX-β-CDs and Amox (stand-ard antibiotic) containing different concentrations in MHB broth against Gram-negative ((a) E. coli, (b) P. aeruginosa) and Gram-positive ((c) S. aureus and (d) B. cereus)

Table 3.3. Minimal inhibitory concentration (MIC(μg/mL)) of OX-β-CDs against *E. coli,* P. aeruginosa, *S. aureus* and *B. cereus* bacteria

Samples	Gram-negative bacteria		Gram-positive bacteria	
	Escherichia coli	*Psedomonas aeruginosa*	*Staphylococcus aureus*	*Bacillus cereus*
	MIC(μg/mL)	MIC(μg/mL)	MIC(μg/mL)	MIC(μg/mL)
OX-β-CD2	8192	>8192	>8192	8192
OX-β-CD4	4096	8192	8192	4096
OX-β-CD5	4096	8192	8192	4096
OX-β-CD7	4096	8192	8192	4096
Amoxcillin	<1024	<1024	<1024	1024<
β-CD	NA	NA	NA	NA

NA: No activity.

Table 3.4. Antibacterial activity of OX-β-CDs against *E. coli*, *P. aeruginosa*, *E. faecalis* and *B. cereus* by disc diffusion method

Samples	Gram-negative bacteria		Gram-positive bacteria	
	Escherichia coli	*Psedomonas aeruginosa*	*Staphylococcus aureus*	*Bacillus cereus*
	inhibition zone (mm)	inhibition zone (mm)	inhibition zone (mm)	inhibition zone (mm)
OX-β-CD2	11.0±0.0	10.0±0.0	9.0±0.0	NA
OX-β-CD4	11.0±0.0	9.0±0.0	8.0±0.0	NA
OX-β-CD5	11.0±0.0	9.0±0.0	8.0±0.0	7.0±0.0
OX-β-CD7	9.0±0.0	10.0±0.0	10.5±0.7	9.5±0.7
Amoxcillin	28.0±0.0	NA	40.0±0.0	8.0±0.0
Control	6.0±0.0	6.0±0.0	6.0±0.0	6.0±0.0

NA: No activity.

3.2. Synthesis of Aldehyde Nanosponge (ALD-NS)

All these studies have shown that OX-β-CDs prepared with higher sodium periodate molar ratio more than molar 4 will lose its ability to form complexes with some molecules, since there will be deterioration in their structural integrity, especially in the hydrophilic cavity. Therefore, OX-β-CD4 prepared with periodate molar ratio 4 was seen as the best optimum synthesized structure in terms of both the high aldehyde amount or oxidation degree and the preservation of structural integrity. So, white solid Aldehyde Nanosponge (ALD-NSs) was obtained (Figure 3.7) in the reaction of OX-β-CD4 and PMDA crosslinker using OX-β-CD4: PMDA 1:2, 1:4 and 1:6 molar ratios with the method described in experimental section and they named as ALD-NS2, ALD-NS4 and ALD-NS6 based on molar amount used for preparations.

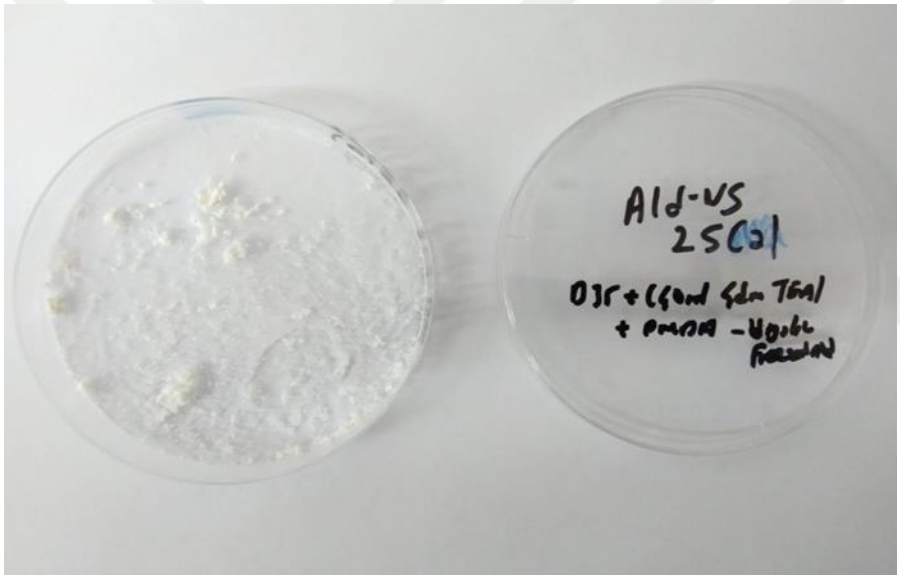

Figure 3.7. Image of synthesized ALD-NS

In order to determine which of the ALD-NSs synthesized with different molar ratios shows the optimum value, a drug loading study was conducted on ALD-NSs with a different drug containing the NH_2 group. For this purpose, AMOX model drug was selected, and the amounts of AMOX in the nanocarrier were calculated using the standard calibration curve of AMOX in methanol at 272 nm (see Appendix 2). The experimental procedure and all the characterization results of AMOX loaded ALD-NS are explained in Appendix 2.

Figure 3.8 also shows the picture of the AMOX-loaded nanostructure obtained in the drug loading study. The amount of AMOX was calculated from the standard

calibration chart of AMOX by taking the UV-vis spectrum at 272 nm of each molar ratio aqueous solution. As can be seen in Figure 3.8, the color of the aqueous solution of ALD-NS4 prepared with molar ratio 4 is lighter than ALD-NS2 and ALD-NS6. This result is an indication that AMOX loaded into the nanostructure obtained in molar ratio 4 more than those obtained from other molar ratios. Apart from this, the drug loading percentages obtained from the standard calibration curve of AMOX were calculated (see Appendix 2) . It is found to be 14,90% for ALD-NS2, 24,46% for ALD-NS4 and 22,05% for ALD-NS6. Thus, the highest AMOX loading ratio was observed (24.46%) in ALD-NS4 synthesized with a molar ratio of 1:4. Therefore, 1:4 molar ratio of OX-β-CD4: PMDA was selected to synthesis of ALD-NS for further studies.

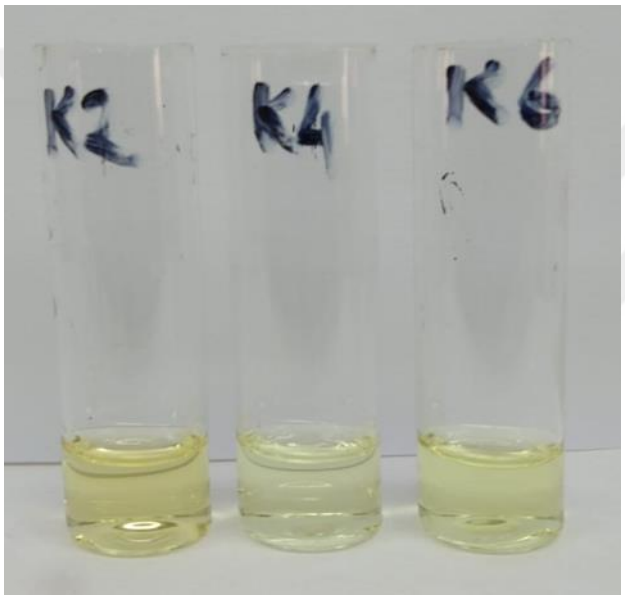

Figure 3.8. Picture of AMOX loaded ALD-NS Nanocarriers (K2: ALD-NS2, K4: ALD-NS4, K4: ALD-NS6) in methanol prepared by three molar ratios of OX-β-CD: PMDA

3.2.1. Characterization of ALD-NS

Figure 3.9 displays the characteristic sharp FT-IR absorption band of ALD-NS at 1721 cm^{-1} which is ascribable to combination of carbonyl (C=O) stretching vibration of the aldehyde and carboxylate linkage. Accordingly, the appearance of carbonyl functional group bands in the spectra of ALD-NS confirmed the cross-linking reaction between PMDA crosslinker and OX-β-CD4 and the formation of ALD-NS. However, a slight downward aldehyde vibration shift was observed in terms of actual aldehyde band at 1730 cm^{-1} due to ALD-NS formation. Other characteristic absorption bands observed for ALD-NS included peaks at 3330 cm^{-1} due to O-H stretching, 1151 cm^{-1} C-O-C stretching and 1077 cm^{-1} C-O stretching vibration band.

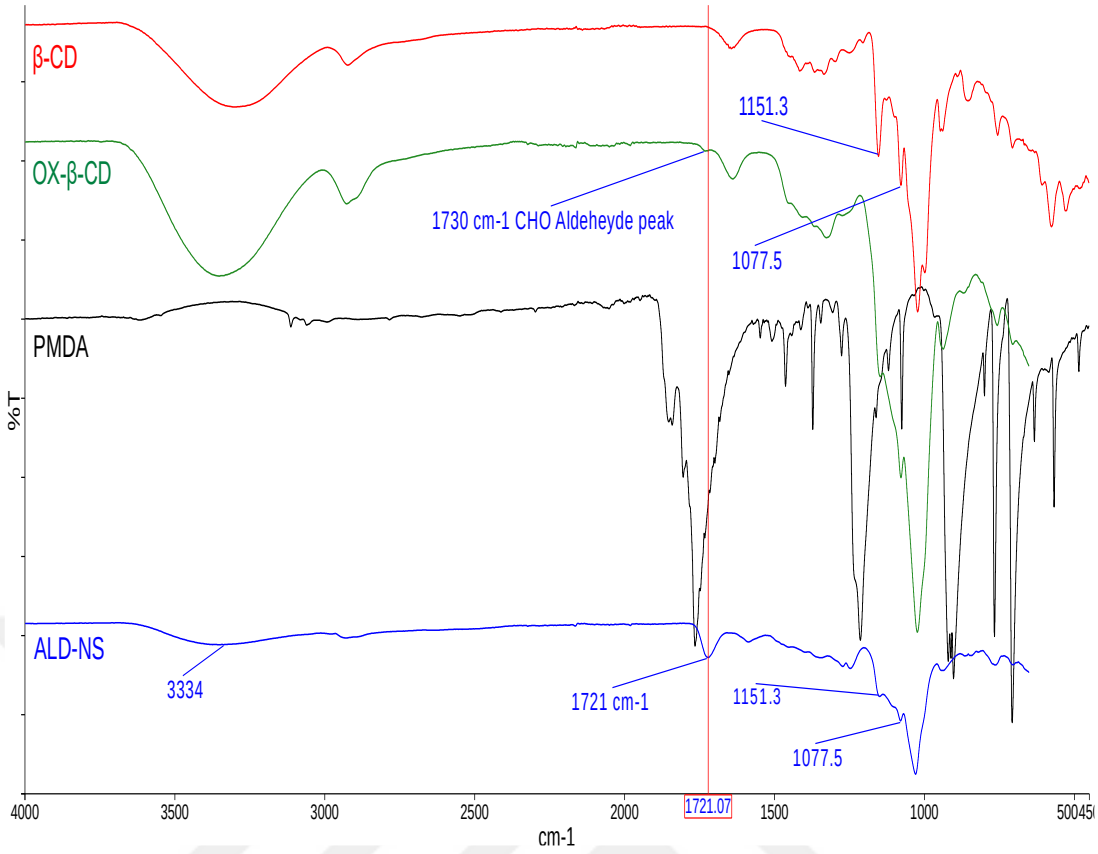

Figure 3.9. FTIR Spectrum of synthesized ALD-NS Nanocarriers

Figure 3.10 shows the proton NMR spectrum of synthesized ALD-NS. For Schiff base formation, if there is an aldehyde group in the synthesized structure, the characteristic CHO peak should be observed in the 9-10 ppm range of the spectrum. As seen in Figure 3.10, the presence of H peak in CHO bound at 9.25 ppm and an H peak in aromatic rings at 8.51 ppm indicates that ALD-NS contains an aldehyde group.

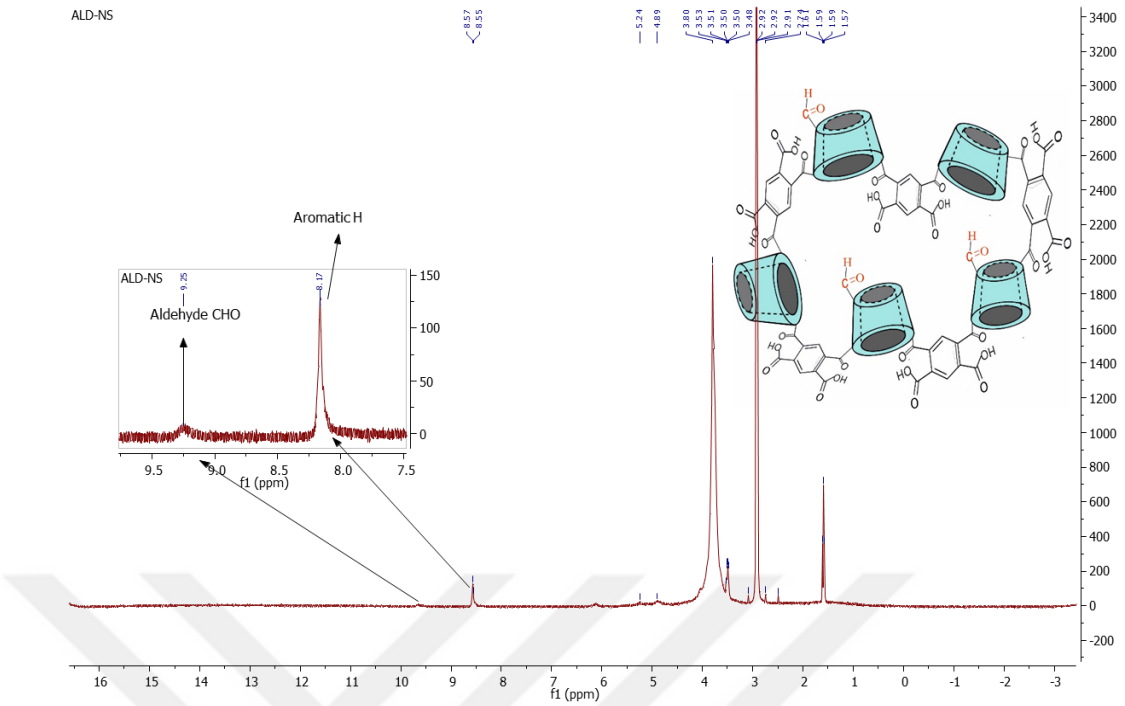

Figure 3.10. ^{1}H-NMR Spectrum of synthesized ALD-NS Nanocarriers

In conclusion, characterization studies have successfully proven that the intended ALD-NS nanocarrier synthesis was successfully achieved.

3.3. Integration of DOX.HCl Anti-Cancer Drug onto ALD-NS

3.3.1. Synthesis of ALD-NS+DOX Complex

The integration of the DOX drug into the nanostructure is predicted by performing it in two mechanisms, as shown in the schematic structure in Figure 2.5 above. The first stage of these can be explained as the acidic environment-sensitive bond (Schiff base bond) that will form between the CHO group of ALD-NS and the NH_2 group of the DOX, and the second stage can be explained as the inclusion of the drug in the hydrophilic cavity of the nanostructure. Thus, the amount of drug loading to the nanostructure and the drug release in the acidic environment would be increased.

3.3.2. Characterization of Drug Loaded ALD-NS+DOX Complex

3.3.2.1. UV-vis, FTIR, SEM, TGA, XRD, ^{13}C-NMR, PS, ZP Measurement

Encapsulation and integration of DOX into the ALD-NS nanocarrier was confirmed and monitored by UV-vis absorption spectroscopy study. Figure 3.11(a,b,c) shows the UV-vis spectra of the aqueous solutions of DOX.HCl, ALD-NS nanocarrier

and ALD-NS+DOX complex. In Figure 3.11(a), three main absorption peaks at 233 nm, 477 nm and 494 nm were observed in the spectrum of free DOX.HCl in methanol. At 295 nm, the characteristic absorbance peak of ALD-NS was observed in the spectrum in Figure 3.11(b).

As seen in Figure 3.11(c), after loading DOX into the ALD-NS nanocarrier, the disappearance of the peak at 233 nm and the presence of the characteristic peak of ALD-NS at 295 nm, as well as the DOX characteristic peak at 494 nm, are clear indications of the formation of ALD-NS+DOX complex. In addition, absorption peaks at 246-252 nm corresponding to the Schiff base groups (Fonkui et al., 2019) were observed both in the ALD-NS nanocarrier before and after DOX- encapsulation and integration, which confirmed that both the ALD-NS nanocarrier and the DOX loaded ALD-NS complex contains Schiff base groups.

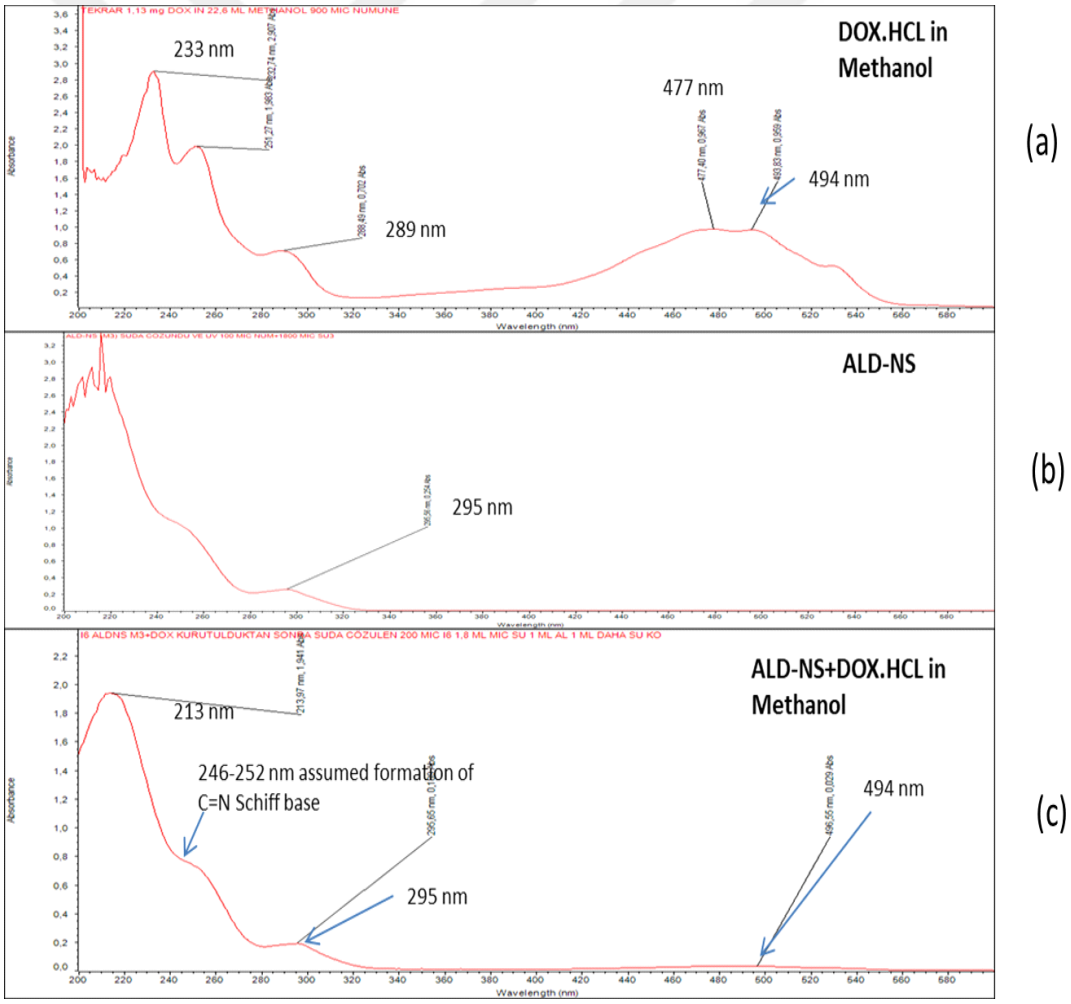

Figure 3.11. UV-vis Spectrum of (a) DOX.HCl, (b) ALD-NS nanocarriers and (c) DOX loaded ALD-NS complex in Methanol

To investigate the formation of inclusion complex of DOX with the ALD-NS

nanocarrier, FTIR analysis was performed. FTIR spectra of pure DOX, ALD-NS and ALD-NS+DOX inclusion complexes are presented in Figure 3.12. The FT-IR spectrum of DOX in Figure 3.12 shows band at 3319 cm-1 due to symmetric stretching vibrations of primary amine group (NH_2). The band at 3528 cm^{-1} is due to OH stretching vibration and the band about 1523 cm^{-1} is due to symmetric bending vibration of NH_2 in pure DOX. As can be seen in Figure 3.12, the NH_2 group of the amine at 3319 cm^{-1} belonging DOX and the NH_2 bending vibration of DOX at 1523 cm^{-1} disappeared as a result of binding to CHO group of ALD-NS. The result of Schiff base binding is seen with the formation of the C=N bond of ALD-NS+DOX at 1645 cm^{-1}(Su et al., 2018). A characteristic band corresponding to the stretching of C=N (1650~1590 cm^{-1}) was also observed in some studies (Xiong et al., 2015).

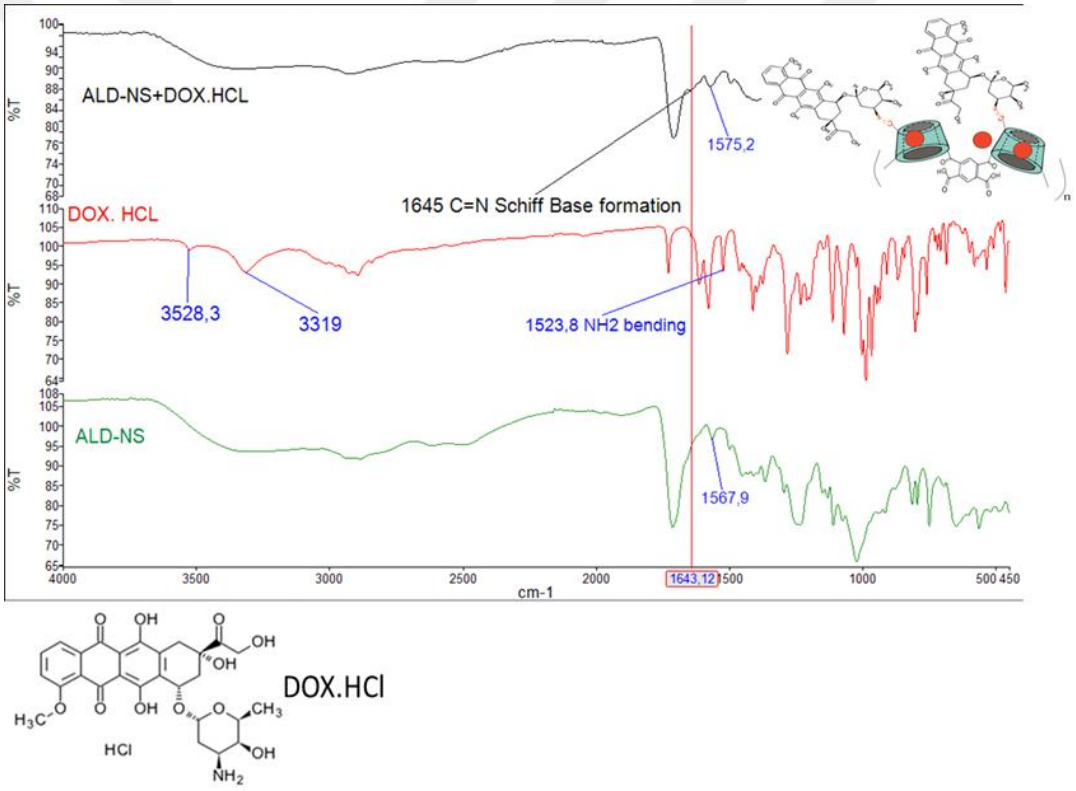

Figure 3.12. FTIR Spectrum of DOX.HCl, ALD-NS nanocarrier and DOX loaded ALD-NS

The surface morphology of DOX.HCL, ALD-NS and ALD-NS+DOX were examined using SEM (Figure 3.13). Unlike ALD-NS and ALD-NS+DOX, DOX.HCL demonstrated highly rough surfaces in square and rectangular crystals shapes of different sizes. However, ALD-NS exhibits both needle or rod shape image and hard irregular crystal structures of different sizes, while the ALD-NS+DOX surface exhibit a rough porous and smooth surface in the porous matrix verifying the formation of

integration and encapsulation of the drug. The same phenomena were observed in rod shape image of $CaCO_3$/Dox nanoparticle (Kamba et al., 2013) or irregular and not spherical-like crystals in physical mixtures of dendrimer/DOX (Kamba et al., 2013; Yousef and Hassan, 2017).

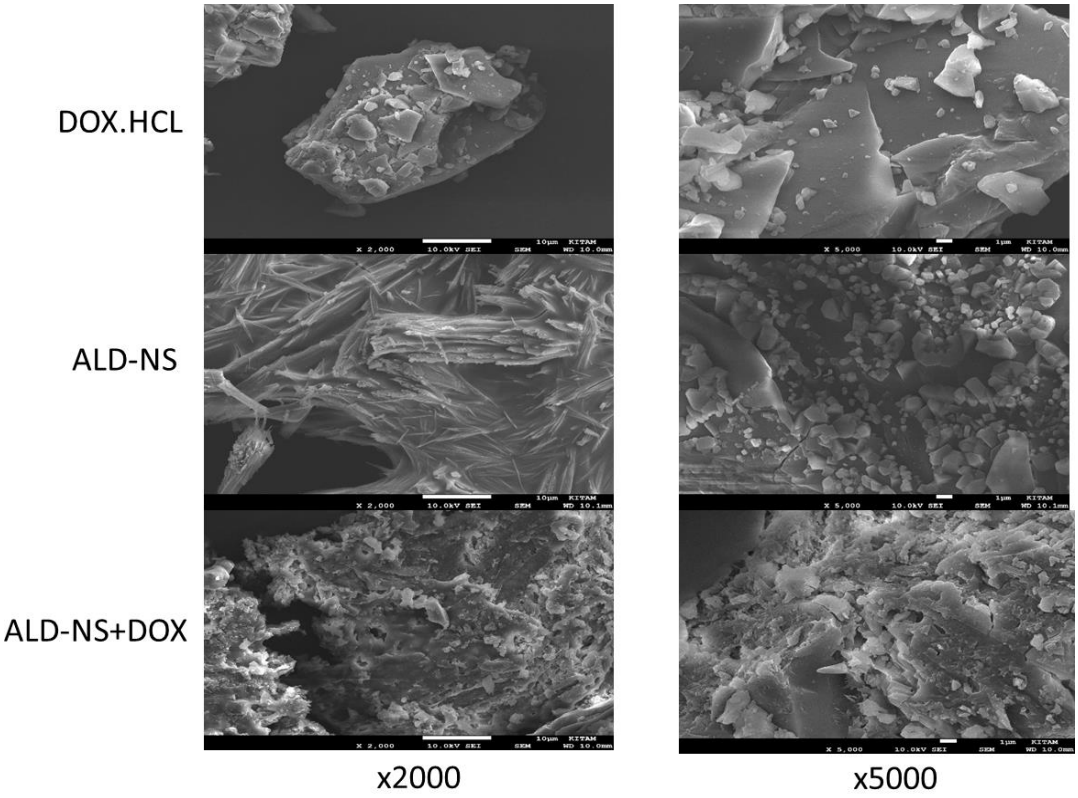

Figure 3.13. SEM image of DOX.HCl, ALD-NS and DOX loaded ALD-NS complex with x2000 and x5000 magnification

Thermal behavior of DOX.HCl, OX- β- CD, ALD-NS drug carrier and physical mixture of ALD-NS+DOX complex were investigated and TGA data of all samples from 30°C to 700°C are shown in Figure 3.14. The TGA thermogram of free drug, OX- β- CD, ALD-NS and ALD-NS+DOX complex exhibits a first endothermic peak around 100°C which could be the initial weight loss as a result of evaporation of adsorbed water. As can be seen in Figure 3.14 that multiple degradation profile was observed in TGA curve of the free DOX (Fasiku et al., 2019).

The % initial weight loss in the DOX.HCl was 3% at 209.7 °C followed by sudden sharp weight loss of 29% at 252.9 °C respectively. The % weight loss in the ALD-NS carrier was 9.3% at 178.37 °C followed by gradual weight loss. The next weight loss of DOX, OX- β- CD and ALD-NS observed around 209°C, 240.7 °C, 178.3°C and 158°C respectively, could be related to the decomposition or degradation

of samples. In addition, the temperatures at which 50% weight loss of pure drug, OX-β- CD, ALD-NS carrier and ALD-NS+DOX complex occurred were around 571.4°C, 291.0 °C, 306.9 °C and 404.7 ^{0}C respectively. Among all samples, 50% weight loss at the lowest temperature occurs in OX- β- CD.

As displayed in the TGA curves of ALD-NS+DOX complex in Figure 3.14, the pattern of weight loss temperature of sample is completely different to that of pure ALD-NS and DOX.HCl. The flattening profile of the ALD-NS+DOX complex in Figure 3.14 without sudden and sharp weight loss can be considered as definitive proof of the molecular integration of DOX in ALD-NS. This confirms successful linking of DOX in the target polymers. In addition, 50% weight loss is observed to be the lowest after the pure drug at high temperature when compared to other samples, confirming the integration between the drug and the nanocarrier.

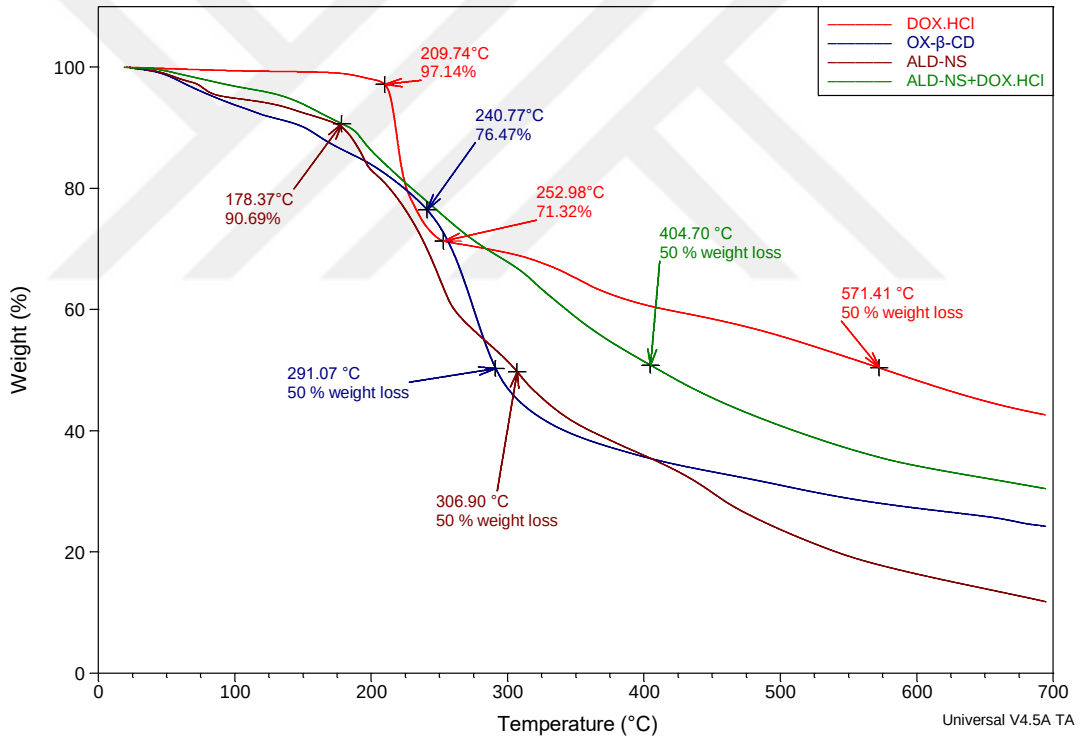

Figure 3.14. TGA image of DOX.HCl, OX-β-CD, ALD-NS nanocarrier and ALD-NS+DOX complex

^{13}C-NMR spectra were used to characterize the imine (C=N) compounds of ALD-NS+DOX complex. The spectra of the compounds were recorded in DMSO- d6 solution and the obtained data has been given in Figure 3.15. The ^{13}C-NMR spectra in Figure 3.15, C=N signals of imine of the synthesized Schiff bases were observed around δ=167.6 ppm as expected (Fonkui et al., 2019). The imine carbons R-CH=N-

R at δ=155–168 ppm was also observed in some studies (Dalgıç et al., 2020). ^{13}C-NMR spectrum confirmed the successful synthesis of the drug loaded nanocarrier bearing Schiff bases.

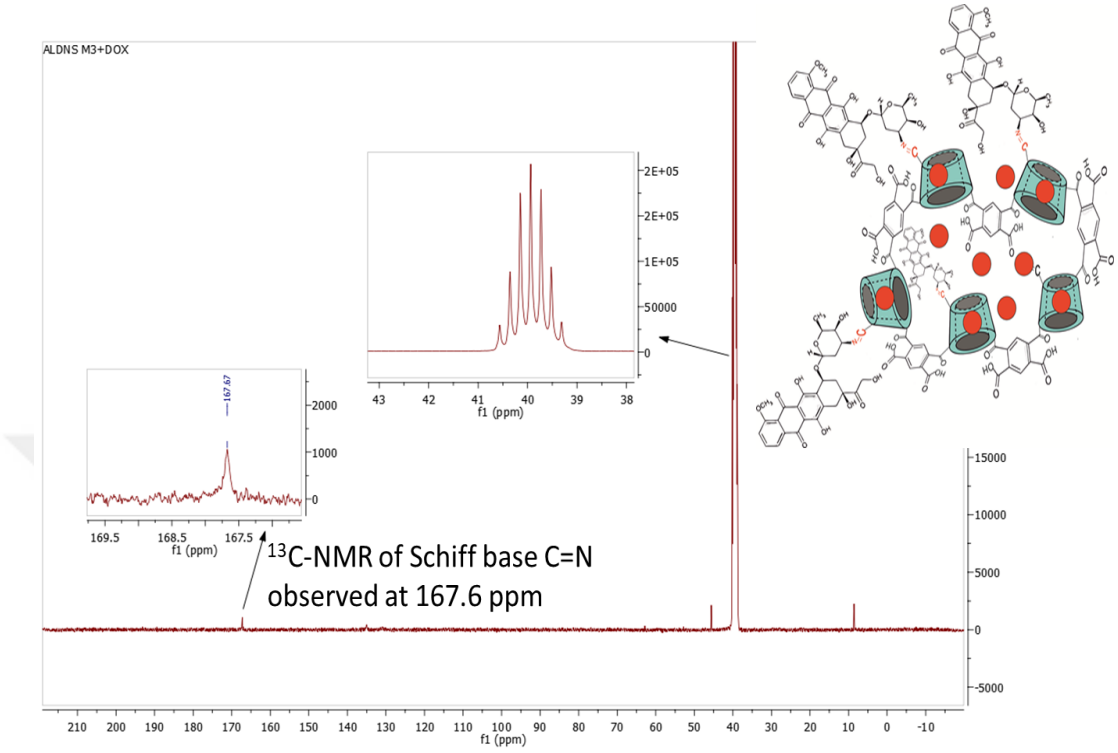

Figure 3.15. ^{13}C-NMR Spectrum of DOX loaded ALD-NS nanocarriers

The XRD technique was applied on account of understanding and evaluating the morphological alteration in the crystallinity and structure of the sample.

Figure 3.16 shows the XRD patterns of β-CD, OX-β-CD, DOX.HCl, ALD-NS nanocarrier and ALD-NS+DOX.HCl complex. In Figure 3.16, multiple distinctive sharp peaks at 2θ 8.8°, 10°, 11.6°, 13.1°, 15°,17.3°, 18.5°,19.3°, 21.9°, 24°, 25.1°, 26.2°, 30.5°, 31.06°, 33.3°, 34.4°, 35.6° and 36.5° respectively, were seen in the XRD pattern of DOX.HCl (Yousef and Hassan, 2017). Several sharp peaks clearly observed in the XRD of β-CD, indicating its crystalline structure. Note that most of peaks have disappeared in the XRD patterns of OX-β-CD (Figure 3.16) indicating O-β-CD is almost amorphous. When the XRD structure of ALS-NS is examined, it is seen in Figure 3.16 that it has an almost amorphous structure, except for a few peaks. However, a broad band pattern with several peaks was observed in the case of ALD-NS+DOX implying the slightly amorphous nature of this complex. This phenomenon is also observed in some studies indicating most of distinctive peaks of DOX

disappeared and the crystallinity of DOX alter to amorphous state (Zha et al., 2020). Interestingly, some of peaks corresponding to the DOX were not observed in the XRD pattern of ALD-NS+DOX in Figure 3.16, which confirmed the formation of Schiff base connection bond as well as integration of hydrophilic parts between ALD-NS and DOX, and consequently it could be concluded that complex was formed.

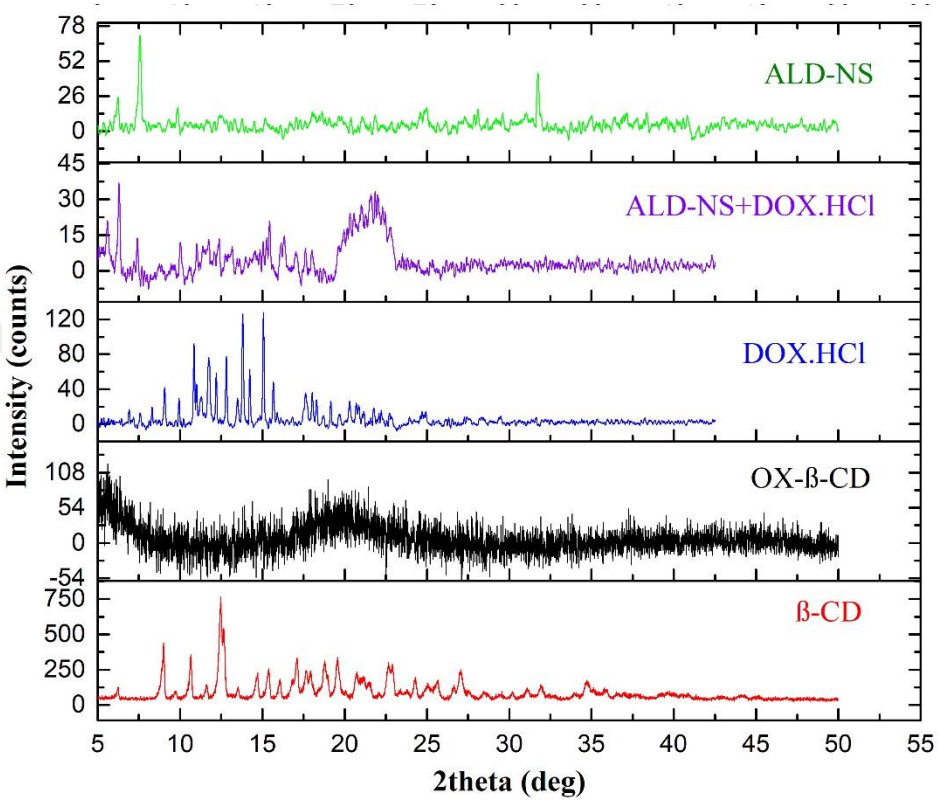

Figure 3.16. XRD image of DOX.HCl, β-CD, OX-β-CD, ALD-NS nanocarriers and DOX loaded ALD-NS complex

3.3.2.2. PS and ZP Measurement

PS and ZP(ζ) are the primary criteria that have an impact on influencing the biological behavior of nanomaterials, such as stability, toxicity, in vivo distribution or bioavailability. PS distribution by intensity curves and ZP(ζ) values of β-CD, OX-β-CD, ALD-NS, DOX.HCl and ALD-NS+DOX complex for each formulation are presented in Table 3.5. Amongst the prepared formulations, β-CD demonstrated the smallest particle size (215 nm). In OX- β-CD, a slightly larger particle size (240 nm) was observed due to the presence of aldehyde groups which formed as a result of oxidation. Whereas DOX.HCl exhibited larger and the highest average particle size (392 nm) values among them. The particle size of the ALD-NS+DOX (372.7 nm) complex demonstrated higher particle size compared to those of the corresponding the

unloaded ALD-NS (323 nm) form (Figure 3.17). However, such an increase could be attributed to Schiff base covalent bonding and drug encapsulation.

As can be seen on Table 3.5 that the mean ZP (ζ) values obtained for all the formulations were negative. Since high ZP(ζ) values (≥ ± 30 mV) are considered reasonable and indicative of a strong repulsive force between particles meaning lower aggregation tendency of particles and higher stability (Bischoff et al., 2020). The ζ value was found to −25.1 mV for ALD-NS nanocarriers in the absence of DOX. However, in the presence of the negatively charged DOX in ALD-NS nanocarriers, the ζ value decreased and was found around −12.8 mV. This decrease in ZP value of ALD-NS+DOX complex in presence of DOX might indicate Schiff base interaction between DOX drug and the nanocarrier. Higher negative ZP(ζ) values of different nanocarrier formulation that was prepared with DOX.HCl was also observed in some studies (Tahir et al., 2019; Dalgıç et al., 2020; Behera et al., 2021).

When the PDI values of samples were compared, which is a parameter used to define the size range of nanocarrier systems or the distribution of size populations in a particular medium for in vitro and in vivo applications, the lowest value was obtained in OX-β-CD (Table 3.5).

Table 3.5. PS, ZP, PDI, EE and DL values of aqueous dispersions of DOX.HCl, β-CD, OX- β- CD ALD-NS and drug loaded ALD-NS+DOX

Formulation	**Particle Size (nm)**	**Mean Zeta Potential (ζ, mV)**	**Polydispersity index (PDI)**	**Entrapment Efficiency (EE) (%)**	**Loading Capacity (DL) (%)**
DOX.HCl	392±2.30	– 27.20±1.05	0.319		
β-CD	215±24.10	-23.40±1.08	0.239		
OX- β- CD	240±4.54	-32.50±1.25	0.053		
ALD-NS	323±5.52	-25.10±1.54	0.254		
ALD-NS+DOX.HCl	372±8.21	-12.80±2.74	0.421	85.53±1.74	8.089 ±1.320

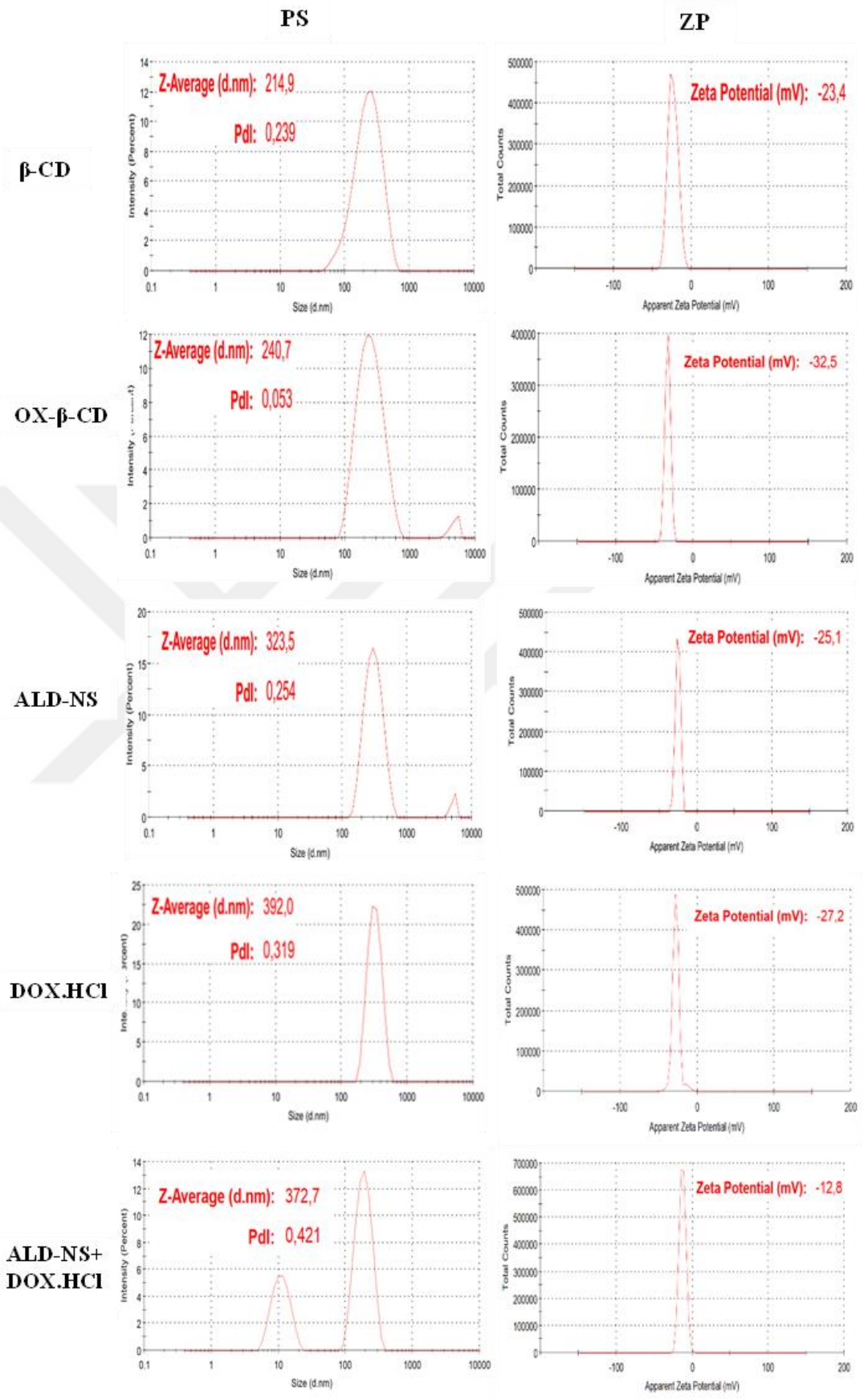

Figure 3.17. PS and ZP (ζ) values of DOX.HCl, β-CD, OX-β-CD, ALD-NS nanocarriers and loaded ALD-NS+DOX complex

The PDI value of the drug-loaded nanostructure, on the other hand, was the highest due to the increase in particle size as a result of multiple loading. The PDI value ranges from 0.0 (molecular particle size is homogeneously distributed and in the same size) to 1.0 (particle size in the population is not homogeneously distributed in the same size, not constant or the sample is dispersed in different sizes) according to the particle size (Danaei et al., 2018). Values higher than 0.7 are not preferred in drug delivery applications because they have a wide particle size distribution and are not suitable for analysis by DSL technique (Danaei et al., 2018). Nanostructures with PDI values between 0.1- 0.4 are considered acceptable as they show moderate polydispersity (Costa et al., 2022).

3.3.2.3. Drug EE and DL Calculation

Before calculating the drug loading effect and capacity, the standard calibration curve graph of the DOX.HCl drug was obtained, and results are shown in Figure 3.18.

Average DL and EE of ALD-NS+DOX complex was obtained by drug loading experiment and the values were calculated from standard calibration curve of DOX. The results are summarized in Table 3.5. Observations revealed very high EE (85.53 %) and DL (8.089%) content for DOX loaded nanocarriers compared to the other studies conducted with the same drug using different nanocarriers (Hervault et al., 2016). The possible explanation is that the drug is both integrated into the hydrophilic outer surface of the nanostructure and attached with C=N Schiff base bond between drug and nanocarrier (aldehyde groups (–CHO) of nanocarrier can bind to the amin group (-NH_2) of DOX by electrostatic interaction). In some studies, it has been reported that drug loading was achieved below 1%, depending on the use of hydrophilic DOX (water-soluble form) and the type of nanocarriers (Yildiz et al., 2018).

Cont. (mg/ml)	Abs at 494 nm
0.0545	1.765
0.0500	1.631
0.0462	1.504
0.0429	1.384
0.0400	1.297
0.0375	1.215
0.0353	1.139
0.0333	1.079
0.0316	1.02
0.0300	0.967

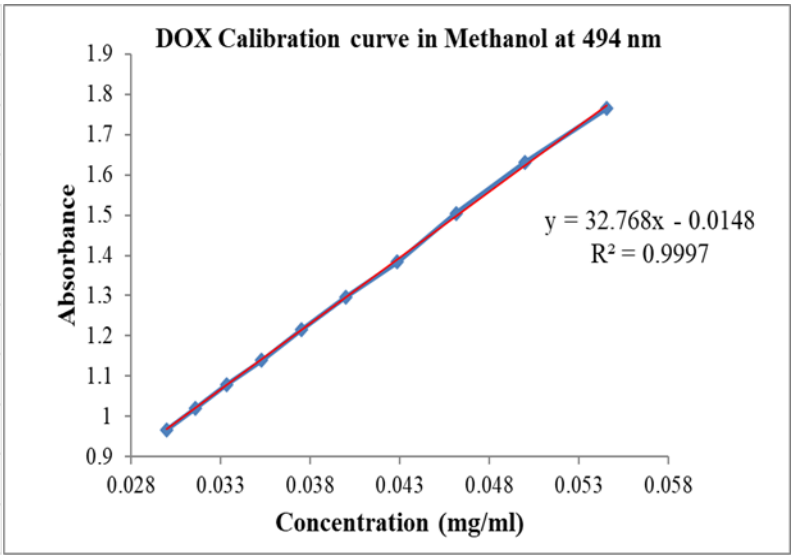

Figure 3.18. Standard calibration curve of DOX.HCl in Methanol

3.3.3. In Vitro DOX Release Studies from ALD-NS+DOX Complex

In vitro pH-triggered release profile of plain DOX dispersion and drug from ALD-NS+DOX formulation was evaluated at 37°C under three different physiological conditions (0.1M PBS at pH 7.4, 0.1M PBS at pH 5.2 and 0.1M NaOAc buffer at pH 5.2) to simulate the lysosomal and tumor intracellular extracellular environment. Figure 3.19 displays cumulative in vitro release profile of drug from ALD-NS+DOX and plain DOX itself. As shown in Figure 3.19, the drug release behavior of ALD-NS+DOX demonstrated an apparent pH-sensitive property and as expected, a slow, controlled and prolonged sustained in vitro release profile of the drug was observed. However, an obvious initial burst release behavior was seen in the first hours for both pure drug and the drug loaded nanocarrier at all pH values. This could be ascribed to the hydrophilic nature of DOX in lower pH and amount of drug existing near the nanocarrier surface.

Free DOX was released quickly (rapid-burst effect) at pH 5.2 in the initial stage and the maximum release of free DOX reached 92,5% in NaOAc buffer and 87.9% in PBS buffer at 24 h of incubation respectively. However, 26.4% of the free DOX at pH 7.4 was released in maximum from PBS buffer after 8 hr. These results showed that the release amount of free DOX is faster in an acidic environment. However, the very rapid drug release profile showed that DOX was completely released after 24 h. “Protonation of the amine groups of pure drugs at low pH may cause partial decomposition of hydrogen-bonding interaction” (Yaghoubi et al., 2022). A rapid

release profile of free drug from different buffer solutions and pH values was also observed in most studies (Nikravan et al., 2019; Yaghoubi et al., 2022).

It is seen in Figure 3.19 that DOX released profile much higher in the acidic mediums at pH 5.2 than that of medium at pH 7.4. In addition, Initial fast drug release effect was also observed from the nanostructure in 8 hours in both acidic buffers at pH 5.2 and natural buffer at pH 7.4 (27.01%), confirming DOX bonding on the nanocarrier by C=N bond. The reason is because the chemical bound (Schiff base) between the CHO functional group added to the nanostructure and the NH_2 group of the drug occurs on the surface of the nanostructure and accordingly the drug release starts on the surface (hydrolysis of the bond in acidic environment) (Fan et al., 2019). In addition, when the drug release in 2 different acidic environments is compared, it was seen in Figure 3.19 that the release of pure DOX as well as the drug from nanocarrier from NaOAc buffer environment was higher than the drug release from PBS buffer condition at same 24 h. For instance, the release of pure DOX from the NaOAc and PBS buffer solution was 92.5 %, and 87.9%, while the release of DOX from the nanocarrier was 64.6% and 62.4% respectively. However, later drug release in amount from nanocarrier in NaOAc buffer is slightly decreased compared to PBS environment.

The cumulative release of DOX from ALD-NS+DOX from PBS at pH 5.2 and from NaOAc buffer at pH 5.2 was 66.8% after 72 h and 64.83 % after 48 h respectively. DOX release from both acidic environments showed a sustained slow DOX release profile after 48 h and 72 h till 168 h compared to free DOX release at same time interval. However, DOX release from PBS at pH 7.4 was only 32.9% in 72 hours. Nevertheless, it exhibited a longer duration of DOX release profile, achieving a maximum drug release of 44.74% at 168 h (Figure 3.19). Some studies also verify that DOX release profile in acidic pH environment much higher than that of physiological (pH 7.4) environment (Islami et al., 2018; Argenziano et al., 2020).

As a result, the constant, continuous and sustained drug release could have been due to the entrapment of DOX in the hydrophilic part of the nanostructure as well as acid-sensitive Schiff base bonding. This is due to the acidic pH value promotes the hydrolysis of the Schiff base bond among nanocarrier and the chemically linked DOX, leading to the release of the drug. Furthermore, hydrophilicity and slight pH sensitivity of DOX also contributed to releases when the pH value descended to 5.2 (microenvironment of cancer cells) (Tahir et al., 2019).

Therefore, drug release from the nanostructure in low pH was much higher due to Schiff base, high drug loading capacity than the pure drug in the same environment. It was found that drug-loaded nanocarrier showed a pH dependent drug release profile and drug release at acidic pH demonstrates the potential for release and targeted tumor drug delivery of the pH-sensitive drug-nanocarriers coupled system.

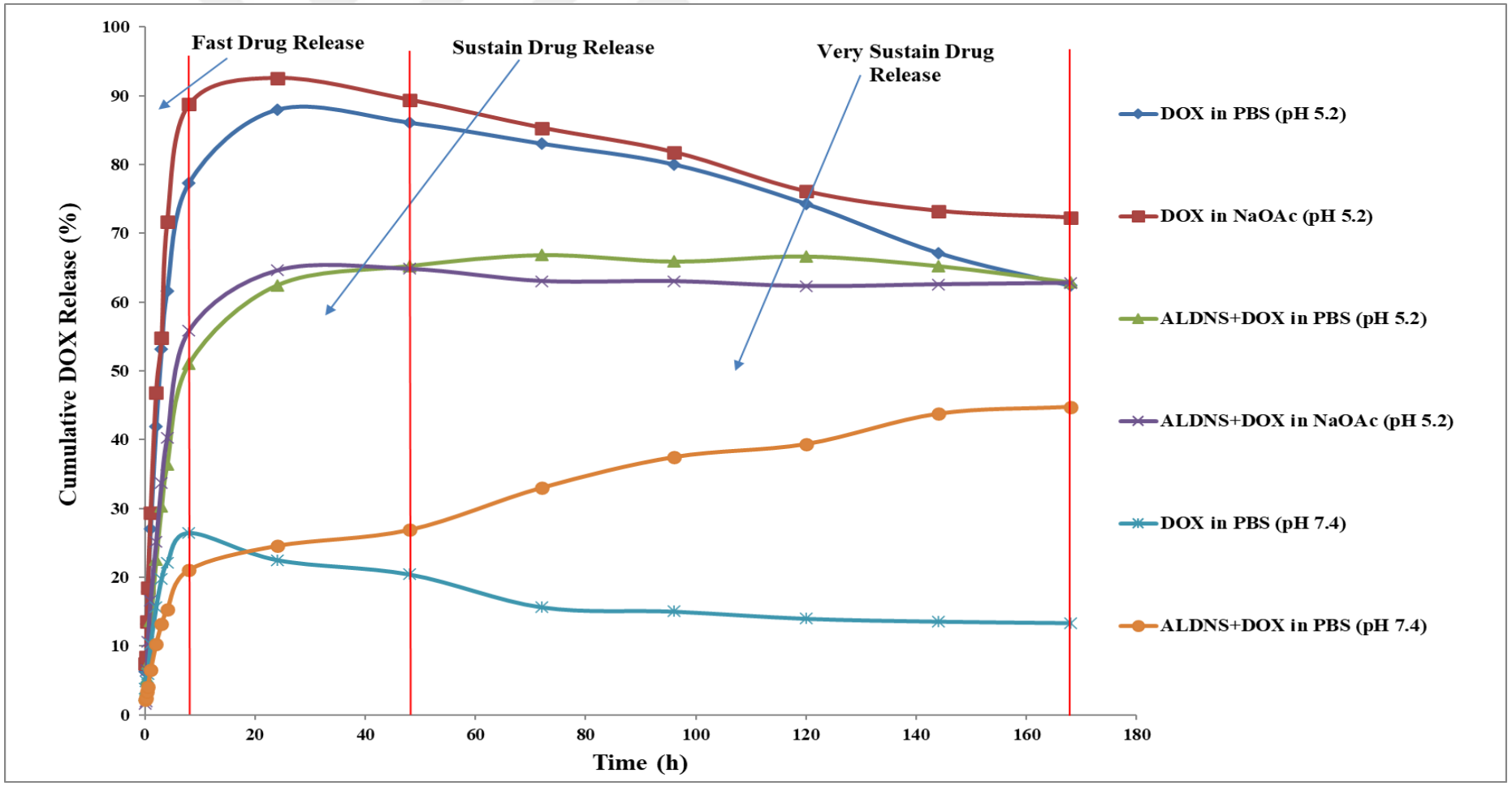

Figure 3.19. In vitro time dependent cumulative release of DOX from ALD-NS+DOX and free DOX at different buffers and pHs

3.4. In Vitro Cytotoxicity of DOX Loaded Nanocarrier

The concentration- and time-dependent cytotoxicity of free drug (DOX.HCl), drug loaded ALD-NS+DOX complex and blank ALD-NS nanocarrier were determined on A549 lung cancer cells after 24h and 48h of incubation at various concentration range of 0.325 to 20 μM by using WST8 assay.

First, the cytotoxicity of the blank nanocarrier was investigated because the application of the synthesized nanocarrier as a drug delivery carrier requires it to be non-toxic. Moreover, the drug loaded ALD-NS+DOX complex was expected to cause cytotoxicity to tumor cells. As shown in Figure 3.20 that the blank ALD-NS nanocarrier showed very low cytotoxicity on the growth inhibition of A549 lung cancer cells in all the tested concentrations. This study shows that the nanocarrier exhibited no cytotoxicity at initial concentrations (0.325 and 0.625 μM) after 24- and 48-hours' treatment and notably, the cell viability had decreased very low after 24 and 48 h over the concentration range of 1.25 to 20 μM. The cell viability rate of blank nanocarrier in A549 cell remained above 86.25% and 85.6 % at 24h and 48h respectively, indicating that the blank ALD-NS nanocarrier possessed excellent cytocompatibility.

The viability of cell activities of free drug and drug-loaded nanocarriers were investigated with various concentrations in A549 cell line at 24 and 48 h. Figure 3.20 shows that free DOX exhibited serious cell viability effect on the A549 cells and displayed remarkably higher cytotoxicity than all samples when the concentrations are increased. As can be clearly seen in Figure 3.20, the percentage of cell viability of free drug decreased by about 75% at 24h and 72.3% at 48h even at low concentration of 1.25 μM indicating high cytotoxicity.

As seen in Figure 3.20, loading of DOX drug on ALD-NS nanocarrier led to a decrease in cell viability. As for the drug loaded nanocarrier, the cell viability effects of the ALD-NS+DOX complex was also time- and dose-dependent (Figure 3.20). The cell viability decreased with increasing concentration. However, it should be noticed that the cell viability values were higher than those with free DOX with the all-equivalent concentration at 24 h and 48 h.

When the time-dependent cell viability rates were examined in Figure 3.20, cell viability in all samples in the 48h period showed more cytotoxicity for each

concentration than in the 24 h period. In many studies also observed that time- and dose dependent cell viabilities of drug loaded nanocarriers have found higher than those with free DOX with the same concentration at various time range (Li et al., 2017; Fan et al., 2019).

In order to examine the cell inhibition of free DOX.HCl, DOX-loaded ALD-NS complexes and ALD-NS nanocarrier, the IC_{50} values of all samples were examined by incubating the A549 cells with various concentrations for 24 h and 48 h. The IC_{50} values and the cell inhibition graph of free DOX.HCl, DOX-loaded ALD-NS complexes and ALD-NS nanocarrier at 24 h and 48 h were displayed in Table 3.6 and in Figure 3.21 respectively. As seen in Figure 3.21, the cell inhibition increased with increasing the concentration and duration of time for all samples.

According to results in Figure 3.21 and Table 3.6, free DOX displayed significant toxic effects on A549 cells. The IC_{50} values of the free DOX with optimal concentrations after 24 and 48 h were 1.09 μM and 0.6924 μM respectively. However, the IC_{50} values of the ALD-NS+DOX nanocarrier were obtained at 1.764 μM and 0.7172 μM respectively after 24 h and 48 h. The lower IC_{50} values of drug loaded nanocarriers compared to free drug could be related to sustained or delayed drug release profile. The existence of such an effect was also observed in some studies conducted by others (Lv et al., 2016; Jalalvandi et al., 2017; Zhou et al., 2018).

As can be seen in Figure 3.21 that the cell inhibition of ALD-NS nanocarrier on A549 cells were all below compared to free DOX and drug loaded complexes for all concentrations both at 24 h and 48 h. For instance, the cell inhibition of ALD-NS nanocarrier is below 65% and 72% in 5μM at 24 h and 48 h respectively which was relatively low even in higher concentrations, indicating that the ALD-NS nanocarrier had no major growing inhibition to cells.

The highest value of incubation shown in Figure 3.21 was obtained on free DOX for all tested concentration compared to unloaded nanocarrier at 24 h. However, it is slightly higher than drug loaded nanocarrier. For possible explanation, it may have occurred as a rapid release of the drug from the mediums.

As expected, the cell growth inhibition efficiency of ALD-ND+DOX complex was observed higher than that of either free DOX or ALD-NS nanocarrier after concentrations was increased from 5 μm to 10 μm at 48 h (Figure 3.21). However, its

values slightly lower compared to the free DOX at 24 h in the same concentration ranges. Reasons for this could be connection of DOX via Schiff base and integration of DOX into hydrophilic part of modified nanocarrier is able to increase the cell inhibition when both duration of time and concentrations were increased versus free DOX at 48 h by increased accumulation of intracellular drug (Zhao et al., 2014).

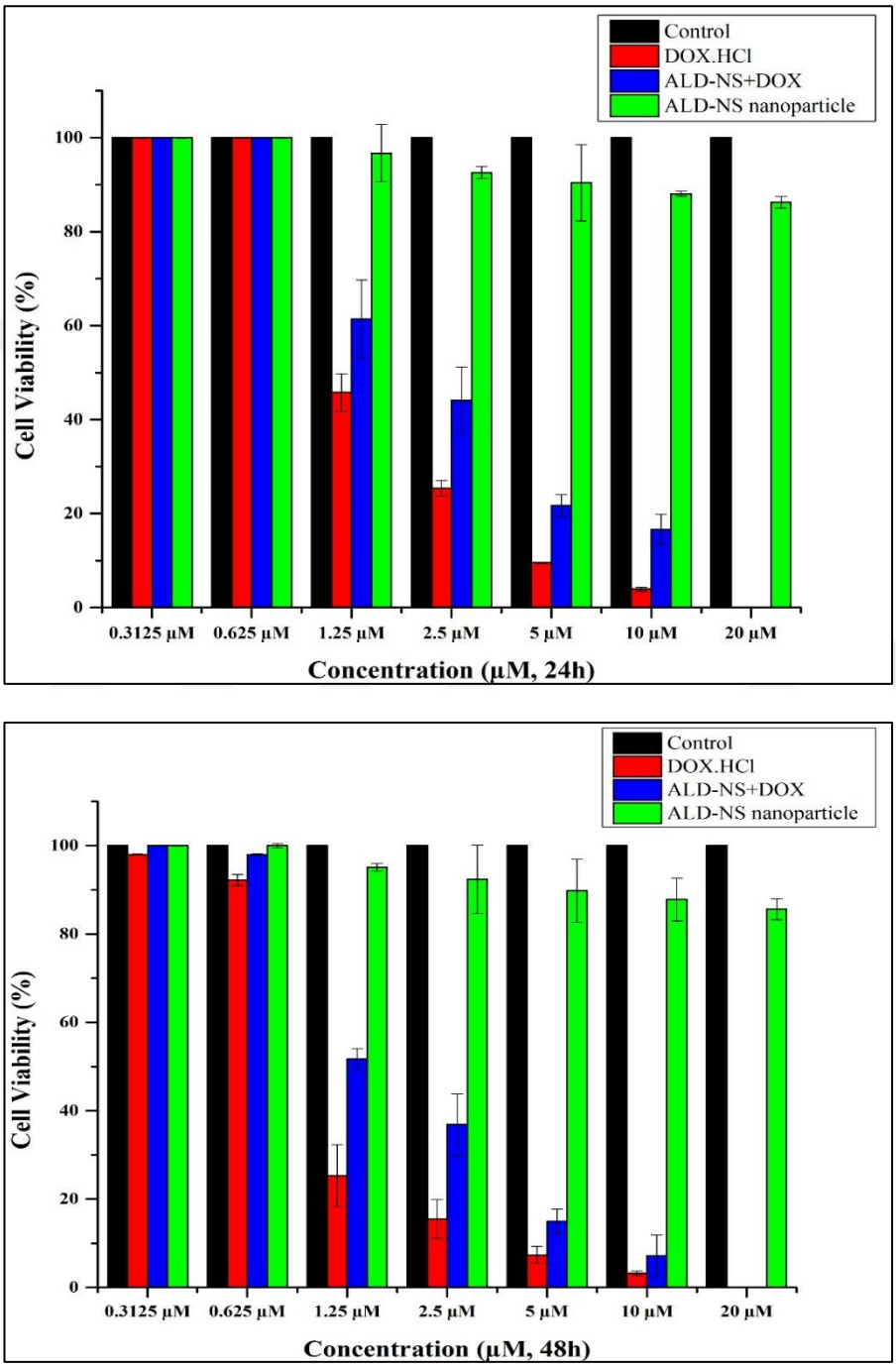

Figure 3.20. In vitro cytotoxicity of ALD-NS nanocarrier, free DOX and ALD-NS+DOX complex at various concentrations after 24h and 48h on A549 cells determined by the WST8 assays (Mean±SD, n =3)

Table 3.6. The IC_{50} values of DOX, ALD-NS+DOX and ALD-NS nanocarrier on A549 cell after 24 h and 48 h

Samples	IC_{50} values (µM) at 24h	IC_{50} values (µM) at 48h
Free DOX	1.109	0.692
ALD-NS+DOX	1.764	0.717
ALD-NS nanocarrier	4.882	2.082

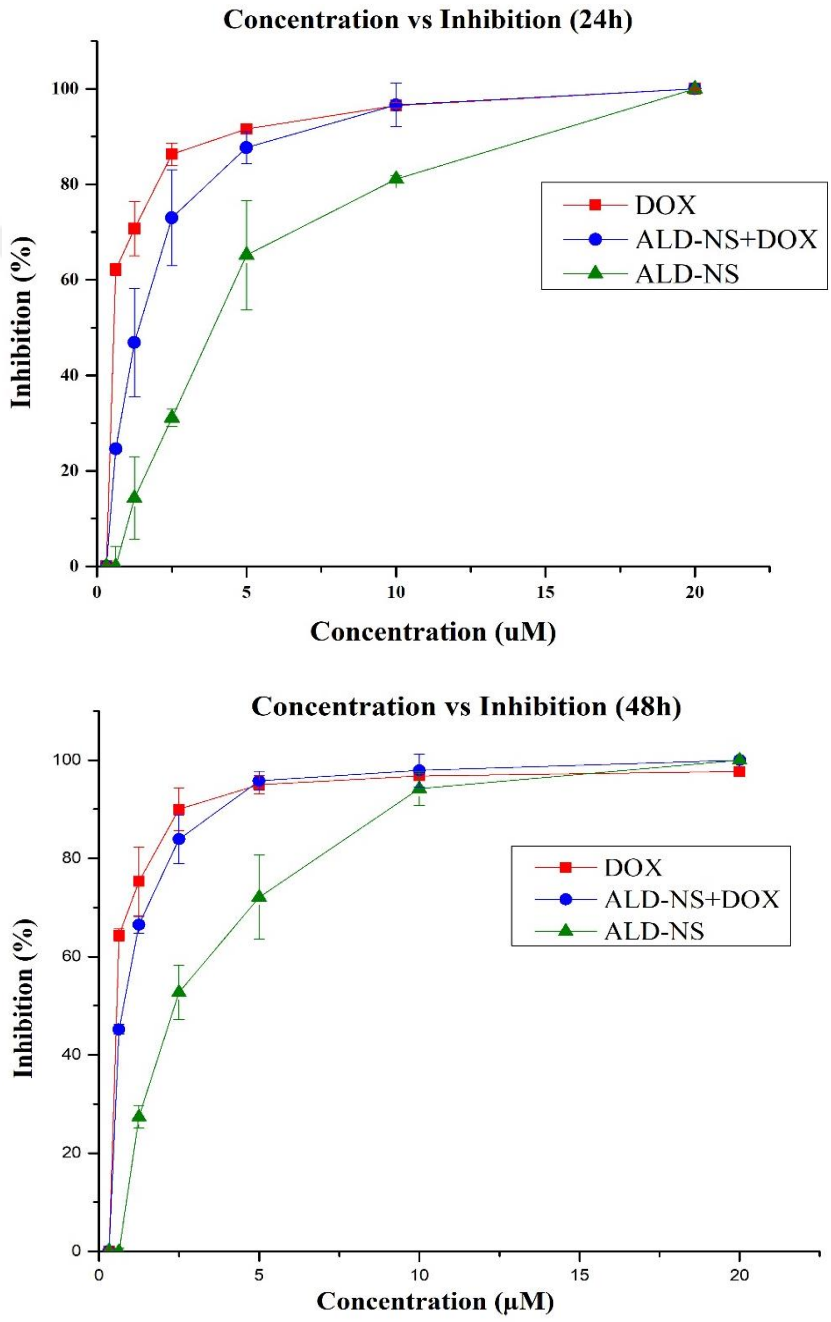

Figure 3.21. The cell inhibition graph of free DOX.HCl, ALD-NS+DOX complex and ALD-NS with various concentrations for 24 h and 48 h on A549 cells evaluated by WST8 assay

3.4.1. Cellular Uptake of DOX-loaded ALD-NS by Fluorescence Microscopy

The cellular uptake behaviors or intercellular distribution of free DOX and drug loaded ALD-NS were investigated in A549 cancer cells by obtaining the overlay images (fluorescense and brightfiled) with a fluorescence microscope. The results of cellular uptake in Figure 3.22 show an increase in fluorescence intensity images of cells after incubation for 12 h with free DOX and ALD-NS formulations, proposing that the fluorescence was activated by the cells. By virtue of the fluorescent characteristics of DOX, no other fluorescent dyes were added to ALD-NS+DOX.

Figure 3.22 displayed that the red fluorescence from DOX was observed in the cytoplasm of A549 cells following 12 h incubation with the DOX-loaded ALD-NS complexes and free DOX. As can be seen in Figure 3.22 that the intensity of red free DOX fluorescence was low in the cytoplasm in A549 cells. However, a larger amount of DOX from the ALD-NS+DOX nanocarriers was distributed in nucleus regions and the cytoplasm of cells. In addition, the intensity of the red fluorescence indicated increase in cancer cell culture compared to free drug suggesting that the cellular uptake of DOX formulations in these cells was time and a dose dependent. The fluorescence images in Figure 3.22 displayed that ALD-NS can enhance drug penetration as a higher concentration of drug accumulation occurs both in the cell nucleus or surface and in the cytoplasm compared to free DOX. This could be due to hydrolysis of Schiff base bound and breaking the crosslinking of NCs agent in acidic medium to release the DOX in the cell and enhancing cell internalization of the drug.

Same observations also depicted in some studies that the fluorescence signals of the drug loaded NCs were mainly accumulated at inner and outer compartments of the cell's nuclei (Lv et al., 2016; Singh et al., 2018; Fan et al., 2019; Behera et al., 2021).

Efficient cellular transport of DOX across the membranes was based on enhanced drug intracellular accumulation and the delivery of drug by ALD-NS. However, this method is quite qualitative and further quantitative experiments, such as HPLC, should be performed to show cellular uptake and cellular kinetic behaviors of the DOX and ALD-NS+ DOX complex.

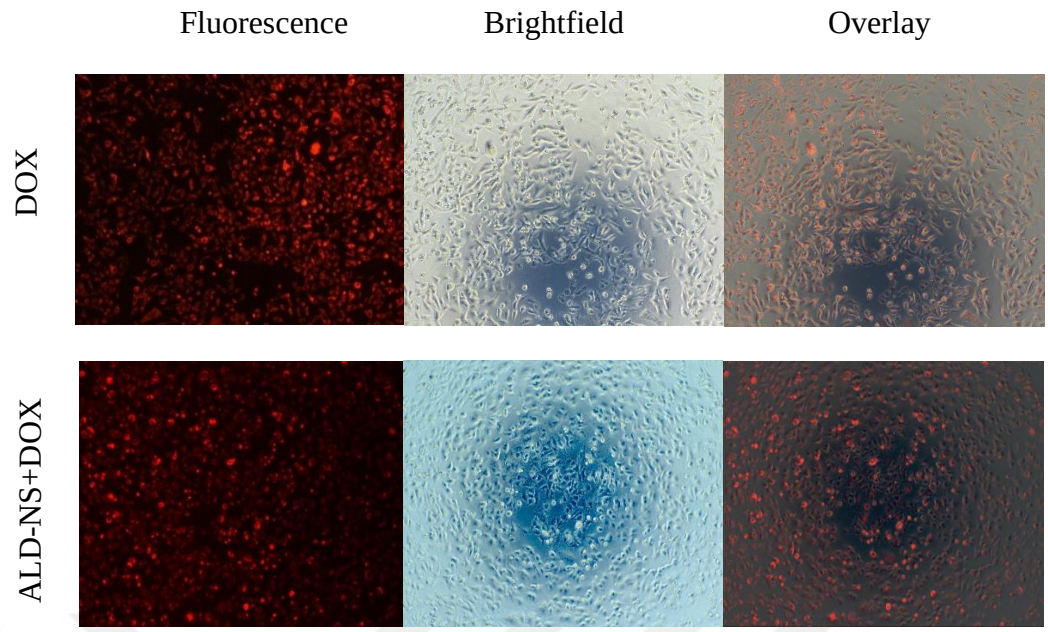

Figure 3.22. Fluorescence, brightfield and overlay images of ALD-NS+DOX and free DOX.HCl for 12 hours in A549 cells

3.5. Mathematical Modeling of Drug Release Kinetics for ALD-NS+DOX Complex

Drug release kinetics with mathematical models is an essential parameter to examine the transport mechanisms involved in the control of drug release. To establish the drug release mechanism as well as the release rate for our system, data obtained from in vitro drug release studies for each pH in different buffer saline solutions (PBS at pH 5.2 and 7.4 and NaOAc at pH 5.2) at body temperature condition were fitted with the most convenient models such as zero order, first order, Higuchi and Korsmeyer-Peppas models (Elmas et al., 2020). By comparing linear correlation coefficient (R^2) and fit parameters of each model, the accuracy of each fitting could be confirmed so that the model which grants the highest R^2 was regarded as the best fit of release data.

Therefore, the mechanism and release kinetic of DOX from the ALD-NS+DOX nanocarrier was defined according to those mathematical models. The results and release parameters for each model (k_0, k_1, k_h, k_{kp} and n) as well as the correlation values (R^2) are shown in Figure 3.23 and Table 3.7.

The zero and first order kinetic model would not fit well with the experimental release data as it displayed lower R^2 values than the other two models indicating the two models were not applicable. Because the zero-degree model is valid for slow drug

release of low soluble drugs, and the first-degree model is applicable mostly in porous matrix systems. Thus, these two models are difficult to describe in rapid release for pH sensitive systems.

The Higuchi model almost fits well with the release data even though it has better R^2 values than the zero and first order model, but it is lower than the Korsmeyer–Peppas model (Figure 3.23). The highest R^2 value was obtained with the Korsmeyer–Peppas model (Figure 3.23). Therefore, in vitro release profile of ALD-NS+DOX complex could be best expressed by Korsmeyer–Peppas, as the plot demonstrated the highest linearity with R^2=0.972 (Figure 3.23) for all buffer solution. In the Korsmeyer-Peppas model, the release kinetics are defined by determining the diffusion coefficient or release exponent "n" values (Table 3.7). The release exponent "n" was found to be lower than 0.5 (n=0.497) in PBS (physiological media) at pH 7.4, indicating a Fickian diffusion mechanism. The same phenomenon was also observed at pH 7.4 in a study of a pH-sensitive drug delivery system using the model drug DOX (Li et al., 2017).

However, an increase in "n" values corresponding to decreasing pH was observed in both PBS and NaOAc buffers at pH 5.2 compared to the basic pH medium. The "n" value for both buffers is between 0.5<n<1 (0.622 for PBS at pH 5.2 and 0.71 for NaOAc at pH 5.2) specifying Anomalous (Non-Fickian) diffusion which suggests that the drug release from the medium depends on both diffusion and dissolution as it is expected. Thus, Korsmeyer–Peppas model was considered as well fitted release kinetic model that the drug release takes place due to both dissolution and diffusion. This can be attributed to the importance of the involvement of C=N bond cleavage in a low pH environment (Tahir et al., 2019). Another study using a hydrogel showed that the release profile fits the Korsmeyer–Peppas model which drug release occurs in response to both swellable porous matrix and Fickian diffusion (Fan et al., 2019; Tran et al., 2022). This may be attributed to the inclusion of cleavage of the imine bond in the medium due to its sensitivity to a low pH environment.

Cyclodextrin, dextran and similar polysaccharides remain stable under physiological pH and temperature, but undergo hydrolysis in aqueous media due to swelling, molecular chain dissolution or solvent penetration effect at high temperatures and pH environments (Fu and Kao, 2010). Therefore, solute transport by polymer dissolution and/or diffusion takes place in polysaccharide-based systems. Polymer dissolution can be described the process by which the substance contained in the

polymer structure, or the substance it carries, begins to release into the surrounding fluid in the presence of a thermodynamically compatible solvent (Loftsson et al., 2005b).

Table 3.7. Correlation coefficients and release parameters based on drug release results with kinetic models

Kinetic Models											
Sample	**Release Media**	**pH**	**Zero Order**		**Fist Order**		**Higuchi Model**		**Krosmeyer-Peppas**		
			R^2	k_o	R^2	k_1	R^2	k_h	n	R^2	k_{kp}
DOX release	PBS	7.4	0.70	0.91	0.48	2.11	0.91	1.68	0.49	0.97	6.59
	PBS	5.2	0.73	2.46	0.46	2.23	0.92	0.74	0.62	0.97	12.58
	NaOAc	5.2	0.71	2.60	0.37	2.20	0.90	1.73	0.71	0.93	12.02

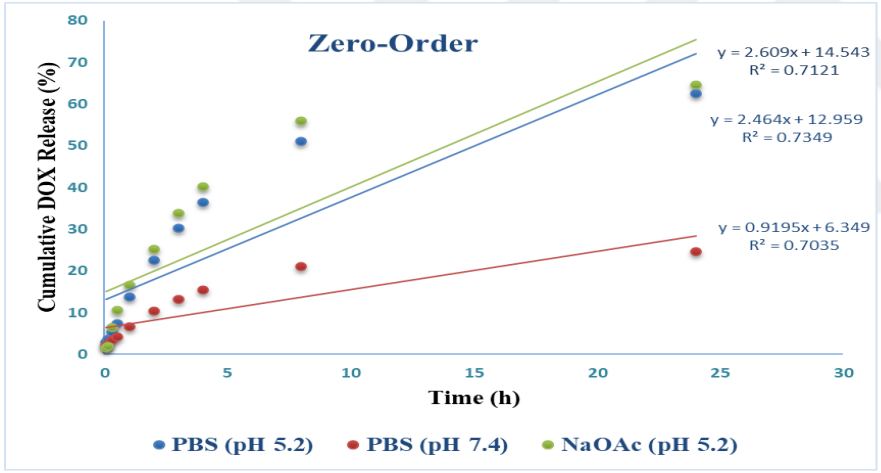

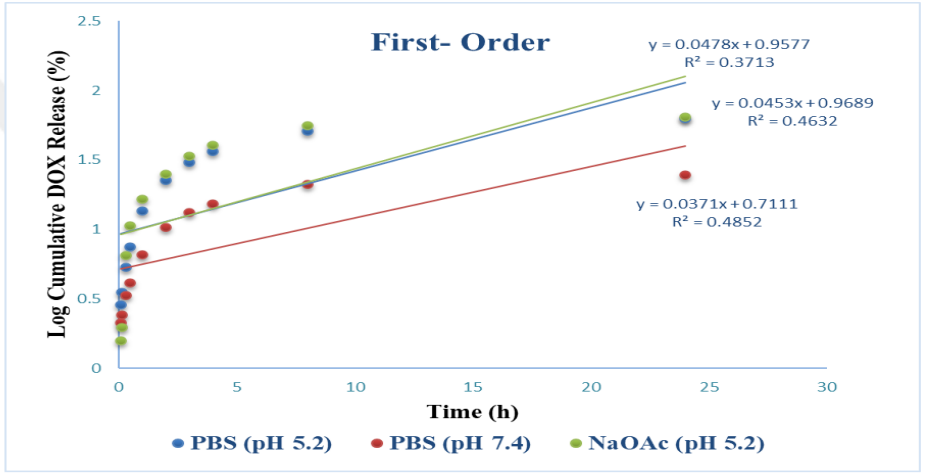

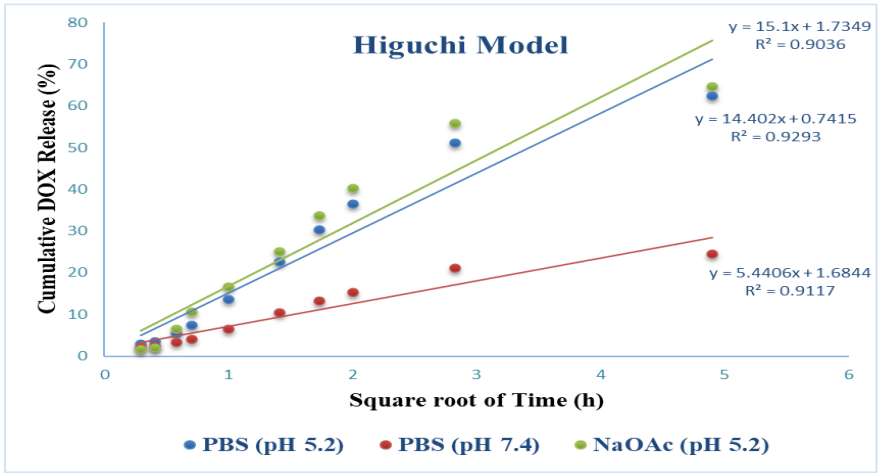

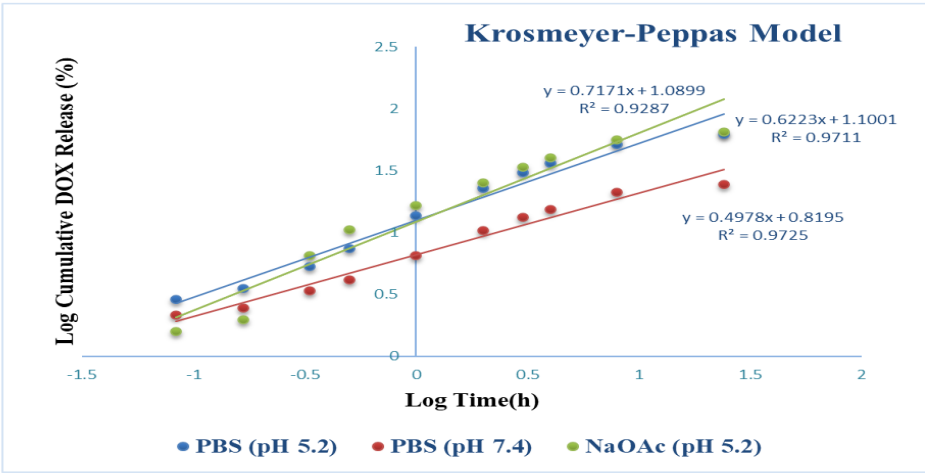

Figure 3.23. The curve of zero order, first order, Higuchi and Korsmeyer-Peppas model of drug release in PBS (pH 5.2), PBS (pH 7.4 and NaOAc (pH 5.2) buffer solutions and rate constant of different kinetic models for ALD-NS+DOX complex

4. CONCLUSIONS

In the present study, firstly, detail synthesis and characterization of an oxidized-β-cyclodextrins via employing periodate oxidation with varying oxidation degree have accomplished and levels of highly reactive aldehyde functional groups introduced into β-CD unit.

It was observed that if sodium periodate could not be removed from the synthesized structure, it underwent a color change from white to yellow after a certain period of time due to the presence of iodate ions in the molecule. Calorimetric titration results showed that the degrees of oxidation or aldehyde content of OX-β-CDs were increased by increasing the dosage of sodium periodate (NaIO4/β-CD molar ratio). FTIR and ^{1}H-NMR studies of OX-β-CDs confirm that aldehyde functional group was successfully introduced into C2 and C3 units of β-CD structure. Furthermore, it has been proven that as the sodium periodate molar ratio increases, morphological changes such as fragmentation in the cyclic structure of β-CD or formation of hemiacetal groups occur besides the formation of the aldehyde. In addition, it has been proven that the modification with the increase of periodate oxidation has impacts on the physicochemical features of OX-β-CDs such as changes in crystal structure and particle shape.

All these studies have shown that OX-β-CDs prepared with higher sodium periodate molar ratio (higher than molar 4) will lose its ability to form complexes with some molecules, since there will be deterioration in their structural integrity, especially in the hydrophilic cavity. Therefore, OX-β-CD4 prepared with periodate molar ratio 4 was seen as the best optimum synthesized structure in terms of both the high aldehyde amount or oxidation degree and the preservation of structural integrity.

It is interesting that MICs and disc diffusion study of OX-β-CDs possessed remarkable antibacterial activity against both Gram-negative (*E. coli, P. aeruginosa)* and Gram-positive (*S. aureus* and *B. cereus)* bacteria. This result showed that the aldehyde functional group present on the synthesized structure caused an antibacterial effect and that the increased amount of aldehyde would have a significant effect on the antibacterial activity, depending on the increase in the molar degree of sodium periodate. This work could help with the use of OX-β-CDs as biomaterials for a new antibacterial agent or targeted drug delivery applications.

Secondly, ALD-NS nanocarrier was obtained by using different molars of OX-

β-CD4 to PMDA crosslinker with an optimal molar ratio and DOX cancer drug was successfully integrated into the obtained ALD-NS by applying the Reflux method. Thus, drug-loaded ALD-NS+DOX nanocarrier, sensitive to acidic environmental conditions, was obtained. In this system, a pH sensitive Schiff base (C=N) bond between the drug molecule and the nanocarrier was performed and formation proved in whole characterization studies. Demonstrated in UV, FTIR, XRD, TGA analyzes that the desired environment-sensitive bond occurs between the model drug and the synthesized ALD-NS nanocarrier with bidirectional manner as well as high loading capacity (8.089 ±1.32 %) and entrapment efficiency (85.53±1.74 %), descend particle size (372 ±8.21 nm) and high negative ZP (-12.8±2.74 mV).

The in vitro drug release study from the ALD-NS+DOX complex was carried out with three buffer solutions at different pH and as a result, it has been proven that drug release profile of ALD-NS+DOX in the acidic environment (pH 5.2) is quite high from the physiological neutral (pH 7.4) environment. As expected, drug release from ALD-NS+DOX occurs sustains, prolong slow-release profile compared to pure DOX which is sudden fast release occur due to its hydrophilic nature. The drug release of ALD-NS nanocarrier is mainly dependent on two mechanisms; firstly, the cleavage of the imine bond (C=N) to release the drug molecules, and secondly diffusion of drug molecules from the polymer matrix based on the surrounding acidic medium.

Thirdly, in vitro concentration- and time-dependent cytotoxicity, the cell inhibition and in vitro cellular uptake behavior of drug loaded ALD-NS+DOX complex was determined on A549 lung cancer cells after 24h and 48h of incubation at various concentrations by using WST8 assays. The results show that the cell viability of ALD-NS+DOX complex decreased with increasing the concentration, but viabilities were higher than those with free DOX with the all-equivalent concentration at 24 h and 48 h. Therefore, cytotoxicity of drug loaded nanostructure display low effect on A549 cells compared with free DOX which exhibited serious cell viability effect and displayed remarkably higher cytotoxicity. However, the cell inhibition of ALD-NS+DOX complex was increased with increasing the concentrations and duration of time. IC_{50} value of ALD-NS+DOX complex found 1.764 μM and 0.7172 μM respectively after 24 h and 48 h. In vitro cellular uptake behaviors of ALD-NS+DOX complex was obtained with the fluorescence microscopy. The overlay fluorescence images displayed that larger amount of DOX from the ALD-NS+DOX

nanocarriers was distributed in nucleus regions and the cytoplasm of cells. Therefore, ALD-NS can enhance drug penetration as a higher concentration of drug accumulation occurs compared to free DOX, suggesting that the cellular uptake of formulation in these cells was time and a dose dependent.

Lastly, drug release kinetics was investigated using the best-known mathematical models and it was seen that drug release was best achieved with the Krosmeyyer-Peppas model with high correlation coefficient (R^2=0.97 and 0.5<n<1). According to this model based on diffusion coefficient "n" was found to be lower than 0.5 (n=0.497) in PBS (physiological media) at pH 7.4 suggesting a Fickian diffusion mechanism. However, an increase in "n" values can be observed in response to decreasing pH in both for PBS and NaOAc buffers at pH 5.2. The "n" value for both buffers is between 0.5<n<1 (0.622 for PBS at pH 5.2 and 0.71 for NaOAc at pH 5.2) specifying anomalous (Non-Fickian) diffusion. It has been proven that DOX drug is released as a result of diffusion from nanostructure and hydrolysis of Schiff base bond of C=N that DOX is bound to nanostructure. Again, in this model, it was concluded that drug release occurs better in an acidic environment.

As a result, it has been proven that the nanostructure formed by the model drug both with an acid-sensitive connection and integrating it into the hydrophilic part of the nanocarrier has the potential to be a nanocarrier sensitive to acidic environmental conditions. However, further in vivo studies are required as well to evaluate the pharmacological effects of our nano drug system. In addition, numerous in vitro and in vivo research on nanostructure is needed to investigate the effects of NH_2 group containing drugs such as amoxicillin, adriamycin, fluvoxamine or carbidopa on drug loading, drug release, cellular uptake behavior as well as its cytotoxicity in the same or different physiological environments.

REFERENCES

Abed, H. F., Abuwatfa, W. H., & Husseini, G. A. (2022). Redox-responsive drug delivery systems: A chemical perspective. *Nanomaterials (Basel, Switzerland)*, *12*(18). doi:10.3390/nano12183183

Afinjuomo, F., Fouladian, P., Barclay, T. G., Song, Y., Petrovsky, N., & Garg, S. (2020). Influence of oxidation degree on the physicochemical properties of oxidized inulin. *Polymers*, *12*(5), 1025. doi:10.3390/polym12051025

Afinjuomo, F., Fouladian, P., Parikh, A., Barclay, T. G., Song, Y., & Garg, S. (2019). Preparation and characterization of oxidized inulin hydrogel for controlled drug delivery. *Pharmaceutics*, *11*(7), 356. doi:10.3390/pharmaceutics11070356

Afzal, O., Altamimi, A. S. A., Nadeem, M. S., Alzarea, S. I., Almalki, W. H., Tariq, A., … Kazmi, I. (2022). Nanoparticles in drug delivery: From history to therapeutic applications. *Nanomaterials (Basel, Switzerland)*, *12*(24), 4494. doi:10.3390/nano12244494

Ahmad, F., Salem-Bekhit, M. M., Khan, F., Alshehri, S., Khan, A., Ghoneim, M. M., … Elbagory, I. (2022). Unique properties of surface-functionalized nanoparticles for bio-application: Functionalization mechanisms and importance in application. *Nanomaterials (Basel, Switzerland)*, *12*(8), 1333. doi:10.3390/nano12081333

Aldughaim, M. S., Muthana, M., Alsaffar, F., & Barker, M. D. (2020). Specific targeting of PEGylated liposomal doxorubicin (Doxil®) to tumour cells using a novel TIMP3 peptide. *Molecules (Basel, Switzerland)*, *26*(1), 100. doi:10.3390/molecules26010100

Ali M. Osmani, R., R. Bhosale, R., Hani, U., Vaghela, R., & K. Kulkarni, P. (2015). Cyclodextrin based nanosponges: Impending carters in drug delivery and nanotherapeutics. *Current Drug Therapy*, *10*(1), 3–19. doi:10.2174/1574885510011508250955l3

Alibolandi, M., Mohammadi, M., Teimouri, R., Babaei, M., Movaffagh, J., & Ramezani, M. (2022, February 14). Carbohydrate-based materials in tissue engineering applications. *Nanoengineering of Biomaterials*, pp. 1–31. doi:10.1002/9783527832095.ch18

Amer, H., Nypelö, T., Sulaeva, I., Bacher, M., Henniges, U., Potthast, A., & Rosenau, T. (2016). Synthesis and characterization of periodate-oxidized polysaccharides: Dialdehyde Xylan (DAX). *Biomacromolecules*, *17*(9), 2972–2980. doi:10.1021/acs.biomac.6b00777

Anandam, S., & Selvamuthukumar, S. (2014a). Fabrication of cyclodextrin nanosponges for quercetin delivery: physicochemical characterization, photostability, and antioxidant effects. *Journal of Materials Science*, *49*(23), 8140–8153. doi:10.1007/s10853-014-8523-6

Anandam, S., & Selvamuthukumar, S. (2014b). Optimization of microwave-assisted synthesis of cyclodextrin nanosponges using response surface methodology. *Journal of Porous Materials*, *21*(6), 1015–1023. doi:10.1007/s10934-014-9851-2

Argenziano, M., Gigliotti, C. L., Clemente, N., Boggio, E., Ferrara, B., Trotta, F., … Dianzani, C. (2020). Improvement in the anti-tumor efficacy of doxorubicin nanosponges in in vitro and in mice bearing breast tumor models. *Cancers*, *12*(1), 162. doi:10.3390/cancers12010162

Aziz, M. A., Cabral, J. D., Brooks, H. J. L., Moratti, S. C., & Hanton, L. R. (2012). Antimicrobial properties of a chitosan dextran-based hydrogel for surgical use. *Antimicrobial Agents and Chemotherapy*, *56*(1), 280–287. doi:10.1128/aac.05463-11

Bano, N., Ray, S. K., Shukla, T., Upmanyu, N., Khare, R., Pandey, S. P., & Jain, P. (2019). Multifunctional nanosponges for the treatment of various diseases: A review. *Asian Journal of Pharmacy and Pharmacology*, *5*(2), 235–248. doi:10.31024/ajpp.2019.5.2.4

Barenholz, Y. (chezy). (2012). Doxil® — The first FDA-approved nano-drug: Lessons learned. *Journal of Controlled Release: Official Journal of the Controlled Release Society*, *160*(2), 117–134. doi:10.1016/j.jconrel.2012.03.020

Behera, S. K., Mohanty, M. E., & Mohapatra, M. (2021). A fluorescence study of the interaction of anticancer drug molecule doxorubicin hydrochloride in pluronic P123 and F127 micelles. *Journal of Fluorescence*, *31*(1), 17–27. doi:10.1007/s10895-020-02630-y

Bergal, A., & Andaç, M. (2021). Nanosponges (NSs): Using as a nanocarrier for anti cancer drug delivery applications. *ACTA Pharmaceutica Sciencia*, *59*(2), 306–320. doi:10.23893/1307-2080.aps.05918

Bhalani, D. V., Nutan, B., Kumar, A., & Singh Chandel, A. K. (2022). Bioavailability enhancement techniques for poorly aqueous soluble drugs and therapeutics. *Biomedicines*, *10*(9), 2055. doi:10.3390/biomedicines10092055

Bischoff, M., Biriukov, D., Předota, M., Roke, S., & Marchioro, A. (2020). Surface potential and interfacial water order at the amorphous TiO_2 nanoparticle/aqueous interface. *The Journal of Physical Chemistry. C, Nanomaterials and Interfaces*, *124*(20), 10961–10974. doi:10.1021/acs.jpcc.0c01158

Boscolo, B., Trotta, F., & Ghibaudi, E. (2010). High catalytic performances of Pseudomonas fluorescens lipase adsorbed on a new type of cyclodextrin-based nanosponges. *Journal of Molecular Catalysis. B, Enzymatic*, *62*(2), 155–161. doi:10.1016/j.molcatb.2009.10.002

Bozzer, S., Dal Bo, M., Grimaldi, M. C., Toffoli, G., & Macor, P. (2022). Nanocarriers as a delivery platform for anticancer treatment: Biological limits and perspectives in B-cell malignancies. *Pharmaceutics*, *14*(9). doi:10.3390/pharmaceutics14091965

Broaders, K. E., Grandhe, S., & Fréchet, J. M. J. (2011). A biocompatible oxidation-triggered carrier polymer with potential in therapeutics. *Journal of the American Chemical Society*, *133*(4), 756–758. doi:10.1021/ja110468v

Cavalli, R., Akhter, A. K., Bisazza, A., Giustetto, P., Trotta, F., & Vavia, P. (2010). Nanosponge formulations as oxygen delivery systems. *International Journal of Pharmaceutics*, *402*(1–2), 254–257. doi:10.1016/j.ijpharm.2010.09.025

Chan, M., Brooks, H., Moratti, S., Hanton, L., & Cabral, J. (2015). Reducing the oxidation level of dextran aldehyde in a chitosan/dextran-based surgical hydrogel increases biocompatibility and decreases antimicrobial efficacy. *International Journal of Molecular Sciences*, *16*(12), 13798–13814. doi:10.3390/ijms160613798

Chandrakala, V., Aruna, V., & Angajala, G. (2022). Review on metal nanoparticles as nanocarriers: current challenges and perspectives in drug delivery systems. *Emergent Materials*, *5*(6), 1593–1615. doi:10.1007/s42247-021-00335-x

Chen, Y. M., Sun, L., Yang, S. A., Shi, L., Zheng, W. J., Wei, Z., & Hu, C. (2017). Self-healing and photoluminescent carboxymethyl cellulose-based hydrogels. *European Polymer Journal*, *94*, 501–510. doi:10.1016/j.eurpolymj.2017.06.008

Chen, Y., Zhang, R., Zheng, B., Cai, C., Chen, Z., Li, H., & Liu, H. (2020). A biocompatible, stimuli-responsive, and injectable hydrogel with triple dynamic bonds. *Molecules (Basel, Switzerland)*, *25*(13), 3050. doi:10.3390/molecules25133050

Chis, A. A., Dobrea, C., Morgovan, C., Arseniu, A. M., Rus, L. L., Butuca, A., … Frum, A. (2020). Applications and limitations of dendrimers in biomedicine. *Molecules (Basel, Switzerland)*, *25*(17), 3982. doi:10.3390/molecules25173982

Cinà, V., Russo, M., Lazzara, G., Chillura Martino, D., & Lo Meo, P. (2017). Pre- and post-modification of mixed cyclodextrin-calixarene co-polymers: A route towards tunability. *Carbohydrate Polymers*, *157*, 1393–1403. doi:10.1016/j.carbpol.2016.11.018

Coseri, S. (2017). Cellulose: To depolymerize… or not to? *Biotechnology Advances*, *35*(2), 251–266. doi:10.1016/j.biotechadv.2017.01.002

Costa, R. de O., Coutinho, J. P., & Santos, R. L. S. R. (2022). Use of mixture design to optimize nanofabrication of dithiocarbazate–loaded polylactic acid nanoparticles. *Journal of Applied Polymer Science*, *139*(3), 51504. doi:10.1002/app.51504

Crini, G., Fourmentin, S., Fenyvesi, É., Torri, G., Fourmentin, M., & Morin-Crini, N. (2018). Cyclodextrins, from molecules to applications. *Environmental Chemistry Letters*, *16*(4), 1361–1375. doi:10.1007/s10311-018-0763-2

Dalgıç, B., Demir, N., Yıldız, M. (2020). Investigation of the synthesis and biological activity of A new imine compound containing ferrocene and benzothiazol. *International Journal of Innovative Approaches in Science Research*, *4*(3), 52–65. doi:10.29329/ijiasr.2020.273.1

Danaei, M., Dehghankhold, M., Ataei, S., Hasanzadeh Davarani, F., Javanmard, R., Dokhani, A., … Mozafari, M. (2018). Impact of particle size and polydispersity index on the clinical applications of lipidic nanocarrier systems. *Pharmaceutics*, *10*(2), 57. doi:10.3390/pharmaceutics10020057

Davis, M. E., & Brewster, M. E. (2004). Cyclodextrin-based pharmaceutics: past, present and future. *Nature Reviews. Drug Discovery*, *3*(12), 1023–1035. doi:10.1038/nrd1576

De, R., Mahata, M. K., & Kim, K.-T. (2022). Structure-based varieties of polymeric nanocarriers and influences of their physicochemical properties on drug delivery profiles. *Advanced Science (Weinheim, Baden-Wurttemberg, Germany)*, *9*(10), e2105373. doi:10.1002/advs.202105373

Dhakar, N. K., Matencio, A., Caldera, F., Argenziano, M., Cavalli, R., Dianzani, C., … Trotta, F. (2019). Comparative evaluation of solubility, cytotoxicity and photostability studies of resveratrol and oxyresveratrol loaded nanosponges. *Pharmaceutics*, *11*(10), 545. doi:10.3390/pharmaceutics11100545

Dhiman, N., Awasthi, R., Sharma, B., Kharkwal, H., & Kulkarni, G. T. (2021). Lipid nanoparticles as carriers for bioactive delivery. *Frontiers in Chemistry*, *9*, 580118. doi:10.3389/fchem.2021.580118

Di, X., Liang, X., Shen, C., Pei, Y., Wu, B., & He, Z. (2022). Carbohydrates used in polymeric systems for drug delivery: From structures to applications. *Pharmaceutics*, *14*(4), 739. doi:10.3390/pharmaceutics14040739

Din, F. ud, Aman, W., Ullah, I., Qureshi, O. S., Mustapha, O., Shafique, S., & Zeb, A. (2017). Effective use of nanocarriers as drug delivery systems for the treatment of selected tumors. *International Journal of Nanomedicine*, *12*, 7291–7309. doi:10.2147/ijn.s146315

Ding, C., & Li, Z. (2017). A review of drug release mechanisms from nanocarrier systems. *Materials Science & Engineering. C, Materials for Biological Applications*, *76*, 1440–1453. doi:10.1016/j.msec.2017.03.130

Dou, Y., Huang, X., Zhang, B., He, M., Yin, G., & Cui, Y. (2015). Preparation and characterization of a dialdehyde starch crosslinked feather keratin film for food packaging application. *RSC Advances*, *5*(34), 27168–27174. doi:10.1039/c4ra15469j

Duan, J., & Kasper, D. L. (2011). Oxidative depolymerization of polysaccharides by reactive oxygen/nitrogen species. *Glycobiology*, *21*(4), 401–409. doi:10.1093/glycob/cwq171

Elmas, A., Akyüz, G., Bergal, A., Andaç, M., Andaç, Ö. (2020). Mathematical modelling of drug release. *Research on Engineering Structures and Materials*. doi:10.17515/resm2020.178na0122

Euvrard, É., Morin-Crini, N., Druart, C., Bugnet, J., Martel, B., Cosentino, C., … Crini, G. (2016). Cross-linked cyclodextrin-based material for treatment of metals and organic substances present in industrial discharge waters. *Beilstein Journal of Organic Chemistry*, *12*, 1826–1838. doi:10.3762/bjoc.12.172

Fam, S. Y., Chee, C. F., Yong, C. Y., Ho, K. L., Mariatulqabtiah, A. R., & Tan, W. S. (2020). Stealth coating of nanoparticles in drug-delivery systems. *Nanomaterials (Basel, Switzerland)*, *10*(4). doi:10.3390/nano10040787

Fan, W., Xu, Y., Li, Z., & Li, Q. (2019). Folic acid-modified β-cyclodextrin nanoparticles as drug delivery to load DOX for liver cancer therapeutics. *Soft Materials*, *17*(4), 437–447. doi:10.1080/1539445x.2019.1624265

Fasiku, V. O., Aderibigbe, B. A., Sadiku, E. R., Lemmer, Y., Owonubi, S. J., Ray, S. S., & Mukwevho, E. (2019). Polyethylene glycol–gum acacia-based multidrug delivery system for controlled delivery of anticancer drugs. *Polymer Bulletin (Berlin, Germany)*, *76*(10), 5011–5037. doi:10.1007/s00289-018-2642-1

Fonkui, T. Y., Ikhile, M. I., Njobeh, P. B., & Ndinteh, D. T. (2019). Benzimidazole Schiff base derivatives: synthesis, characterization and antimicrobial activity. *BMC Chemistry*, *13*(1), 127. doi:10.1186/s13065-019-0642-3

Fu, Y., & Kao, W. J. (2010). Drug release kinetics and transport mechanisms of non-degradable and degradable polymeric delivery systems. *Expert Opinion on Drug Delivery*, *7*(4), 429–444. doi:10.1517/17425241003602259

Gangadharappa, H. V., Chandra Prasad, S. M., & Singh, R. P. (2017). Formulation, in vitro and in vivo evaluation of celecoxib nanosponge hydrogels for topical application. *Journal of Drug Delivery Science and Technology*, *41*, 488–501. doi:10.1016/j.jddst.2017.09.004

Gim, S., Zhu, Y., Seeberger, P. H., & Delbianco, M. (2019). Carbohydrate-based nanomaterials for biomedical applications. *Wiley Interdisciplinary Reviews. Nanomedicine and Nanobiotechnology*, *11*(5). doi:10.1002/wnan.1558

Griffiths, H., & MacLeod, K. T. (2003). The voltage-sensitive release mechanism of excitation contraction coupling in rabbit cardiac muscle is explained by calcium-induced calcium release. *The Journal of General Physiology*, *121*(5), 353–373. doi:10.1085/jgp.200208764

Gunasekaran, S., Govindan, S., & Ramani, P. (2021). Sulfated modification, characterization and bioactivities of an acidic polysaccharide fraction from an edible mushroom Pleurotus eous (Berk.) Sacc. *Heliyon*, *7*(1), e05964. doi:10.1016/j.heliyon.2021.e05964

Guo, J., Ge, L., Li, X., Mu, C., & Li, D. (2014). Periodate oxidation of xanthan gum and its crosslinking effects on gelatin-based edible films. *Food Hydrocolloids*, *39*, 243–250. doi:10.1016/j.foodhyd.2014.01.026

He, H., Chen, S., Zhou, J., Dou, Y., Song, L., Che, L., … Li, X. (2013). Cyclodextrin-derived pH-responsive nanoparticles for delivery of paclitaxel. *Biomaterials*, *34*(21), 5344–5358. doi:10.1016/j.biomaterials.2013.03.068

Hervault, A., Dunn, A. E., Lim, M., Boyer, C., Mott, D., Maenosono, S., & Thanh, N. T. K. (2016). Doxorubicin loaded dual pH- and thermo-responsive magnetic nanocarrier for

combined magnetic hyperthermia and targeted controlled drug delivery applications. *Nanoscale*, *8*(24), 12152–12161. doi:10.1039/c5nr07773g

Hoshyar, N., Gray, S., Han, H., & Bao, G. (2016). The effect of nanoparticle size on in vivo pharmacokinetics and cellular interaction. *Nanomedicine (London, England)*, *11*(6), 673–692. doi:10.2217/nnm.16.5

Ibrahim, M., Abuwatfa, W. H., Awad, N. S., Sabouni, R., & Husseini, G. A. (2022). Encapsulation, release, and cytotoxicity of doxorubicin loaded in liposomes, micelles, and metal-organic frameworks: A review. *Pharmaceutics*, *14*(2), 254. doi:10.3390/pharmaceutics14020254

Ijaz, M., Matuszczak, B., Rahmat, D., Mahmood, A., Bonengel, S., Hussain, S., … Bernkop-Schnürch, A. (2015). Synthesis and characterization of thiolated β-cyclodextrin as a novel mucoadhesive excipient for intra-oral drug delivery. *Carbohydrate Polymers*, *132*, 187–195. doi:10.1016/j.carbpol.2015.06.073

Ijaz, M., Prantl, M., Lupo, N., Laffleur, F., Hussain Asim, M., Matuszczak, B., & Bernkop-Schnürch, A. (2017). Development of pre-activated α-cyclodextrin as a mucoadhesive excipient for intra-vesical drug delivery. *International Journal of Pharmaceutics*, *534*(1–2), 339–347. doi:10.1016/j.ijpharm.2017.10.054

Islami, M., Zarrabi, A., Tada, S., Kawamoto, M., Isoshima, T., & Ito, Y. (2018). Controlled quercetin release from high-capacity-loading hyperbranched polyglycerol-functionalized graphene oxide. *International Journal of Nanomedicine*, *13*, 6059–6071. doi:10.2147/ijn.s178374

Isogai, A., Saito, T., & Fukuzumi, H. (2011). TEMPO-oxidized cellulose nanofibers. *Nanoscale*, *3*(1), 71–85. doi:10.1039/c0nr00583e

Jain, A., Prajapati, S. K., Kumari, A., Mody, N., & Bajpai, M. (2020). Engineered nanosponges as versatile biodegradable carriers: An insight. *Journal of Drug Delivery Science and Technology*, *57*(101643), 101643. doi:10.1016/j.jddst.2020.101643

Jalalvandi, E., Hanton, L. R., & Moratti, S. C. (2017). Schiff-base based hydrogels as degradable platforms for hydrophobic drug delivery. *European Polymer Journal*, *90*, 13–24. doi:10.1016/j.eurpolymj.2017.03.003

Jansook, P., Ogawa, N., & Loftsson, T. (2018). Cyclodextrins: structure, physicochemical properties and pharmaceutical applications. *International Journal of Pharmaceutics*, *535*(1–2), 272–284. doi:10.1016/j.ijpharm.2017.11.018

Jia, T., Huang, S., Yang, C., & Wang, M. (2017). Unimolecular micelles of amphiphilic cyclodextrin-core star-like copolymers with covalent pH-responsive linkage of anticancer prodrugs. *Molecular Pharmaceutics*, *14*(8), 2529–2537. doi:10.1021/acs.molpharmaceut.6b00708

Jiang, M., Liu, Q., Zhang, Y., Wang, H., Zhang, J., Chen, M., … Wang, Y. (2022). Construction of magnetic drug delivery system and its potential application in tumor theranostics. *Biomedecine & Pharmacotherapie [Biomedicine & Pharmacotherapy]*, *154*(113545), 113545. doi:10.1016/j.biopha.2022.113545

Joudeh, N., & Linke, D. (2022). Nanoparticle classification, physicochemical properties, characterization, and applications: a comprehensive review for biologists. *Journal of Nanobiotechnology*, *20*(1), 262. doi:10.1186/s12951-022-01477-8

Kamba, S., Ismail, M., Hussein-Al-Ali, S., Ibrahim, T., & Zakaria, Z. (2013). In vitro delivery and controlled release of doxorubicin for targeting osteosarcoma bone cancer. *Molecules (Basel, Switzerland)*, *18*(9), 10580–10598. doi:10.3390/molecules180910580

Kaushik, N., Borkar, S. B., Nandanwar, S. K., Panda, P. K., Choi, E. H., & Kaushik, N. K. (2022). Nanocarrier cancer therapeutics with functional stimuli-responsive mechanisms. *Journal of Nanobiotechnology*, *20*(1), 152. doi:10.1186/s12951-022-01364-2

Khalid, A., Asim-Ur-Rehman, Ahmed, N., Chaudhery, I., Al-Jafary, M. A., Al-Suhaimi, E. A., … Elaissari, A. (2021). Polysaccharide chemistry in drug delivery, endocrinology, and vaccines. *Chemistry (Weinheim an Der Bergstrasse, Germany)*, *27*(33), 8437–8451. doi:10.1002/chem.202100204

Khodaei, A., Jahanmard, F., Madaah Hosseini, H. R., Bagheri, R., Dabbagh, A., Weinans, H., & Amin Yavari, S. (2022). Controlled temperature-mediated curcumin release from magneto-thermal nanocarriers to kill bone tumors. *Bioactive Materials*, *11*, 107–117. doi:10.1016/j.bioactmat.2021.09.028

Kolosnjaj-Tabi, J., Gibot, L., Fourquaux, I., Golzio, M., & Rols, M.-P. (2019). Electric field-responsive nanoparticles and electric fields: physical, chemical, biological mechanisms and therapeutic prospects. *Advanced Drug Delivery Reviews*, *138*, 56–67. doi:10.1016/j.addr.2018.10.017

Korin, N., Kanapathipillai, M., Matthews, B. D., Crescente, M., Brill, A., Mammoto, T., … Ingber, D. E. (2012). Shear-activated nanotherapeutics for drug targeting to obstructed blood vessels. *Science (New York, N.Y.)*, *337*(6095), 738–742. doi:10.1126/science.1217815

Kristiansen, K. A., Potthast, A., & Christensen, B. E. (2010). Periodate oxidation of polysaccharides for modification of chemical and physical properties. *Carbohydrate Research*, *345*(10), 1264–1271. doi:10.1016/j.carres.2010.02.011

Kumar, K., Sheetu, Sharma, A., Singh, G., & Kumar, R. (2022). Natural carbohydrates-based nanoparticles: A review of pharmaceutical applications. *The Natural Products Journal*, *12*. doi:10.2174/2210315512666220826145928

Li, B., Shan, M., Di, X., Gong, C., Zhang, L., Wang, Y., & Wu, G. (2017). A dual pH- and reduction-responsive anticancer drug delivery system based on PEG–SS–poly(amino acid) block copolymer. *RSC Advances*, *7*(48), 30242–30249. doi:10.1039/c7ra04254j

Li, D., & Ma, M. (2000). Nanosponges for water purification. *Clean Technologies and Environmental Policy*, *2*(2), 0112–0116. doi:10.1007/s100980000061

Li, M., Zhao, G., Su, W.-K., & Shuai, Q. (2020). Enzyme-responsive nanoparticles for anti-tumor drug delivery. *Frontiers in Chemistry*, *8*, 647. doi:10.3389/fchem.2020.00647

Liu, J., Yu, P., Sollogoub, M., & Zhang, Y. (2019). Functionalized Cyclodextrins and Their Applications in Biodelivery. In *Handbook of Macrocyclic Supramolecular Assembly* (pp. 1–39). Singapore: Springer Singapore.

Liu, H., Li, F., & Luo, P., (2019). Effect of carboxymethylation and phosphorylation on the properties of polysaccharides from Sepia esculenta ink: Antioxidation and anticoagulation in vitro. *Marine Drugs*, *17*(11), 626. doi:10.3390/md17110626

Liu, P., Gao, C., Chen, H., Vong, C. T., Wu, X., Tang, X., … Wang, Y. (2021). Receptor-mediated targeted drug delivery systems for treatment of inflammatory bowel disease: Opportunities and emerging strategies. *Acta Pharmaceutica Sinica. B*, *11*(9), 2798–2818. doi:10.1016/j.apsb.2020.11.003

Loftsson, T., Hreinsdóttir, D., & Másson, M. (2005a). Evaluation of cyclodextrin solubilization of drugs. *International Journal of Pharmaceutics*, *302*(1–2), 18–28. doi:10.1016/j.ijpharm.2005.05.042

Loftsson, T., Jarho, P., Másson, M., & Järvinen, T. (2005b). Cyclodextrins in drug delivery. *Expert Opinion on Drug Delivery*, *2*(2), 335–351. doi:10.1517/17425247.2.1.335

Longo, C., Gambara, G., Espina, V., Luchini, A., Bishop, B., Patanarut, A. S., … Liotta, L. A. (2011). A novel biomarker harvesting nanotechnology identifies Bak as a candidate melanoma biomarker in serum: Bak as a candidate melanoma biomarker. *Experimental Dermatology*, *20*(1), 29–34. doi:10.1111/j.1600-0625.2010.01187.x

Lou, C., Tian, X., Deng, H., Wang, Y., & Jiang, X. (2020). Dialdehyde-β-cyclodextrin-crosslinked carboxymethyl chitosan hydrogel for drug release. *Carbohydrate Polymers*, *231*(115678), 115678. doi:10.1016/j.carbpol.2019.115678

Lou, C., Yin, Y., Tian, X., Deng, H., Wang, Y., & Jiang, X. (2020a). Hydrophilic finishing of PET fabrics by applying chitosan and the periodate oxidized β-cyclodextrin for wash resistance improvement. *Fibers and Polymers*, *21*(1), 73–81. doi:10.1007/s12221-020-9269-1

Lou, C., Yin, Y., Tian, X., Deng, H., Wang, Y., & Jiang, X. (2020b). Modification of wool via grafting β-cyclodextrin oxidized by sodium periodate. *Fibers and Polymers*, *21*(8), 1669–1677. doi:10.1007/s12221-020-9983-8

Lv, L., Liu, C., Chen, C., Yu, X., Chen, G., Shi, Y., … Li, G. (2016). Quercetin and doxorubicin co-encapsulated biotin receptor-targeting nanoparticles for minimizing drug resistance in breast cancer. *Oncotarget*, *7*(22), 32184–32199. doi:10.18632/oncotarget.8607

Matar, G. H., & Andac, M. (2021). Antibacterial efficiency of silver nanoparticles-loaded locust bean gum/polyvinyl alcohol hydrogels. *Polymer Bulletin (Berlin, Germany)*, *78*(11), 6095–6113. doi:10.1007/s00289-020-03418-7

Matencio, A., Caldera, F., Cecone, C., López-Nicolás, J. M., & Trotta, F. (2020). Cyclic oligosaccharides as active drugs, an updated review. *Pharmaceuticals (Basel, Switzerland)*, *13*(10), 281. doi:10.3390/ph13100281

Meyer, C. D., Joiner, C. S., & Stoddart, J. F. (2007). Template-directed synthesis employing reversible imine bond formation. *Chemical Society Reviews*, *36*(11), 1705. doi:10.1039/b513441m

Minelli, R., Cavalli, R., Ellis, L., Pettazzoni, P., Trotta, F., Ciamporcero, E., … Pili, R. (2012). Nanosponge-encapsulated camptothecin exerts anti-tumor activity in human prostate cancer cells. *European Journal of Pharmaceutical Sciences: Official Journal of the European Federation for Pharmaceutical Sciences*, *47*(4), 686–694. doi:10.1016/j.ejps.2012.08.003

Mitchell, M. J., Billingsley, M. M., Haley, R. M., Wechsler, M. E., Peppas, N. A., & Langer, R. (2021). Engineering precision nanoparticles for drug delivery. *Nature Reviews. Drug Discovery*, *20*(2), 101–124. doi:10.1038/s41573-020-0090-8

Mognetti, B., Barberis, A., Marino, S., Berta, G., Francia, S., Trotta, F., & Cavalli, R. (2012). In vitro enhancement of anticancer activity of paclitaxel by a Cremophor free cyclodextrin-based nanosponge formulation. *Journal of Inclusion Phenomena and Macrocyclic Chemistry*, *74*(1–4), 201–210. doi:10.1007/s10847-011-0101-9

Mohan, P., & Rapoport, N. (2010). Doxorubicin as a molecular nanotheranostic agent: Effect of doxorubicin encapsulation in micelles or nanoemulsions on the ultrasound-mediated intracellular delivery and nuclear trafficking. *Molecular Pharmaceutics*, *7*(6), 1959–1973. doi:10.1021/mp100269f

Moradi Kashkooli, F., Jakhmola, A., Hornsby, T. K., Tavakkoli, J. J., & Kolios, M. C. (2023). Ultrasound-mediated nano drug delivery for treating cancer: Fundamental physics to future directions. *Journal of Controlled Release: Official Journal of the Controlled Release Society*, *355*, 552–578. doi:10.1016/j.jconrel.2023.02.009

Moreira, M. P., Andrade, G. R. S., de Araujo, M. V. G., Kubota, T., & Gimenez, I. F. (2016). Ternary cyclodextrin polyurethanes containing phosphate groups: Synthesis and

complexation of ciprofloxacin. *Carbohydrate Polymers*, *151*, 557–564. doi:10.1016/j.carbpol.2016.05.101

Nikravan, G., Haddadi-Asl, V., & Salami-Kalajahi, M. (2019). Stimuli-responsive DOX release behavior of cross-linked poly(acrylic acid) nanoparticles. *E-Polymers*, *19*(1), 203–214. doi:10.1515/epoly-2019-0021

Nonsuwan, P., Matsugami, A., Hayashi, F., Hyon, S.-H., & Matsumura, K. (2019). Controlling the degradation of an oxidized dextran-based hydrogel independent of the mechanical properties. *Carbohydrate Polymers*, *204*, 131–141. doi:10.1016/j.carbpol.2018.09.081

Nypelö, T., Berke, B., Spirk, S., & Sirviö, J. A. (2021). Review: Periodate oxidation of wood polysaccharides—Modulation of hierarchies. *Carbohydrate Polymers*, *252*(117105), 117105. doi:10.1016/j.carbpol.2020.117105

Osmani, R. A., Kulkarni, P., Manjunatha, S., Vaghela, R., & Bhosale, R. (2018). Cyclodextrin nanosponge-based systems in drug delivery and nanotherapeutics. In *Organic Materials as Smart Nanocarriers for Drug Delivery* (pp. 659–717). Elsevier.

Ouyang, J., Li, Z., Miao, J., Wang, Y., Hu, L., & Wang, X. (2022). *Antibacterial activity of carboxymethyl chitosan dialdehyde starch Schiff base and its metal complex*. doi:10.21203/rs.3.rs-1669122/v1

Păduraru, D. N., Niculescu, A.-G., Bolocan, A., Andronic, O., Grumezescu, A. M., & Bîrlă, R. (2022). An updated overview of cyclodextrin-based drug delivery systems for cancer therapy. *Pharmaceutics*, *14*(8), 1748. doi:10.3390/pharmaceutics14081748

Paiva-Santos, A. C., Ferreira, L., Peixoto, D., Silva, F., Soares, M. J., Zeinali, M., … Veiga, F. (2022). Cyclodextrins as an encapsulation molecular strategy for volatile organic compounds— Pharmaceutical applications. *Colloids and Surfaces. B, Biointerfaces*, *218*(112758), 112758. doi:10.1016/j.colsurfb.2022.112758

Pan, J.-F., Yuan, L., Guo, C.-A., Geng, X.-H., Fei, T., Fan, W.-S., … Mo, X.-M. (2014). Fabrication of modified dextran–gelatin in situ forming hydrogel and application in cartilage tissue engineering. *Journal of Materials Chemistry. B, Materials for Biology and Medicine*, *2*(47), 8346–8360. doi:10.1039/c4tb01221f

Pandit, A. H., Mazumdar, N., & Ahmad, S. (2019). Periodate oxidized hyaluronic acid-based hydrogel scaffolds for tissue engineering applications. *International Journal of Biological Macromolecules*, *137*, 853–869. doi:10.1016/j.ijbiomac.2019.07.014

Patnaik, S., Gorain, B., Padhi, S., Choudhury, H., Gabr, G. A., Md, S., … Kesharwani, P. (2021). Recent update of toxicity aspects of nanoparticulate systems for drug delivery. *European Journal of Pharmaceutics and Biopharmaceutics: Official Journal of Arbeitsgemeinschaft Für Pharmazeutische Verfahrenstechnik e.V*, *161*, 100–119. doi:10.1016/j.ejpb.2021.02.010

Pawar, S., Shende, P., & Trotta, F. (2019). Diversity of β-cyclodextrin-based nanosponges for transformation of actives. *International Journal of Pharmaceutics*, *565*, 333–350. doi:10.1016/j.ijpharm.2019.05.015

Perlin, A. S. (2006). Glycol-Cleavage Oxidation. In *Advances in Carbohydrate Chemistry and Biochemistry Volume 60* (pp. 183–250). Elsevier.

Poon, W., Kingston, B. R., Ouyang, B., Ngo, W., & Chan, W. C. W. (2020). A framework for designing delivery systems. *Nature Nanotechnology*, *15*(10), 819–829. doi:10.1038/s41565-020-0759-5

Poulson, B. G., Alsulami, Q. A., Sharfalddin, A., El Agammy, E. F., Mouffouk, F., Emwas, A.-H., … Jaremko, M. (2021). Cyclodextrins: Structural, chemical, and physical properties, and applications. *Polysaccharides*, *3*(1), 1–31. doi:10.3390/polysaccharides3010001

Pushpalatha, R., Selvamuthukumar, S., & Kilimozhi, D. (2017). Nanocarrier mediated combination drug delivery for chemotherapy – A review. *Journal of Drug Delivery Science and Technology*, *39*, 362–371. doi:10.1016/j.jddst.2017.04.019

Pushpalatha, R., Selvamuthukumar, S., & Kilimozhi, D. (2018). Cross-linked, cyclodextrin-based nanosponges for curcumin delivery - Physicochemical characterization, drug release, stability and cytotoxicity. *Journal of Drug Delivery Science and Technology*, *45*, 45–53. doi:10.1016/j.jddst.2018.03.004

Rafaque, Z., Abid, N., Liaquat, N., Afridi, P., Siddique, S., Masood, S., … Iqbal Dasti, J. (2020). In-vitro investigation of antibiotics efficacy against uropathogenic Escherichia coli biofilms and antibiotic induced biofilm formation at sub-minimum inhibitory concentration of ciprofloxacin. *Infection and Drug Resistance*, *13*, 2801–2810. doi:10.2147/idr.s258355

Rahim, M. A., Jan, N., Khan, S., Shah, H., Madni, A., Khan, A., … Thu, H. E. (2021). Recent advancements in stimuli responsive drug delivery platforms for active and passive cancer targeting. *Cancers*, *13*(4), 670. doi:10.3390/cancers13040670

Rao, M., Bajaj, A., Khole, I., Munjapara, G., & Trotta, F. (2013). In vitro and in vivo evaluation of β-cyclodextrin-based nanosponges of telmisartan. *Journal of Inclusion Phenomena and Macrocyclic Chemistry*, *77*(1–4), 135–145. doi:10.1007/s10847-012-0224-7

Ren, H., Lyu, Y., Li, X., Zhang, S., Ye, Y., Li, D., & Mu, C. (2018). Preparation and characterization of dialdehyde β-cyclodextrin with broad-spectrum antibacterial activity. *Food Research International (Ottawa, Ont.)*, *111*, 237–243. doi:10.1016/j.foodres.2018.05.039

Santos, A. C., Costa, D., Ferreira, L., Guerra, C., Pereira-Silva, M., Pereira, I., … Veiga, F. (2021). Cyclodextrin-based delivery systems for in vivo-tested anticancer therapies. *Drug Delivery and Translational Research*, *11*(1), 49–71. doi:10.1007/s13346-020-00778-5

Sapino, S., Carlotti, M. E., Cavalli, R., Ugazio, E., Berlier, G., Gastaldi, L., & Morel, S. (2013). Photochemical and antioxidant properties of gamma-oryzanol in beta-cyclodextrin-based nanosponges. *Journal of Inclusion Phenomena and Macrocyclic Chemistry*, *75*(1–2), 69–76. doi:10.1007/s10847-012-0147-3

Selvamuthukumar, Anandam, Krishnamoorthy, K., & Rajappan, M. (2012). Nanosponges: A novel class of drug delivery system - review. *Journal of Pharmacy & Pharmaceutical Sciences: A Publication of the Canadian Society for Pharmaceutical Sciences, Societe Canadienne Des Sciences Pharmaceutiques*, *15*(1), 103. doi:10.18433/j3k308

Sharma, R., & Pathak, K. (2011). Polymeric nanosponges as an alternative carrier for improved retention of econazole nitrate onto the skin through topical hydrogel formulation. *Pharmaceutical Development and Technology*, *16*(4), 367–376. doi:10.3109/10837451003739289

Sharma, S., Parveen, R., & Chatterji, B. P. (2021). Toxicology of nanoparticles in drug delivery. *Current Pathobiology Reports*, *9*(4), 133–144. doi:10.1007/s40139-021-00227-z

Shende, P. K., Gaud, R. S., Bakal, R., & Patil, D. (2015). Effect of inclusion complexation of meloxicam with β-cyclodextrin- and β-cyclodextrin-based nanosponges on solubility, in vitro release and stability studies. *Colloids and Surfaces. B, Biointerfaces*, *136*, 105–110. doi:10.1016/j.colsurfb.2015.09.002

Shende, P., Kulkarni, Y. A., Gaud, R. S., Deshmukh, K., Cavalli, R., Trotta, F., & Caldera, F. (2015). Acute and repeated dose toxicity studies of different β-cyclodextrin-based

nanosponge formulations. *Journal of Pharmaceutical Sciences*, *104*(5), 1856–1863. doi:10.1002/jps.24416

Sherje, A. P., Dravyakar, B. R., Kadam, D., & Jadhav, M. (2017). Cyclodextrin-based nanosponges: A critical review. *Carbohydrate Polymers*, *173*, 37–49. doi:10.1016/j.carbpol.2017.05.086

Singh, P., Ren, X., Guo, T., Wu, L., Shakya, S., He, Y., … Zhang, J. (2018). Biofunctionalization of β-cyclodextrin nanosponges using cholesterol. *Carbohydrate Polymers*, *190*, 23–30. doi:10.1016/j.carbpol.2018.02.044

Sirviö, J., Honka, A., Liimatainen, H., Niinimäki, J., & Hormi, O. (2011). Synthesis of highly cationic water-soluble cellulose derivative and its potential as novel biopolymeric flocculation agent. *Carbohydrate Polymers*, *86*(1), 266–270. doi:10.1016/j.carbpol.2011.04.046

Spangler, D., Rothenburger, S., Nguyen, K., Jampani, H., Weiss, S., & Bhende, S. (2003). *in vitro* antimicrobial activity of oxidized regenerated cellulose against antibiotic-resistant microorganisms. *Surgical Infections*, *4*(3), 255–262. doi:10.1089/109629603322419599

Strätz, J., Liedmann, A., Trutschel, M.-L., Mäder, K., Groth, T., & Fischer, S. (2019). Development of hydrogels based on oxidized cellulose sulfates and carboxymethyl chitosan. *Cellulose (London, England)*, *26*(12), 7371–7382. doi:10.1007/s10570-019-02596-6

Su, H., Jia, Q., & Shan, S. (2016). Synthesis and characterization of Schiff base contained dextran microgels in water-in-oil inverse microemulsion. *Carbohydrate Polymers*, *152*, 156–162. doi:10.1016/j.carbpol.2016.06.091

Su, H., Zhang, W., Wu, Y., Han, X., Liu, G., Jia, Q., & Shan, S. (2018). Schiff base-containing dextran nanogel as pH-sensitive drug delivery system of doxorubicin: Synthesis and characterization. *Journal of Biomaterials Applications*, *33*(2), 170–181. doi:10.1177/0885328218783969

Su, S., & Kang, P. M. (2020). Systemic review of biodegradable nanomaterials in nanomedicine. *Nanomaterials (Basel, Switzerland)*, *10*(4). doi:10.3390/nano10040656

Subhan, M. A., Yalamarty, S. S. K., Filipczak, N., Parveen, F., & Torchilin, V. P. (2021). Recent advances in tumor targeting via EPR effect for cancer treatment. *Journal of Personalized Medicine*, *11*(6), 571. doi:10.3390/jpm11060571

Sultana, A., Zare, M., Thomas, V., Kumar, T. S. S., & Ramakrishna, S. (2022). Nano-based drug delivery systems: Conventional drug delivery routes, recent developments and future prospects. *Medicine in Drug Discovery*, *15*(100134), 100134. doi:10.1016/j.medidd.2022.100134

Swaminathan, S., Cavalli, R., Trotta, F., Ferruti, P., Ranucci, E., Gerges, I., … Vavia, P. R. (2010b). In vitro release modulation and conformational stabilization of a model protein using swellable polyamidoamine nanosponges of β-cyclodextrin. *Journal of Inclusion Phenomena and Macrocyclic Chemistry*, *68*(1–2), 183–191. doi:10.1007/s10847-010-9765-9

Swaminathan, Shankar, Cavalli, R., & Trotta, F. (2016). Cyclodextrin-based nanosponges: a versatile platform for cancer nanotherapeutics development. *Wiley Interdisciplinary Reviews. Nanomedicine and Nanobiotechnology*, *8*(4), 579–601. doi:10.1002/wnan.1384

Swaminathan, S., Shankar L., Pastero, L., Serpe, L., Trotta, F., Vavia, P., Aquilano, D., … Cavalli, R. (2010a). Cyclodextrin-based nanosponges encapsulating camptothecin: Physicochemical characterization, stability and cytotoxicity. *European Journal of Pharmaceutics and Biopharmaceutics: Official Journal of Arbeitsgemeinschaft Für*

Pharmazeutische Verfahrenstechnik e.V, *74*(2), 193–201. doi:10.1016/j.ejpb.2009.11.003

Swaminathan, Shankar, Vavia, P. R., Trotta, F., & Torne, S. (2007). Formulation of betacyclodextrin based nanosponges of itraconazole. *Journal of Inclusion Phenomena and Macrocyclic Chemistry*, *57*(1–4), 89–94. doi:10.1007/s10847-006-9216-9

Tahir, N., Madni, A., Correia, A., Rehman, M., Balasubramanian, V., Khan, M. M., & Santos, H. A. (2019). Lipid-polymer hybrid nanoparticles for controlled delivery of hydrophilic and lipophilic doxorubicin for breast cancer therapy. *International Journal of Nanomedicine*, *14*, 4961–4974. doi:10.2147/ijn.s209325

Teixeira, M. I., Lopes, C. M., Amaral, M. H., & Costa, P. C. (2023). Surface-modified lipid nanocarriers for crossing the blood-brain barrier (BBB): A current overview of active targeting in brain diseases. *Colloids and Surfaces. B, Biointerfaces*, *221*(112999), 112999. doi:10.1016/j.colsurfb.2022.112999

Tian, B., Hua, S., & Liu, J. (2020). Cyclodextrin-based delivery systems for chemotherapeutic anticancer drugs: A review. *Carbohydrate Polymers*, *232*(115805), 115805. doi:10.1016/j.carbpol.2019.115805

Tran Vo, T. M., Piroonpan, T., Preuksarattanawut, C., Kobayashi, T., & Potiyaraj, P. (2022). Characterization of pH-responsive high molecular-weight chitosan/poly (vinyl alcohol) hydrogel prepared by gamma irradiation for localizing drug release. *Bioresources and Bioprocessing*, *9*(1). doi:10.1186/s40643-022-00576-6

Trotta, F., Cavalli, R., Tumiatti, W., Zerbinati, O., Roggero, C., & Vallero, R. (2007). *Patent No. Pat 1786841A1*. Retrieved from https://patents.google.com/patent/US20080213384A1/en

Trotta, Francesco, Zanetti, M., & Cavalli, R. (2012). Cyclodextrin-based nanosponges as drug carriers. *Beilstein Journal of Organic Chemistry*, *8*, 2091–2099. doi:10.3762/bjoc.8.235

Ulldemolins, A., Seras-Franzoso, J., Andrade, F., Rafael, D., Abasolo, I., Gener, P., & Schwartz, S., Jr. (2021). Perspectives of nano-carrier drug delivery systems to overcome cancer drug resistance in the clinics. *Cancer Drug Resistance*, *4*(1), 44–68. doi:10.20517/cdr.2020.59

van de Manakker, F., Vermonden, T., van Nostrum, C. F., & Hennink, W. E. (2009). Cyclodextrin-based polymeric materials: Synthesis, properties, and pharmaceutical/biomedical applications. *Biomacromolecules*, *10*(12), 3157–3175. doi:10.1021/bm901065f

Westin, C. B., Nagahara, M. H. T., Decarli, M. C., Kelly, D. J., & Moraes, Â. M. (2020). Development and characterization of carbohydrate-based thermosensitive hydrogels for cartilage tissue engineering. *European Polymer Journal*, *129*(109637), 109637. doi:10.1016/j.eurpolymj.2020.109637

Wibowo, F. R., Saputra, O. A., Lestari, W. W., Koketsu, M., Mukti, R. R., & Martien, R. (2020). PH-triggered drug release controlled by poly(styrene sulfonate) growth hollow mesoporous silica nanoparticles. *ACS Omega*, *5*(8), 4261–4269. doi:10.1021/acsomega.9b04167

Wicki, A., Witzigmann, D., Balasubramanian, V., & Huwyler, J. (2015). Nanomedicine in cancer therapy: challenges, opportunities, and clinical applications. *Journal of Controlled Release: Official Journal of the Controlled Release Society*, *200*, 138–157. doi:10.1016/j.jconrel.2014.12.030

Xin, Y., & Yuan, J. (2012). Schiff's base as a stimuli-responsive linker in polymer chemistry. *Polymer Chemistry*, *3*(11), 3045. doi:10.1039/c2py20290e

Xiong, L., Luo, Q., Wang, Y., Li, X., Shen, Z., & Zhu, W. (2015). An injectable drug-loaded hydrogel based on a supramolecular polymeric prodrug. *Chemical Communications (Cambridge, England)*, *51*(78), 14644–14647. doi:10.1039/c5cc06025g

Yaghoubi, F., Motlagh, N. S. H., Naghib, S. M., Haghiralsadat, F., Jaliani, H. Z., & Moradi, A. (2022). A functionalized graphene oxide with improved cytocompatibility for stimuli-responsive co-delivery of curcumin and doxorubicin in cancer treatment. *Scientific Reports*, *12*(1). doi:10.1038/s41598-022-05793-9

Yagublu, V., Karimova, A., Hajibabazadeh, J., Reissfelder, C., Muradov, M., Bellucci, S., & Allahverdiyev, A. (2022). Overview of physicochemical properties of nanoparticles as drug carriers for targeted cancer therapy. *Journal of Functional Biomaterials*, *13*(4), 196. doi:10.3390/jfb13040196

Yakan, H., Cakmak, S., Kutuk, H., Yenigun, S., & Ozen, T. (2020). Synthesis, characterization, antioxidant, and antibacterial activities of new 2,3-dimethoxy and 3-acetoxy-2-methyl benzamides. *Research on Chemical Intermediates*, *46*(5), 2767–2787. doi:10.1007/s11164-020-04118-7

Yamamura, H. (2017). Chemical modification of cyclodextrin and amylose by click reaction and its application to the synthesis of poly-alkylamine-modified antibacterial sugars. *Chemical & Pharmaceutical Bulletin*, *65*(4), 312–317. doi:10.1248/cpb.c16-00739

Yamamura, H., Sugiyama, Y., Murata, K., Yokoi, T., Kurata, R., Miyagawa, A., … Katsu, T. (2014). Synthesis of antimicrobial cyclodextrins bearing polyarylamino and polyalkylamino groups via click chemistry for bacterial membrane disruption. *Chemical Communications (Cambridge, England)*, *50*(41), 5444. doi:10.1039/c3cc49543d

Yan, Y., & Ding, H. (2020). PH-responsive nanoparticles for cancer immunotherapy: A brief review. *Nanomaterials (Basel, Switzerland)*, *10*(8), 1613. doi:10.3390/nano10081613

Ye, Y., Ren, H., Zhu, S., Tan, H., Li, X., Li, D., & Mu, C. (2017). Synthesis of oxidized β-cyclodextrin with high aqueous solubility and broad-spectrum antimicrobial activity. *Carbohydrate Polymers*, *177*, 97–104. doi:10.1016/j.carbpol.2017.08.123

Yildiz, T., Gu, R., Zauscher, S., & Betancourt, T. (2018). Doxorubicin-loaded protease-activated near-infrared fluorescent polymeric nanoparticles for imaging and therapy of cancer. *International Journal of Nanomedicine*, *13*, 6961–6986. doi:10.2147/ijn.s174068

Yin, P., Zhou, W., Dong, X., Guo, B., & Huang, Y. (2020). Effect of oxidized wood pulp fibers on the performance of the thermoplastic corn starch composites. *Advances in Polymer Technology*, *2020*, 1–7. doi:10.1155/2020/8976713

Yousef, T., & Hassan, N. (2017). Supramolecular encapsulation of doxorubicin with β-cyclodextrin dendrimer: in vitro evaluation of controlled release and cytotoxicity. *Journal of Inclusion Phenomena and Macrocyclic Chemistry*, *87*(1–2), 105–115. doi:10.1007/s10847-016-0682-4

Zha, L., Wang, B., Qian, J., Fletcher, B., Zhang, C., Dong, Q., … Hong, L. (2020). Preparation, characterization and preliminary pharmacokinetic study of pH-sensitive Hydroxyapatite/Zein nano-drug delivery system for doxorubicin hydrochloride. *The Journal of Pharmacy and Pharmacology*, *72*(4), 496–506. doi:10.1111/jphp.13223

Zhang, C., Yang, X., Hu, W., Han, X., Fan, L., & Tao, S. (2020). Preparation and characterization of carboxymethyl chitosan/collagen peptide/oxidized konjac composite hydrogel. *International Journal of Biological Macromolecules*, *149*, 31–40. doi:10.1016/j.ijbiomac.2020.01.127

Zhang, C.-W., Zhang, J.-G., Yang, X., Du, W.-L., Yu, Z.-L., Lv, Z.-Y., & Mou, X.-Z. (2022). Carbohydrates based stimulus responsive nanocarriers for cancer-targeted

chemotherapy: a review of current practices. *Expert Opinion on Drug Delivery*, *19*(6), 623–640. doi:10.1080/17425247.2022.2081320

Zhang, L., Ge, H., Xu, M., Cao, J., & Dai, Y. (2017). Physicochemical properties, antioxidant and antibacterial activities of dialdehyde microcrystalline cellulose. *Cellulose (London, England)*, *24*(5), 2287–2298. doi:10.1007/s10570-017-1255-4

Zhang, Y.-M., Liu, Y.-H., & Liu, Y. (2020). Cyclodextrin-based multistimuli-responsive supramolecular assemblies and their biological functions. *Advanced Materials (Deerfield Beach, Fla.)*, *32*(3), e1806158. doi:10.1002/adma.201806158

Zhao, G., Long, L., Zhang, L., Peng, M., Cui, T., Wen, X., … Che, L. (2017). Smart pH-sensitive nanoassemblies with cleavable PEGylation for tumor targeted drug delivery. *Scientific Reports*, *7*(1). doi:10.1038/s41598-017-03111-2

Zhao, M.-X., Zhao, M., Zeng, E.-Z., Li, Y., Li, J.-M., Cao, Q., … Mao, Z.-W. (2014). Enhanced anti-cancer efficacy to cancer cells by doxorubicin loaded water-soluble amino acid-modified β-cyclodextrin platinum complexes. *Journal of Inorganic Biochemistry*, *137*, 31–39. doi:10.1016/j.jinorgbio.2014.03.012

Zhao, W., Zhao, Y., Wang, Q., Liu, T., Sun, J., & Zhang, R. (2019). Remote light-responsive nanocarriers for controlled drug delivery: Advances and perspectives. *Small*, *15*(45), e1903060. doi:10.1002/smll.201903060

Zheng, L., Xiong, L., Li, J., Li, X., Sun, J., Yang, S., & Xia, J. (2008). Synthesis of a novel β-cyclodextrin derivative with high solubility and the electrochemical properties of ferrocene-carbonyl-β-cyclodextrin inclusion complex as an electron transfer mediator. *Electrochemistry Communications*, *10*(2), 340–345. doi:10.1016/j.elecom.2007.12.015

Zhou, T., Li, J., Jia, X., Zhao, X., & Liu, P. (2018). PH/reduction dual-responsive oxidized alginate-doxorubicin (mPEG-OAL-DOX/cys) prodrug nanohydrogels: Effect of complexation with cyclodextrins. *Langmuir: The ACS Journal of Surfaces and Colloids*, *34*(1), 416–424. doi:10.1021/acs.langmuir.7b03990

Zhu, M., Ge, L., Lyu, Y., Zi, Y., Li, X., Li, D., & Mu, C. (2017). Preparation, characterization and antibacterial activity of oxidized κ-carrageenan. *Carbohydrate Polymers*, *174*, 1051–1058. doi:10.1016/j.carbpol.2017.07.029

Zi, Y., Zhu, M., Li, X., Xu, Y., Wei, H., Li, D., & Mu, C. (2018). Effects of carboxyl and aldehyde groups on the antibacterial activity of oxidized amylose. *Carbohydrate Polymers*, *192*, 118–125. doi:10.1016/j.carbpol.2018.03.060

Ziegler-Borowska, M., Wegrzynowska-Drzymalska, K., Chelminiak-Dudkiewicz, D., Kowalonek, J., & Kaczmarek, H. (2018). Photochemical reactions in dialdehyde starch. *Molecules (Basel, Switzerland)*, *23*(12), 3358. doi:10.3390/molecules23123358

(N.d.). Retrieved May 5, 2023, from Europa.eu website: https://www.ema.europa.eu/en/documents/scientific-guideline/questions-answers-cyclodextrins-used-excipients-medicinal-products-human-use_en.pdf

Appendix 1

A1.1. Iodometric Titration Method

2M 1 ml HCL and 1 ml sample are added to 25 ml 0.25 gr potassium iodide solution and mixed. At this stage, the color of the solution becomes dark yellow brownish. Then, it is titrated with the prepared 0.05 M sodium thiosulfate ($Na_2S_2O_3$) solution until the color turns pale yellow and the amount spent is recorded in ml. 4 ml of 0.5% starch solution is added and the color of the solution becomes dark blue. Then, titration is continued with 0.05 M sodium thiosulfate solution until the color of the solution turns white and the total amount of sodium thiosulfate spent is recorded in ml.

Figure A1. 1. Color change of OX-β-CDs after 3-4 mounts with no addition of $CaCl_2$

The amount of iodate (IO_3^-) is calculated based on the stoichiometry of the following reaction. In the Eq. (1) below, 6 moles of S_2O_3 corresponding to 1 mole of iodate enter the reaction.

$$IO_3^-(aq) + 6\,S_2O_3^{2-}(aq) + 6H^+(aq) \rightarrow I^-(aq) + 3\,S_2O_3^{2-}(aq) + 3H_2O(l) \qquad (\mathbf{1})$$

IO_3^- concentration <u>NO addition of $CaCl_2$;</u>

Vconsumed $S_2O_3^{-2}$ (ml) = 23.03 ml

0.05 = n/ (23.03/1000) = $1.15\times10^{-3}/6 = 1.191\times10^{-4}$ mol×174.9 gr/mo l= 34mg/ml

IO_3^- = 34 mg/ml

IO_3^- concentration <u>after addition of $CaCl_2$</u>;

Vconsumed $S_2O_3^{-2}$ (ml) = 1 ml

IO_3^- =1.45 mg/ml

The amount of iodate in the synthesized substance was calculated using the titration method without and with the addition of $CaCl_2$. According to this result, the amount of iodate in the solution was reduced 23.44 times with the addition of $CaCl_2$, that is, 95% of iodate was removed.

Appendix 2

A2.1. Preparation of AMOX Loaded ALD-NS

It was examined whether the obtained ALD-NS could bind to the drug containing the NH_2 group, both by the Schiff base reaction and hydrophilic part of the nanoparticle depicted in Figure A2.1. Therefore, AMOX model drug was selected for drug loading (DL) and entrapment efficiency (EE) study of the synthesized nanostructure (ALD-NS2, ALD-NS4 and ALD-NS6) by using standard calibration graph of AMOX (Figure A2.3). In order to prove the formation of the Schiff base formation, the FTIR method was applied as a characterization study and the presence of the C=N bond confirmed this formation.

Accurately weighed amount of AMOX was dispersed in aqueous suspensions of ALD-NS in weight ratios (1:1) and stirred magnetically for 24 h. These suspensions were then centrifuged at 5000 rpm for 15 min to separate out the non-complexed drug as a residue below the colloidal supernatant. The colloidal supernatants were then subjected to freeze-drying to obtain the AMOX loaded ALD-NS nanocarriers.

After that, EE and DL were determined by quantitative estimation of AMOX loaded ALD-NS. Certain amount of ALD-NS+AMOX (10 mg) were dissolved in methanol, sonicated 15 s for breaking the complex and centrifuged for 15 min. Centrifuged supernatant was diluted and then analyzed by UV-vis at 272 nm (0.1–1 mg/ml, $R^2 = 0.9916$). EE and DL of ALD-NS+AMOX complex was determined using equations shown in the text (section 3.3.2.3).

A2.2. Characterization

A2.2.1. FTIR

The FT-IR spectrum of AMOX in Figure A2.2 shows bands at 3453 cm^{-1} due to symmetric stretching vibrations of primary amine group. The band at 2969 cm^{-1} is due to CH_2 stretching vibration. Bands about 1774 cm^{-1}, 1684 cm^{-1}and1575 cm^{-1} are due to C=O stretching for lactam, carboxyl group, COO^- asymmetric and symmetric stretching vibration, respectively.

As can be seen in Figure A2.2, the NH_2 group of the amine at 3453 cm^{-1} belonging AMOX disappeared as a result of binding to CHO group of ALD-NS. The result of Schiff base binding is seen with the formation of the C=N bond of ALD-NS at 1688

cm^{-1}. A characteristic band corresponding to the stretching of C=N (1690~1590 cm^{-1}) was observed.

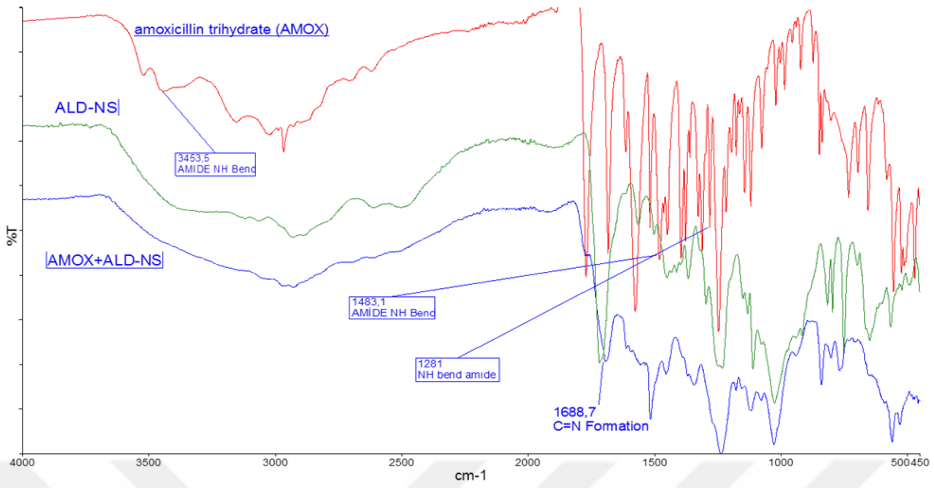

Figure A2. 1. FTIR Spectra of AMOX, ALD-NS and AMOX loaded ALD-NS

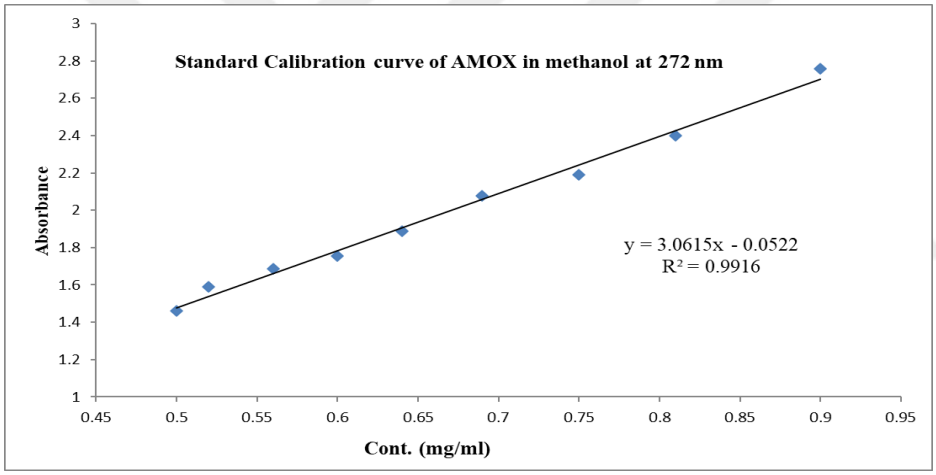

Figure A2. 2. Standard calibration curve of AMOX in methanol at 272 nm

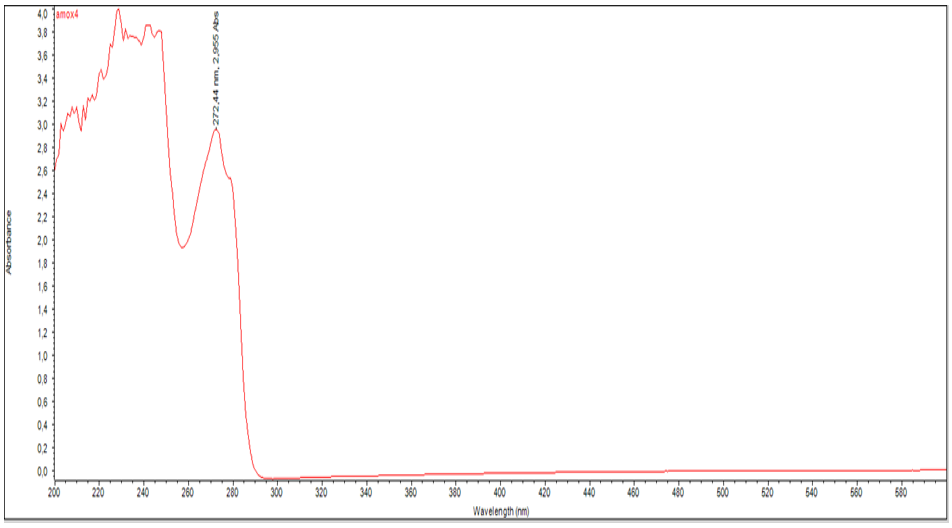

Figure A2. 3. UV-vis spectrum of AMOX in methanol (High absorbance peak observed at 272 nm)

CURRICULUM VITEA

After graduating from Pamukkale University, Faculty of Arts and Sciences, Department of Chemistry in 2003, Ayhan Bergal went to the United States for pursuing his master's degree. He completed his Master's Degree in Chemical Engineering at The City University of New York in 2011. Following his graduation, he returned to Türkiye and worked in private companies. He subsequently entered Ondokuz Mayis University for his Ph.D. education and completed his Ph.D. study in the Department of Nanoscience and Nanotechnology at Ondokuz Mayis University and graduated in 2023.

Contact Information :

ORCID ID : **0000-0002-5930-9104**

Publications :

1. Bergal, A., Matar, G. H., & Andaç, M. (2022). Olive and green tea leaf extracts mediated green synthesis of silver nanoparticles (AgNPs): comparison investigation on characterizations and antibacterial activity. *BioNanoScience*, *12*(2), 307–321. https://doi.org/10.1007/s12668-022-00958-2
2. Bergal, A., & Andaç, M. (2021). Nanosponges (NSs): Using as a nanocarrier for anti cancer drug delivery applications. *ACTA Pharmaceutica Sciencia*, *59*(2), 306–320. https://doi.org/10.23893/1307-2080.aps.05918
3. Elmas, A., Akyuz, G., Bergal, A., Andac, M., & Andac, O. (2021). Enhanced analytic approach for describing pH triggered fast drug release systems. *Current Drug Delivery*, *18*(8), 1130–1136. https://doi.org/10.2174/1567201818999210112181853
4. Elmas, A., Akyüz, G., Bergal, A., Andaç, M., Andaç, Ö. (2020). Mathematical modelling of drug release. *Research on Engineering Structures and Materials*, 6(4), 327-350. https://doi.org/10.17515/resm2020.178na0122
5. Bergal A, Elmas A, Akyüz G. (2019). A New Type and Effective Approach for Anti-Cancer Drug Delivery Application: Nanosponge. *Nano Res Appl*, Vol.5 No.2:3 https://doi.org/ 10.36648/2471-9838.5.1.43

Won Awards, Incentives and Scholarships

1. YOK 100/2000 Ph.D. Scholarship
2. TUBITAK 2214-A - International Research Fellowship Program for Ph.D. Students
3. TUBITAK 2211-C National Ph.D. Scholarship Program in the Priority Fields in Science and Technology